Novel automated treatment planning approaches to deal with microscopic disease in radiotherapy

by

I. Briggeman

to obtain the degree of Master of Science
at the Delft University of Technology,
to be defended on Wednesday May 27, 2020 at 11:00 AM.

Student number:	4270142	
Project duration:	September 2 2019 – May 27, 2020	
Thesis committee:	Dr. ir. A. Denkova,	TU Delft, chair
	Dr. ir D. Lathouwers,	TU Delft, supervisor
	Dr. Z. Perko,	TU Delft
	Prof. B. Heijmen,	Erasmus MC, supervisor
	MSc. L. Rossi,	Erasmus MC, daily supervisor

Abstract

The scope of a radiotherapy treatment is to induce damage to tumor cells by irradiating them with ionizing radiation. The radiation should target the tumor as visible in images, also called the macroscopic disease. There is, however, a risk of small, invisible groups of cancer cells in the area surrounding the macroscopic tumor, the microscopic disease. For an optimal clinical outcome of radiotherapy, the microscopic disease needs to be irradiated as well. In current treatment planning, the macroscopic tumor is extended with a margin to better ensure full disease coverage. Because there is uncertainty in the extent of the microscopic disease, also the margin definition is uncertain. Moreover, in current planning, the same margin is used for all patients, and there is no patient-specific exploration of the trade-offs between dose extensions to cover potentially present microscopic disease vs radiation-induced toxicity because of enhanced dose in organs at risk (OARs) surrounding the tumor.

This study aimed to explore whether the margin concept could be replaced by more advanced, individualized approaches for irradiation of volumes just outside the macroscopic tumor. All plans were generated automatically to avoid bias by human planners and to reduce workload. Two novel treatment planning approaches were investigated.

The first focused on increasing dose coverage of the microscopic disease while at the same time controlling the resulting increased dose to the healthy tissues surrounding the macroscopic tumor, including OARs. Several treatment plans were generated to explore a range of trade-offs between dose in microscopic disease and dose in OARs. The results showed that for optimal microscopic disease irradiation, both low and high OAR doses needed to worsen. However, the most significant increase in microscopic disease coverage could be obtained when accepting higher OAR low doses, that is generally less important for induction of negative side-effects.

In the second approach, an expected Tumor Control Probability (expected TCP) cost function was used to control dose delivery in areas close to the macroscopic tumor. Basis of the expected TCP model was a function describing the probability of finding microscopic disease at a specific distance from the macroscopic tumor. The results again demonstrated opportunities to increase dose to areas close to the tumor, at the cost of enhanced doses in OARs.

In conclusion, both approaches had a positive impact on microscopic disease dose coverage. However, improved irradiation of the microscopic disease was always at a price of enhanced dose in OARs. Complementary studies, involving clinicians, need to be carried out to investigate if and how the approaches could be used to replace the current planning with fixed margins.

Contents

List of abbreviations

Abbreviations

ADC	Adenocarcinoma
BED	Biologically Effective Dose
COP	Coverage Optimized Planning
CT	Computed Tomography
CTD	Clinical Target Distribution
CTV	Clinical Target Volume
DCH	Dose Coverage Histogram
DVH	Dose Volume Hisogram
ECE	ExtraCapsular Extension
EPE	ExtraProstatic Extension
EQD	Equivalent Dose
E(TCP)	Expected TCP
EUD	Equivalent Uniform Dose
GTV	Gross Tumor Volume
Gy	Gray
IMRT	Intensity Modulation Radiotherapy
IOV	Inter-observer Variability
LTCP	Logarithm of the TCP
LQ	Linear Quadratic
MDE	Microscopic Disease Extension
MRI	Magnetic Resonance Imaging
NSCLC	Non-Small-Cell Lung Cancer
NTCP	Normal Tissue Complication Probability
OAR	Organ At Risk
PDF	Probability Density Function
PET	Positron Emission Tomography
PTV	Planning Target Volume
SBRT	Stereotactic Body Radiotherapy
SCC	Squamous Cell Carcinoma
SF	Surviving Fraction
TCP	Tumor Control Probability
TODT	Target OAR Dose Tradeoff
TPS	Treatment planning system

1 Introduction

Cancer is currently one of the major causes of death worldwide [1]. Tumor development initiates when cells start reproducing without control. Tumors can be either non-cancerous, *benign*, or cancerous, *malignant*. Non-cancerous tumors grow locally and do not invade nearby tissues. Malignant tumors, on the other hand, may infiltrate and spread throughout the body. When a group of these uncontrolled cells becomes large enough to be discovered either via physical examination or imaging techniques, it can be called *macroscopic* disease or Gross Tumor Volume (GTV). Generally, there is a risk of a spread of cancer cells in the surroundings of the macroscopic disease. This is referred to as *microscopic* disease. A simple graphical representation is visualized in figure 1.1. The maximum extent of microscopic disease from the macroscopic disease edge is patient-specific, tumor-specific, and generally unknown. Even with current technological advances and new imaging techniques, visualizing the microscopic disease is not possible.

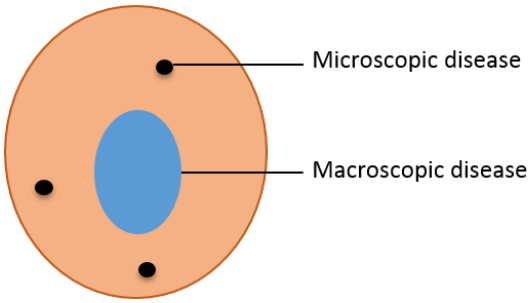

Figure 1.1: Simple tumor example, showing a macroscopic disease surrounded by microscopic diseases.

There are several types of cancer treatment, including surgery, chemotherapy, and radiation therapy. This work focuses on prostate cancer (most theory also holds for all other tumor sites), for which radiotherapy is one of the primary treatment modalities. Prostate cancer is the most prevalent cancer among men and incidence increases, especially due to the aging population [2]. Death rates vary widely [3]. This may be explained by the fact that prostate cancer is well treatable and has high survival rates when it is localized, while this rate drops for patients with distal disease spreads [4].

For an optimal clinical outcome of radiotherapy treatment, microscopic disease should be irradiated, next to the macroscopic disease. Currently, the margin concept is used for irradiation of microscopic disease. Margins define expansions around the GTV to create a radiotherapy target called Clinical Target Volume (CTV) that also includes microscopic disease (this could, for example, be the total brown volume in figure 1.1). Generally, the CTV is defined in patient images. Because of limitations in visibility of the macroscopic tumor in these images and the uncertainty in the (invisible) patient-specific extent of microscopic disease, the CTV definition has large uncertainties. The uncertainties might also lead to so-called inter-observer variability in established CTVs. This variability is aggravated by the fact that margins are a yes/no decision; either an area belongs to the target volume or not.

Uncertainties of up to where these margins might extent can currently not be incorporated in the generation of a patient-specific treatment plan, i.e. the dose distribution delivered to the patient is not optimized for uncertainties in the margin.

1.1. Goal of this research

The goal of this master project is to investigate two novel approaches to deal with microscopic disease uncertainties in treatment planning. In the first method, prioritized multi-criteria optimization, referred to as 'prioritized optimization', the trade-off of between irradiating larger volumes around the tumor, for killing potentially present microscopic disease, and the higher doses obtained in the healthy tissues surrounding this volume, is studied. In the second approach, called the 'probabilistic planning approach', treatment planning is based on a probabilistic cost function that explicitly models the probability that microscopic disease is located at certain distances from the macroscopic tumor.

1.2. Outline

Chapter 2 gives an introduction to the key concepts of radiotherapy. First, it will provide insights into the biological effects of radiation, followed by a description of the radiotherapy workflow. Here special attention is paid to the establishment of margins and the uncertainties. Chapter 3 is a modified version of the literature study, as part of this project, elaborating on microscopic disease and on the use of histopathological studies to investigate microscopic disease extent. It also introduces previous studies on probabilistic planning to replace current margin-based planning. Chapter 4 focuses on the use of prioritized optimization as a replacement of the classical use of margins for microscopic disease, while Chapter 5 describes the use of a probabilistic cost function for the same purpose. Finally, chapter 6 provides an overall conclusion.

2

Background

Radiotherapy is used for the treatment of tumors, and can either be curative or palliative. The final goal is always to induce biological damage in tumors tissues, causing cell death. Radiotherapy makes use of radiation, which could either arise from external beams or a radiation source implanted in the proximity of the tumor. In external beam radiation, beams of ionizing radiation are aimed at the tumor to deliver a specified dose, expressed in Gray (Gy). The rationale behind the dose needed for tumor irradiation is radiobiology. Section 2.1 provides fundamental insights into radiobiology. The sections following, 2.2, 2.3 and 2.4, will focus on the radiotherapy workflow.

2.1. Radiobiology

When living organisms are irradiated with ionizing beams, this induces a reaction. A major pathway to cell death by radiotherapy is the induction of DNA breaks. The science that evaluates the biological effects of radiation is called radiobiology [5]. For radiotherapy, the impact of the treatment on both healthy tissues and tumor cells should preferentially be known in detail to make a balanced trade-off between tumor control and normal tissue complication probability possible. The balance is handled by delivering dose in multiple sessions, also called *fractions*. With fractionation, the total irradiation dose is not given at once but instead delivered in smaller doses spread over several days. In this way, there is time between the sessions to let the normal tissue cells recover from possible damage. However, tumor cells may, to some extent, also benefit from a prolonged treatment due to so-called re-population. Therefore, the optimal fractionation scheme should be defined to maximize the damage to the tumor while minimizing the damage to the healthy tissues. In conventional external beam radiotherapy, the dose is fractionated in 2 Gy fractions, i.e. instead of irradiation with 60 Gy at once, 30 fractions of 2 Gy are prescribed. Another, more recent approach, is hypofractionation, in which the total dose is divided into larger dose fractions [6], e.g. with stereotactic body radiotherapy (SBRT).

Radiobiological models have been introduced to evaluate the effects of different fractionation schemes [7]. Typically, in these models, physical parameters, as the number of fractions, total dose or overall treatment time are converted into biological quantities.

2.1.1. Radiobiological models

Linear-Quadratic model

The biological impact of fractionation can be calculated with the Linear-Quadratic (LQ) model for cell survival, where the surviving fraction (SF) for a single fraction treatment is expressed as

$$SF_d = e^{-\alpha d+\beta d^2} \tag{2.1}$$

Here α and β are parameters for cell sensitivity, and d is the fraction dose. The ratio α/β determines the sensitivity for fractionation and differs per tissue type. For fractionated treatment, with N_f fractions of dose d, the total dose becomes $D = N_f d$, the LQ-model can be rewritten as:

$$SF_{N_f d} = (SF_d)^{N_f} \tag{2.2}$$

$$SF_{N_f d} = e^{-N_f(\alpha d + \beta d^2)} \tag{2.3}$$

$$SF_{N_f d} = e^{-(\alpha D + \beta D^2 / N_f)} \tag{2.4}$$

This is the same as

$$SF_{N_f d} = e^{-\alpha BED} \tag{2.5}$$

Where BED is the Biologically Effective Dose

$$BED = D(1 + d/\frac{\alpha}{\beta}) \tag{2.6}$$

BED can be regarded as the biological dose delivered to a tissue having a specific α/β ratio. If BED values are the same for two different fractionation schemes, a similar biological effect is induced by the two treatments. From the BED it can be seen that the biological effect is larger for tissues with smaller α/β values, which is the case for late toxicity in most organs at risk (normal tissue), compared to tumor cells. In practice, this means that fractionation, with a lower d, is beneficial for the organs at risk. The total dose can be increased so that the effect for the tumor remains constant, while the BED of the organs at risk is reduced. This way the surviving fraction is increased, resulting in fewer complications.

Tumor Control Probability
The Tumor Control Probability (TCP), which describes the probability of local tumor control [8], is dependent on the average number of surviving cells in the tumor, μ. Taking the most general model for TCP, depending on the Poisson distribution, the TCP depending on fraction dose d for a fixed number of fractions N_f becomes

$$TCP = e^{-\mu} = e^{-N_0 e^{-N_f(\alpha d + \beta d^2)}} \tag{2.7}$$

With N_0 the initial number of tumor cells. Similar as in the LQ-model, N_f is the number of fractions, α and β are parameters for cell sensitivity and d is the fraction dose. Rewriting the TCP in terms of total dose D, the model looks like

$$TCP = e^{-\mu} = e^{-N_0 e^{-(\alpha D + \beta D^2 / N_f)}} \tag{2.8}$$

The optimal TCP value is 1. The TCP model can both be used for plan evaluation, or plan optimization.

Normal Tissue Complication Probability
For a treatment plan, a balance should be found between the TCP and the Normal Tissue Complication Probabilities (NTCP). The NTCP refers to the probability that a given dose will cause complications in a specific tissue [9]. A general way to model NTCPs was introduced by Lyman [10] and called the Lyman Kutcher Burman NTCP model.

2.2. Radiotherapy workflow

The radiotherapy workflow after diagnosis can be divided into various steps: 1. patient immobilization preparation, 2. image acquisition (planning computed tomography (CT)), 3. volume definition of targets and sensitive tissues in the planning CT, 4. treatment planning, 5. plan evaluation, 6. patient set-up, 7. radiation treatment and 8. follow- up. For this research, the focus will be mainly on steps 3 and 4, and 5, i.e. targets and sensitive tissues definition in the planning CT, treatment planning, and plan evaluation. Treatment planning is performed on the structures defined in the CT by optimizing and evaluating the dose distribution that will be delivered to the patient, and in particular to the delineated organs at risk and targets.

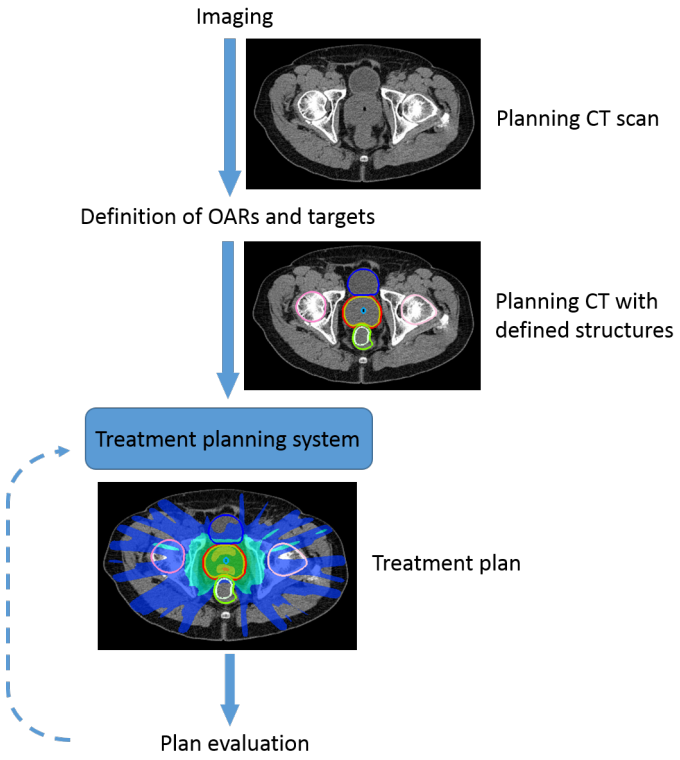

Figure 2.1: Schematic simplified overview of the radiotherapy treatment planning workflow. After the patient has been immobilized, imaging is performed. This results in at least a planning CT scan, used for definition of several structures. The treatment planning system uses this as input and generates a treatment plan. Plan evaluation needs to be performed and if needed improved treatment plans should be created.

2.3. Definition of structures used for planning

After immobilizing the patient, 3D images for the 3D definition of the targets and OARs are acquired. The images with the defined volumes, i.e. structures are used to steer the treatment planning. The volumes GTV, CTV and Planning Target Volume (PTV), have been for proposed in the International Commission on Radiation Units and Measurements (ICRU) 50 guidelines [11] for the first time . In this section, more details will be provided. In figure 2.1 a schematic overview is presented.

2.3.1. Definitions

Gross tumor Volume (GTV)

The GTV is the tumor visible in the image and is also the first and central volume to be defined in the planning CT-scan. Often, an additional imaging modality such as Magnetic Resonance Imaging (MRI) or Positron Emission Tomography (PET) is used next to CT, to provide supplementary information for the establishment of the GTV in the planning CT. The planning CT-scan is the basis for planning as it contains information on electron densities that is needed for dose calculations. Due to limitations in imaging of the GTV (e.g. related to low contrast) and the fact that different imaging modalities may give rise to a different contour (even though the same physician does contouring), delineation uncertainties arise.

Clinical Target Volume (CTV)

To obtain the CTV, the GTV is expanded with a margin to include potential microscopic disease extensions located outside of the GTV. Microscopic disease extent is patient-specific; histopathological studies, have shown that there are patients that have no microscopic extensions while for others microscopic disease can be found up to 12 mm from the tumor edge [12]. By definition, microscopic disease is not visible in the patient images, so the GTV-CTV margin cannot be made patient-specific. In practice, the applied margin is often a balance between optimal tumor control (large margin including likely microscopic disease presence) and avoidance of severe radiotherapy-induced toxicity (small margin).

Currently, in each treatment centre, the applied margin is generally fixed for patients with the same tumor type.

Planning Target Volume (PTV)
To make sure that the full CTV receives the prescribed dose, despite geometrical uncertainties such as variations in daily patient set-up relative to the treatment isocenter, a CTV-PTV margin is normally added to the CTV. In planning, the aim is then to deliver a high dose to the largest part of the PTV, e.g. 98%. Daily total setup errors consist of both random and systematic errors. The random errors are day-to-day variations of the tumor relative to the radiation beam, e.g. due to organ motion and differs between fractions. The systematic error has the same value for every fraction. For each patient, it is a fixed error, occurring every day. The most commonly used way to define the PTV margin is by using the margin recipe introduced by van Herk et al. [13], where the extension, M, is:

$$M = 2.5\Sigma + 0.7\sigma \tag{2.9}$$

Σ is a standard deviation describing the distribution of systematic errors in a patient population, while σ is a standard deviation representing day-to-day variations in the random error. As can be seen from the equation, the systematic error has a much higher weight than the random error.

Organs at Risk (OAR)
OARs are organs that are located in the surroundings of the volume to be treated, or located further away but still relevant. Their irradiation may lead to damage resulting in functional problems, reduced quality of life or even death [14]. There are two types of OARs, namely serial-like and parallel-like organs. It is essential to know the type of OAR to be delineated since it affects the area needing delineation. In serial-like organs, the functional subunits are arranged in series. They can be seen as a chain of links. If damage is done to one of the links, this will affect the entire organ [15]. Since the effect depends on a single subunit, only the part close to the irradiated area, carefully defined, can be delineated (e.g. part of the spinal cord). Parallel-like organs, on the other hand, are organized as functional subunits that behave more independently of each other. Damage to one of these subunits does not influence the entire organ [15]. Instead, the organ is sensitive to irradiation of a relative part. The liver and lungs are examples of parallel-like organs. Since they have a volume dependence, these organs need to be fully delineated.

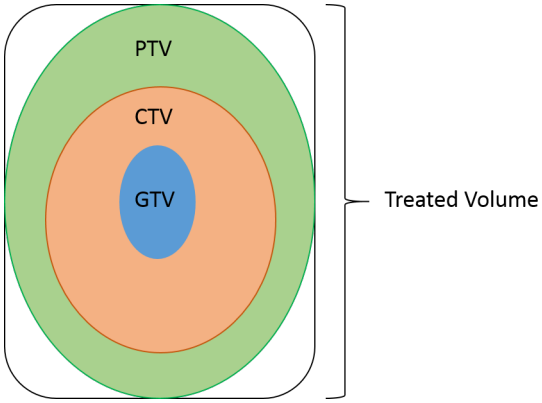

Figure 2.2: Different target volumes that need to be delineated. From inside to outside the Gross tumor Volume (GTV), Clinical Target Volume (CTV) and the Planning Target Volume (PTV). The PTV is the area to be covered with high dose in treatment planning. Adapted from [11]

2.3.2. Definition of the prostate structures

In clinical practice, for SBRT prostate treatment, the complete prostate volume is delineated as the GTV, and there is no extension for microscopic disease, ie. CTV=GTV. Often a 3 mm PTV margin is used. Relevant OARs for treatment planning are rectum, bladder, urethra and the left and right femoral heads. An overview of all structures to be defined can be seen in figure 2.3. The bladder, rectum and femoral heads are serial-like organs; high doses could induce serious complications. To prevent loss

of function, irradiating these OARs with high doses needs to be minimized, while urethra volumes need to be controlled at medium-high doses.

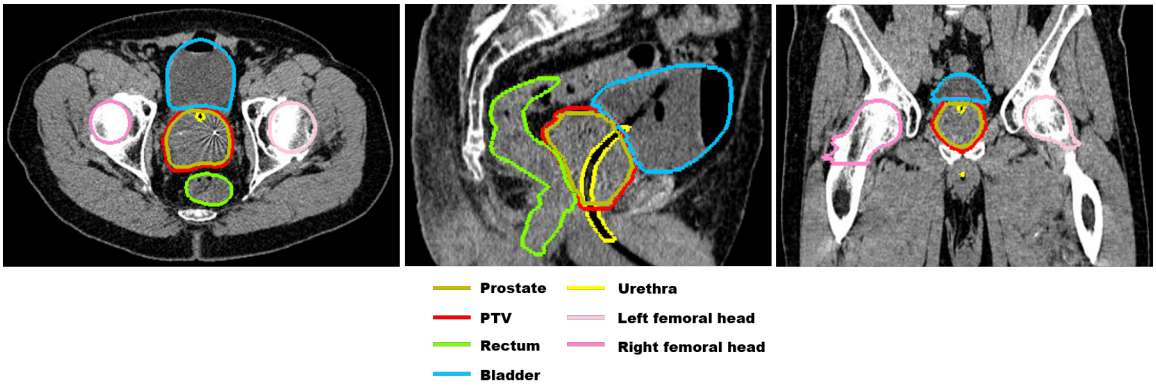

Figure 2.3: CT scan of a prostate cancer patient with defined target and OARs. From left to right, 2D patient slices in the axial, sagittal and coronal direction are presented. All structures relevant for prostate treatment planning are visualized; the prostate and PTV as the target volumes and the rectum, bladder, urethra and left and right femoral heads as relevant OARs.

2.4. Treatment planning

2.4.1. Clinical protocol for prostate SBRT

The clinical protocol includes clinical requirements that should not be violated in treatment planning. The requirements are dose constraints, for either targets structures or OARs. For a treatment plan to be accepted, the planned dose values should be within limits. Even though constraints in the wish-list usually regulate these values, it should always be checked if the clinical protocol has not been violated.

The clinical constraints for prostate SBRT are reported below (table 2.1). For the PTV, the volume that receives the prescribed dose should be above 95%, while for the prostate, the minimum dose is constrained (Dmin > 34.0 Gy). For both rectum and bladder the D0.03cc and D1cc are used to define clinical requirements. D0.03cc is called the near-maximum dose; it is less sensitive than Dmax for high doses in a single or a few voxels. The dose in the urethra is constrained using D50%, D10% and the D5%, the dose in 50, 10, and 5% of the structure, respectively. The goal of each treatment plan is to irradiate the patients without exceeding constraints.

Structure	Parameter	Constraint	Min/Max
PTV	*V38Gy*	95.0%	Min
Prostate	*Dmin*	34.0 Gy	Min
Rectum	*D0.03cc*	38.0 Gy	Max
	D1cc	32.3 Gy	Max
Bladder	*D0.03cc*	41.8 Gy	Max
	D1cc	38.0 Gy	Max
Urethra	*D50%*	40.0 Gy	Max
	D10%	42.5 Gy	Max
	D5%	45.0 Gy	Max

Table 2.1: Clinical protocol of the prostate showing the protocol parameters and corresponding values for all structures included: the PTV, prostate and the rectum, bladder and prostate as OARs. The values are reported in Gy, except for the V38Gy, the volume receiving 38Gy. Min/max refers to whether it is a minimum of maximum constraint.

2.4.2. Erasmus-iCycle

After definition of the OARs and the targets, and the clinical protocol has been defined, treatment plans can be created. This is done using a treatment planning system (TPS). In the Erasmus MC, a system for the automation of the treatment planning process has been developed named Erasmus-iCycle [16]. In this research, Erasmus-iCycle is used for generation of all treatment plans, so a short introduction is given.

Erasmus-iCycle is an algorithm for automated treatment planning using an a priori multi-criteria approach to optimize beam profiles and angles [16]. The algorithm optimizes based on a tumor site-specific wish-list. This list contains hard constraints and objectives of which the priorities are defined [16]. Constraints are fixed requirements that need to be met. Objectives will be optimized as much as possible to their defined goals, starting iteratively with the one having the highest priority. When an objective is optimized it becomes a constraint for the next objective. The algorithm optimizes two times through the wish-list, in two phases. In the first phase, each objective will have a value that is equal or higher than its goal [16]. If it is possible to reach a value better than the goal, the algorithm will not fully optimize in the first phase, but instead, it will stop at the goal and continue to optimize all other objectives first. In the second phase the optimizer will try to further improve on the objectives that could be further optimized in the first phase and goal values are fully minimized to the best attainable value. With Erasmus-iCycle the user can upfront define a fixed beam configuration. Otherwise, the algorithm selects the optimal beam directions from a pool of candidate beams.

2.4.3. Plan evaluation

Dose Volume Histograms

For plan evaluation, Dose Volume Histograms (DVHs) are the most commonly used tool. Treatment planning, results in a 3D dose distribution, which can be difficult to fully quantify. DVHs provide a graphical representation of the dose that is delivered to specific 3D volumes [17]. These specific volumes can either be target volumes or OARs. There are two types of DVHs, cumulative and differential. The most used one is the cumulative DVH, which shows the percentage of volume receiving a certain dose or higher (see figure 2.4 for an example). The graphs start with 100% volume in the 0 Gy dose bin. With increasing dose, the percentage of volume receiving that dose or higher decreases. Because DVHs provide quick insights in the percentage volume receiving a specific dose, they can be used to compare plans easily. The DVHs can be used as an evaluation tool, and can also be used to calculate the expected TCP and NTCP. A disadvantage of DVHs is that, because it is a 2D plot of a 3D distribution, spatial information is lost.

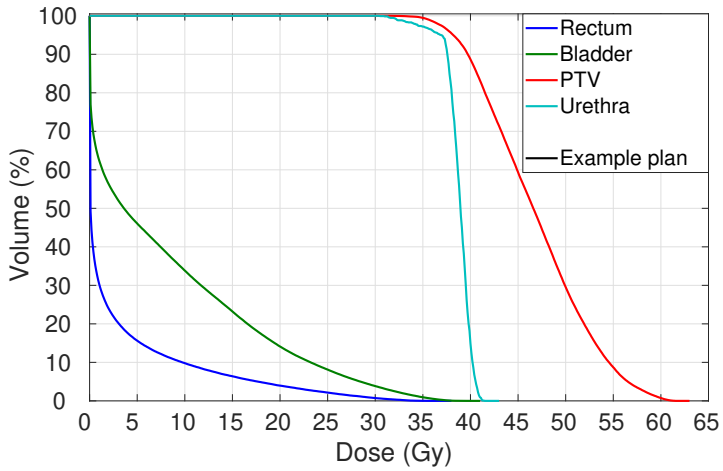

Figure 2.4: An example cumulative dose volume histogram showing the doses in the PTV and OARs.

3

Literature study

This chapter is a modified version of my literature study: *The introduction of probabilistic planning to deal with uncertainties in tumor extensions*. The study elaborates on microscopic disease extensions and the information histopathological studies might provide and introduces previous work on probabilistic planning as a method to overcome the limitations of the currently used margin concept.

3.1. Microscopic disease extensions

It is known that most solid tumors can have microscopic disease extension(s) (MDE(s)) that are not visualized by currently used imaging modalities [18]. Only histopathological studies provide information about the MDE distance, i.e. distance from the macroscopic tumor edge to the MDE. There are different ways to refer to it: extension distance, MDE distance, radial extension, however, it all comes down to the same. Incorporating MDE distance information in margin definitions could result in better reproducible CTV margins. Therefore, several studies have been performed for different tumor locations.

3.1.1. Pathological MDE studies

Pathological MDE studies in the prostate will be discussed as this is the focus of the research. Literature findings in this section are reported as consistent as possible. However, the way in which MDE data is reported differs considerably per study. This topic will be further discussed in section 3.1.3.

Microscopic disease extension in the prostate

Microscopic extension of prostate cancer can be categorized as extraprostatic extension (EPE), also called extracapsular extension (ECE) i.e., the local spread of prostate cancer beyond the prostate boundaries [19]. EPE is associated with unfavorable prognostic factors [4]. Knowing the radial extent of EPE, tumor volume margins could be better defined, thereby improving therapy outcomes [20].

In 1999, the radial distance of EPE was studied by Davis et al. [4]; 416 specimens were studied, of which 126 were identified with EPE (30%). For each specimen, the maximum radial EPE distance was measured from the edge of the prostate (the known tumor volume). The maximum EPE distance had a mean (mean value over all specimens showing EPE) of 0.9 mm, with a range from 0.04 to 5.7 mm. Treating the prostate with brachytherapy, a margin of 3-5 mm would cover 100% of the MDEs in 96% to 99% of the specimens in this specific study [4].

Sohayda et al. [20] analyzed 256 prostatectomy specimens, of which 92 showed EPE (36%). Measurements were performed for 79 of the 92 EPE cases (79/256). In these 79 cases, 98 EPE sites were found (some cases had more sites). The median distance of all EPE sites was 1.1 mm (mean 1.7mm). The minimal distance found was 0.1 mm, while the maximum was 8 mm (range 0.1 – 8mm). Taking a margin of 3.8 mm, would cover 100% of the EPE in 90% of the cases, resulting in a 90% accuracy.

In a larger study by Teh. et al [12] in 2003, 712 specimens were studied. Of these specimens, 299 (42%) were identified with EPE. The median radial distance was 2.0 mm, with a range from 0.5-12 mm. The maximum distance of 12 mm is higher than the values found in previous studies [4] [20].

The reason behind this could be that this study had the largest number of samples so far [12]. Since radial extension distances vary between patients, having a higher number of samples, increases variation. In a successive study [21], it was concluded that a margin of 5 mm around the GTV would be sufficient to cover 97.2% of the MDEs in 100% of the samples.

Schwartz et al. [22] studied 404 patients, 121 were categorized as having EPE (30%). Over all EPE samples, the EPE distance range was 0.0-5.7 mm, with a mean of 0.9 mm and a median of 0.6 mm. Most extensions were located posterolaterally [22].

Similar extension distances were found in a study by Chao et al. [23]. Of the 371 prostatectomy specimens, 121 (33%) showed EPE, with a median distance of 2.4 mm in and in a range of having a of 0.05-7.0 mm. Also in this study, most extensions were located in a posterolateral direction from the prostate.

An overview of the literature findings can be found in table 3.1.

Author	**MDE samples /total (no.)**	**MDE distance (mm)**	**Range MDE (mm)**	**Suggested margin (mm)**	**Accuracy (%)**
Davis et al. [4]	126/416	Mean: 0.9	0.04 - 5.7	3 - 5	96 - 99
Sohayda et al. [20]	92/256	Median: 1.1	0.1 - 8.0	3.8	90
Teh et al. [12] [21]	299/712	Median 2.0	0.5 - 12	5	97.5
Schwartz et al. [22]	121/404	Mean: 0.9 Median: 0.6	0.0 - 5.7		
Chao et al. [23]	121/371	Mean: 2.3 Median: 2.4	0.07 - 7	5	90

Table 3.1: Findings per article of the number of prostate cancer samples with MDE vs the total number studied, the median/mean MDE distances over all samples to the tumor edge, the range of distances found, the suggested tumor margin and the accuracy of the suggested margin.

It can be concluded that MDEs are a frequently occurring phenomenon, underpinning the need to account for them when defining tumor volumes. However, the radial extent distances of the MDEs vary between different studies. This suggests that increasing the number of samples may help in drawing more consistent conclusions from the data

3.1.2. Probability density functions

Definition

Distance information of MDEs can be incorporated in a probability density function (PDF). The distribution of the probability of finding an MDE between r and dr is given by $P(r)dr$, where r is the distance to the GTV and $P(r)$ is the probability density. Taking the integral from 0 to infinity results in

$$\int_0^\infty P(r)dr = 1 \tag{3.1}$$

If a patient has an MDE, taking into account the entire tumor surroundings, the probability of finding an MDE is 1. To derive $P(r)$, MDE distribution information, as the chances of finding MDEs up to a certain distance, or the number of patients having MDEs up to a specific distance r should be known. This knowledge could be gathered from histopathological studies. In literature, several probability density functions have been proposed. Most of them are based on histopathological lung studies.

Literature findings

A study by Siedschlag et al. [24] formulated a probability density P(r) of the MDEs , which can be found below. This function was based on the MDE distribution found in the histopathological study by van Loon et al. [25] and derived by fitting the data to a simple function. In the model, r corresponds to the distance to the GTV, the visible tumor border, in mm and C is a normalization constant.

$$P(r) = C * r * e^{-0.2r} \tag{3.2}$$

This formula was used to run a computer simulation using the Monte Carlo approach to study the effect of the MDEs on the tumor control probability. Various values were taken for geometric uncertainties, and both conventional treatment and stereotactic treatment were analysed.

They concluded that MDEs were not completely irradiated neither using conformal nor stereotactic radiotherapy. Treatment failure decreases with distance from the tumor contour because of the decreasing probability of finding microscopic extensions. The result from Siedschlag et al. confirms that the MDEs have an influence on the TCP that is non-negligible and an improved value can be obtained by increasing the CTV margin.

When studying the distance of MDEs, Grills et al. [26] plotted the percentage of cases (percentage of samples) vs the maximum microscopic disease distance. Here the percentage of cases could be interpreted as the probability of finding microscopic disease up to a certain distance. The obtained curve does not show exponential decay as the equation above.

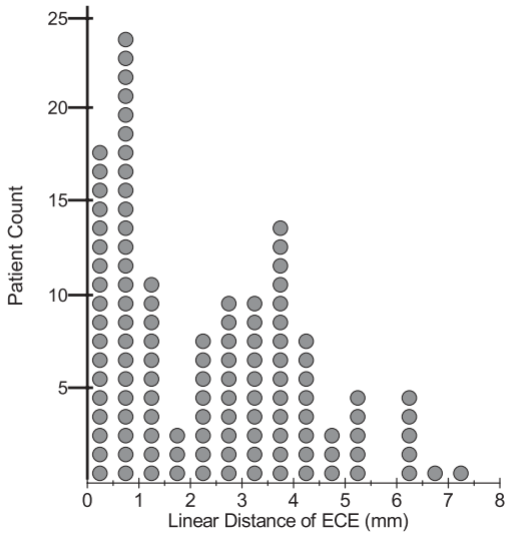

Figure 3.1: Dot density plot provided by Chao et al. [23], displaying the distribution of linear distance of EPE in 121 patients, where each dot represents one patient

Chao et al. [23] created a dot density plot displaying the distribution of the linear distance of EPE in the 121 patients having an MDE, as can be seen in figure 3.1. The distance is subdivided into 0.5 mm bins and each dot represents one patient. The assumption is made that the linear distance of EPE displayed is the maximum distance at which an extension was found per patient. If percentages instead of patients counts were used, this figure would also display the probability density P(r). As can be seen the figure does not really show exponential behaviour.

As could be seen in the literature findings, not all studies formulate the same probability distribution. The literature findings from Siedschlag et al. [24] suggests that the probability density function should resemble an exponential. However, data from Grills et al. [26] and Chao et al. [23] suggest a different behaviour. To define the right probability function for MDEs, distance data is needed as an input.

3.1.3. Reporting MDE data

Some general data is always reported in histopathological studies, as the number of patients, the number of samples and the percentage of samples found to have MDEs. However, how MDE information is reported differs significantly per study, as can also be concluded from section 3.1.1. This makes it hard to compare results from different studies and to derive a probability density function from the reported data. Reported data distributions that might be of interest are the cumulative percentage of patients with MDEs up to a certain distance and the cumulative distribution of MDEs per patient.

This section will first elaborate on how histopathological data is currently being reported in the literature. Then, a recommendation will be made on how the data should be reported to be comparable and which information should be included to derive the optimal probability density function for the MDEs.
There are five main histopathological prostate studies ([4], [20], [12] and [21], [23], [22]). Some data is always reported, as the number of patients, the percentage of EPE, the amount of measurable disease,

whether there is accounted for the shrinkage factor or not, the EPE distance (mostly median), the EPE range and the clinical stage of the patients.

1. In the article by Davis et al. [4] only general information as the maximum and mean radial distances are reported over all patients, which could not be used as input to derive a probability function.

2. Sohayda et al. [20] reports the maximum distance found per patient (if a patient had more than one site, only the EPE site with the largest distance from the tumor was evaluated) in distance ranges (with possible ranges of <0.1 mm, 0.1 – 0.9 mm, 1.0 – 1.9 mm, 2.0 – 2.9 mm, 3.0 – 4.9 mm and 5.0 to 10.0 mm), i.e. 15 patients had an EPE with a maximum distance between 0.1-0.9 mm.

3. Teh et al. [12] [21] reported the number of patients and the cumulative percentage of patients with EPE at a certain dept in mm. This depth is the radial distance of the EPE from the tumor and is divided in ranges of 0, <2, 2-5 and >5 mm. Again the maximum distances are taken.

4. Chao et al. [23] used a different approach to display the extension data. A dot density plot was provided as was seen in figure 3.1. Next to the dot density plot, a plot with the percentage of all patients with EPE at a given linear distance beyond the prostate capsule, grouped by the number of unfavorable risks is shown. From the plot, one would assume that at a distance of 4 mm, 20% of the patients with two unfavorable factors have an extension. In conclusion, the authors comment that the analysis indicates that with the two unfavorable factors, 20% of the patients are at risk for EPE extending 4 to 5 mm beyond the prostate capsule. A discussion could arise whether it means up to a certain distance, as patients can have multiple extensions.

5. Schwartz et al. [22] subdivided the extent of EPE into two ranges. The first range was 0.01-0.59 mm (less than the median EPE), the second one >= 0.6 mm (greater or equal to the median EPE). The authors commented to have created a mathematical model for the prediction of the extent of EPE when pretreatment variables are known. They provided hierarchical diagrams of the predicted percentage of patients with certain EPE distances. Unfortunately, the extent was only described as falling into either one of these two ranges, e.g. with specific pre-therapy characteristics, the risk that a patient had an EPE at a distance of more than 0.6 mm was 4%. No exact distance information was provided.

To start with some high-level observations when looking at the studies as discussed above. First, there is no consistency in the terms articles use when reporting their data. Secondly, even though sometimes studies report the exact same information, data may be displayed or reported differently. This may lead to confusion when comparing various studies. For example, both the study by Sohayda et al. [20] and Teh et al. [12] [21] report the maximum EPE distance per patient, where Sohayda et al. is talking about distances, while Teh et al. is referring to depths. Also, extensions are subdivided in different ranges, making their results not directly comparable.

Next to inconsistency, which can be seen as a minor issue, most studies, as described above, have some limitations in the information provided. First of all, shrinkage of the tumor sample can occur once a biopsy is created of fresh tissue, depending on the specific tumor site [27]. For example, a study to renal tumors showed that the shrinkage factor between fresh and histological samples was 11.4% [27]. Not in every study, the shrinkage factor was taken into account. When comparing different studies and results, one should always keep in mind to check whether or not the authors have compensated for this factor. If not, the radial distances reported are not directly comparable to each other.

Another factor introducing a scaling difference is that most studies address the histopathologic data and not the radiographic data [28]. If MDE data is incorporated into margin definitions, this correlation factor should be known.

When MDE distance data is used, and especially when different studies are compared, the same area around the tumor should be studied. For this reason, it is essential that the cutting margin beyond the tumor and the slice-thickness of the sample are reported per study.

Furthermore, biopsies are always 2D sections of the tumor and the reported distances are mostly given in 1D. Frequently, only the maximum MDE distance per patient is provided.

Looking at figure 3.2, where a and b represent two patients. When only the maximum distance is reported, both patients would give similar values (d1). All other MDE data, as the number of sites per patient (2 vs 4) and distances per site (d2, d3) is ignored, even though it gives much more information about the MDE distribution.

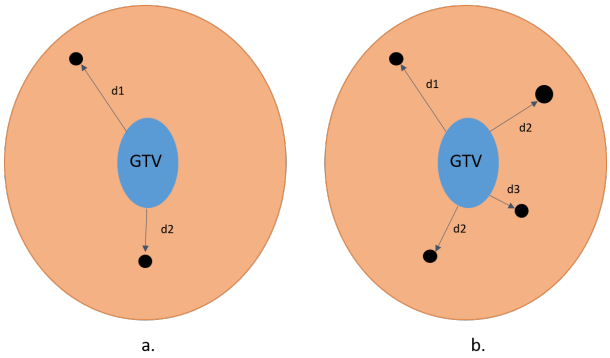

Figure 3.2: Two phantom examples of possible MDE distributions around the GTV. With d the distance between the MDE and GTV. Only taking maximum distances into account a and b would be similar, while the MDE distribution differs.

A more logical output would be the distance per MDE site per patient. Combining the MDE information of all patients, the probability density P(r) could be derived. Probably this type of information was already gathered in the studies as discussed above. Unfortunately, when reporting the results, this full overview was discarded.

In the ideal situation, next to radial distance information, also the MDE size and the MDE distances in 3D should be reported. This would provide knowledge about the 3D distribution of the MDEs around the GTV and give information on the location of the MDEs with respect to each other and the GTV. All examples in figure 3.3 would have similar maximum extension distances being reported (d1). Comparing example b and c, even when the distances for all separate MDE to the GTV are provided in 2-D, the reported values would be the same, even though the MDE distribution is entirely different (one MDE at distance d1, one MDE at distance d3 and two MDEs at distance d2). Example c only has MDEs in particular regions around the GTV, while for example b the MDEs are spread throughout the volume. Also, when information on MDE size is discarded, both MDEs with a distance of d2 in example b would be similar on paper. However, it might be that irradiating an MDE with a larger size is of higher importance. Including the data of both MDE sizes and 3D distributions could have a significant influence on the preferred dose distribution. However, because current literature is usually lacking this kind of information, there is no way to account for it in dose optimization.

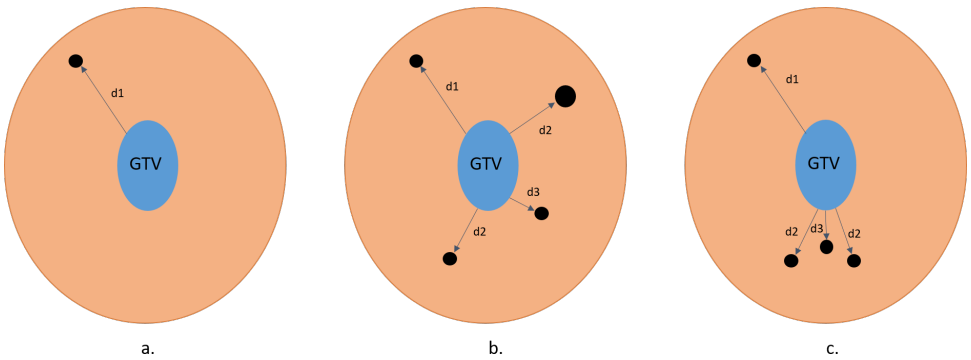

Figure 3.3: Three phantom examples of possible MDE distributions around the GTV. With d the distance between the MDE and GTV. All examples have similar maximum extension distances (d1). Including information on MDE size and 3D distribution, would be more provide a more accurate description of the real situation.

3.1.4. Dose to control MDE

Interesting is how much dose would be needed to control the MDEs. In the literature, several different approaches are discussed. Taking the article from Chao et al. [23], it is concluded that for patients with a high risk of MDEs the CTV margin should be expanded. This suggests that the MDE area should receive the prescribed dose. Another common approach is to assume that a biologically equivalent EQD_{2Gy} of 55 Gy would be sufficient for MDE irradiation [26] [29] [30]. In a study by Grills et al. [26] the effect of different fractionation schemes, 20 Gy in 3 fractions and 12 Gy in 4 fractions on MDE coverage was studied. For 20 Gy in 3 fractions, 6mm outside of the GTV was already covered with 55 Gy by the dose fall off without CTV expansion (i.e. CTV-to-GTV margin =0 mm). While for 12 Gy in 3 fractions, 6 mm outside of the GTV was covered with 55 Gy if a CTV expansion of 3.5 mm would be used. This concludes that MDE coverage is heavily dependent on the fractionation scheme and dose distribution.

3.2. Probabilistic planning

For probabilistic planning, volume uncertainties are directly incorporated in treatment plan optimization [31] [32]. For the CTV-PTV margin, this would mean ignoring the PTV margin and including the geometrical uncertainties on the CTV directly. For the GTV-CTV margin, the CTV would be neglected and uncertainties in the extent of MDEs are directly optimized on the GTV. This way, probabilistic planning could result in a more consistent planning method without the hindrance of delineation uncertainties.

Probabilistic planning is not a new concept. However, variation occurs in its definition and its implementation in treatment planning. Also, the approach is different for the PTV and CTV margins. Probabilistic planning of the CTV-PTV margin is not the main focus of this research work. However, to familiarize with the concept, the most interesting literature findings will be discussed.

3.2.1. Probabilistic planning to replace the CTV-PTV margin

The main goal of the PTV is to make sure that the CTV fully receives the prescribed dose, despite the geometrical uncertainties. The dose is planned to the whole PTV volume as if there is no uncertainty in its definition [33]. However, there are some limitations to the PTV concept. Either the PTV might not offer full coverage of the CTV, or it does ensure coverage, but does not provide the best trade-off between CTV coverage and OAR saving [32]. This can be explained by the fact that the PTV margin can overlap with OAR volumes (something that could never happen for the GTV and CTV). The OARs coinciding with the PTV will receive a similar planning dose as the tumor, without being tumor tissue. This results in sub-optimal treatment plans and possibly unnecessary toxicity.

Currently, PTV delineation is based on general margin recipe models [33]. Many of these margin recipes use the population distribution of systematic and random errors [34]. The error value for an individual patient is unknown; instead, the population approximations are used. Moreover a higher number of fractions is assumed in the error definitions, and they are not always adapted to treatments using a lower number of fractions.

Instead of using the general margin recipe models to define the PTV contour, probabilistic planning could offer a way to optimize for geometrical uncertainties on the CTV directly.

In 2006, Baum et al. [34] suggested the usage of voxel coverage probabilities for IMRT of prostate cancer. These are the probabilities that the CTV occupies a voxel in treatment room coordinates. The values can be calculated from several CT images and the population distribution of the systematic setup error. (CT data of 10 patients, where for each patient, five pre-treatment and three to five treatment CT datasets were acquired.) The cumulative probabilities are used as local weights in treatment planning cost functions, to find the best dose distribution in optimization. To evaluate the obtained dose distributions, the EUD distributions (reflecting the dose distribution) of the target volume and the OARs were compared between margin-based and probabilistic planning. It was concluded that the incorporation of the coverage probabilities in treatment planning, resulted in more information about the overlap region between the PTV and rectum as OAR [34], which could allow for better sparing the rectum. Also, especially when having a lot of organ motion in a patient, the approach leads to robust treatment plans.

Witte et al. [35] introduced another probabilistic planning method (for IMRT optimization) where geometrical uncertainties, including both the random and the systematic errors, can be integrated into the

planning process. With this integration, the TCP and NTCP models were optimized and could directly be used for plan evaluation [35]. For their calculations, they used the TCP model as introduced by Webb and Nahum [8]. Assuming 3D Gaussian distributions for the systematic error and each of the random errors, the expected TCP is obtained. Similarly, functions for the EUD and NTCP were derived, and all functions together were implemented in a general function. To evaluate the outcomes, their treatment plan evaluation software-generated dose sensitivity maps for the TCP and NTCP. These maps show how much the TCP/NTCP would change if the dose in a single voxel increased by 1Gy. It was shown that with probabilistic planning, better trade-offs could be made between the TCP and NTCP than with standard PTV margins in a conventional treatment plan.

Gordon et al. [33] proposed coverage optimized planning (COP). This planning method is based on dose coverage histogram criteria (DCH). Usually, for plan evaluation, the cumulative dose-volume frequency distribution is plotted in a dose-volume histogram (DVH). These histograms plot the volume (tumor or OAR) against dose (v against D). Instead, the DHC plots the probability (Q) that D_v exceeds D, where D_v is the dose delivered to a specific volume (v) of a structure. In a static dose distribution D_v would have one specific value. However, when there are geometric uncertainties, D_v can have a range of different values. Using the DHC, the PTV is discarded and the criteria are directly enforced on the CTV and OARs. To find the optimal plan, a DCH cost function was implemented into an automated optimizer. In this paper, the evaluation of treatment plans was done using Target OAR Dose Tradeoff (TODT) curves. These curves quantify the performance of the plan. Comparing different plans, a better plan results in a lower TODT curve (lower OAR dose for the same target dose). It was shown that since there were no predefined PTV values, doses to the OARs could be increased, without exceeding their clinical constraints. This resulted in wider dosimetric margins around the CTV.

The first paper that claims to have created a probability-based plan optimization that is directly comparable to the conventional margin-based approach, with a CTV-PTV expansion of 5 mm in all directions, dates back to 2013, written by Fontanarosa et al. [36]. Head and neck cancer patients were studied. To realize probabilistic planning, the PTV was discarded, and instead the CTVs were used as targets. They performed a target probabilistic planning (TPP) approach, using Monte-Carlo evaluations of geometrical errors. For plan generation, CTV coverage was optimized and maximum doses were set to critical structures. The evaluation was done using D99%, D98%, D2%, and Dmean calculated on the distribution of CTV doses. The probabilistic planning resulted in better OAR sparing with the same CTV coverage as obtained with original plans.

Even though this is only a short overview of research done on probabilistic planning for the CTV-PTV margin, it shows that in general, a better balance between PTV coverage and OAR saving can be obtained. Using this planning approach, it is possible to overcome the most significant limitation of the current PTV definition.

3.2.2. Probabilistic planning to replace the GTV-CTV margin

Replacing the CTV margin by probabilistic planning, is the main focus of this study. The publication of Shusharina et al. [37] introduced a concept that is most similar to what we would like to achieve. In the article, the clinical target distribution (CTD) is proposed. This is a continuous probabilistic concept of the CTV. Using the current CTV margin, a voxel i can either have a probability 1 or 0 (p_i=1 or p_i=0) of containing tumor cells. Using the CTD instead, the voxel probabilities, p_i, can have continuous (not-binary) values [37]. This means that voxel probabilities can take any value between 1 and 0 (generally, a voxel probability of 1 is defined near the GTV and 0 far away from the GTV).

The way the authors propose to derive the CTD distribution is by making a physician draw shells around the tumor volume with probabilities that a tumor can be found outside that specific shell. Figure 3.4 gives an example of this approach; the likelihood of finding tumor outside of the orange shell would be 60% (60% of the patients would have tumor outside of that cell). Voxel probabilities p_i can be derived from the probability shells.

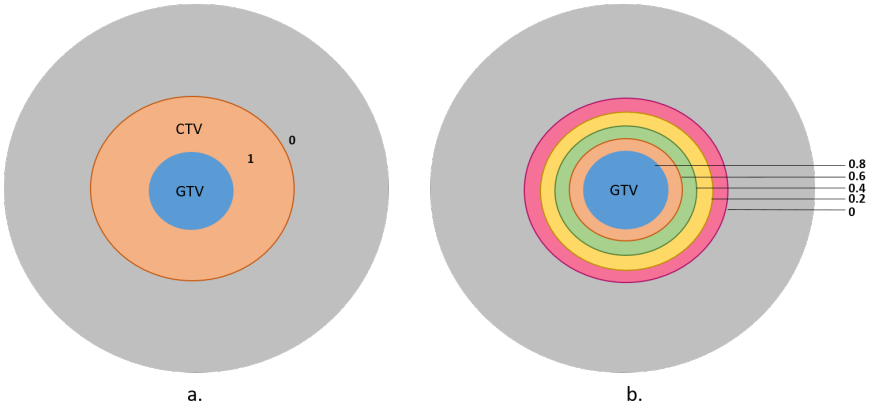

Figure 3.4: Two phantom examples showing the CTV margin (a) and the clinical target distribution (b). In a. the voxel probability is either 1 or 0 (1 inside the CTV, 0 outside). In b. probability shells are drawn around the GTV, accounting for the probability of finding tumor volume inside of a voxel outside of the respective shell. Adapted from [37]

Creating treatment plans, a common way to optimize is taking an objective function that sums dose depending terms. Taking, for example, a simple function that aims to keep the planned dose as close to the prescribed dose as possible, the function per voxel is:

$$f = (d - d_{prescribed})^2 \tag{3.3}$$

With d the dose per voxel and $d_{prescribed}$ the prescription dose per voxel.

Over all voxels, the objective function becomes

$$F = \sum_i f_i \tag{3.4}$$

For the CTD, the voxel probabilities will be introduced in this objective function, resulting in

$$F = \sum_i p_i f_i \tag{3.5}$$

The function can be implemented in a commercial treatment planning system. The introduction of the probabilistic term, p_i, into the objective function, is the only mathematical difference between their probabilistic margin and the common CTV margin.

The research concluded that the CTD allows the physician to realize a better-optimized expansion of the high dose region beyond the GTV. Better trade-offs could be made between OAR sparing and irradiating regions with high chances of having MDEs, resulting in better dose distributions. The clinical target distribution Shusharina et al. proposed could be considered as the starting point of the master project.

However, there are some important aspects that the paper does not explicitly solve. First of all, the paper only introduces a concept, it does demonstrate that the CTD could result in better-optimized plans (but no demonstration for a large patient population) but does not explain how to derive the CTD. It is suggested that physicians delineate probability shells on the CT images. This means that the definition is still susceptible to IOV and it is a binary decision, just now having more levels (either an area falls into a specific isodose line or not). If an area falls into an isodose line, it will receive the same dose as all the other areas within the volume contoured by the isodose line, as the dose is homogeneously distributed. A homogeneous dose distribution is not optimal, it would be more interesting to include distance weights instead, and let the dose distribution be dependent on these weights. This way, an area currently within a certain isodose line, but situated closer to the target volume, could receive a higher dose than another area further away from the target. Another important point is that this research focuses the GTV-CTV expansion. However, it is unclear how to add the PTV from the CTD. A method could start from the GTV+PTV, so already account for the geometric uncertainties and then add the probabilistic optimization for microscopic disease. Furthermore, Shusharina et al. did not evaluate the outcome of the suggested approach. In our research, we want to introduce clear evaluation methods to validate the probabilistic plans and compare them to the plans obtained with current margin definitions. Chapter 5 focuses on our probabilistic planning approach.

4

Prioritized optimization to improve MDE coverage

As explained in section 1.1, this master project investigates two novel approaches to account for MDEs in treatment planning; prioritized multi-criteria optimization to steer MDE coverage in a balance with dose delivered to OARs (this chapter), also referred to as 'prioritized optimization', and the introduction of a probabilistic cost function to improve MDE irradiation (chapter 5).

Generally, in planning, MDE is accounted for by using a CTV margin (section 2.3). However, the focus in this thesis is on prostate cancer treated with SBRT (section 2.3.2). For this treatment, CTV margins are not used in clinical planning in order to maximally protect OARs.

This chapter starts with a general description of prioritized optimization. After that, an explanation of the implementation of prioritized optimization to increase MDE coverage is given. The last section shows the results and provides a conclusion.

4.1. Methods

Erasmus-iCycle optimizes treatment plans with a tumor-site specific wish-list, containing hard constraints and prioritized objectives. In this study, we kept the hard constraints, reflecting the clinical requirements and modified the objective priorities and goals. The approach, elaborated below, assures plan acceptability and is a straightforward method, making it relevant for introduction in the clinic. The final goal of this procedure is twofold. We want to reveal whether there is any space to irradiate and cover more MDEs outside of the PTV, without exceeding hard constraints, and to find out the trade-offs that need to be made in OAR doses when irradiating a larger MDE volume. Several approaches were investigated with different priorities of increasing MDE coverage versus sparing OARs surrounding the PTV.

Plans were performed for 5 SBRT patients, aiming to explore possibilities for clinically usable approaches in a pilot study. For definitive conclusions more patients need to be included.

Using prioritized optimization as a method to improve MDE coverage as a replacement for the current CTV margin definition, we want to directly optimize on the GTV. Therefore, the CTV is neglected. Contrary to previous studies, we also include the PTV margin before optimizing for the MDE uncertainties. With this choice, variations in patient set-up and anatomy are decoupled from uncertainties in MDEs.

4.1.1. iCycle wish-list construction

For prioritized optimization, the starting point was the prostate wish-list that reflects the clinical protocol previously developed at the Erasmus MC [38]. Wish-lists were already introduced in section 2.4.2, table 4.1 shows the wish-list used for this project. Included in the table are priorities of the objectives, the name of the structures, whether there is minimization or maximization of the objective function, and which type of cost function is used linear, LTCP, EUD or mean.

- Linear: The linear function tries to either provide a point-wise minimum for the dose, with cost function $f(x) = min(d(x))$, or a point-wise maximum, $f(x) = max(d(x))$
- LTCP: The LTCP is the logarithm of the TCP. Taking the log of the TCP reduces computational complexity, yielding a convex optimization problem. Minimization of the LTCP aims at reducing the underdosed volume inside the PTV.
- EUD: in the 'Equivalent Uniform Dose' cost function, voxel doses are weighted according to the k-parameter. E.g. k=1 corresponds to the Dmean, while for k=20, as defined in our wish-list, the optimizer focuses on reduction of the high doses. The formula for the cost function is

$$f(x) = \frac{1}{k}\sum_{i=1}^{k} d_i(x) \tag{4.1}$$

- Mean: By minimizing the mean as an objective, the mean dose to the specified structures will be reduced.

Priority	Structure	Min/Max	Type	Goal	Parameters
Constraint	PTV	Minimize	linear	61.5	
Constraint	Rectum	Minimize	linear	36.5	
Constraint	Rectum Mucosa	Minimize	linear	27	
Constraint	Rectum_Dummy	Minimize	linear	38	
Constraint	UrethraPlan	Minimize	EUD	39	3
Constraint	UrethraPlan	Minimize	linear	50	
Constraint	Bladder_Dummy	Minimize	linear	41.8	
Constraint	Bladder	Minimize	linear	39.5	
Constraint	Bladder_Dummy2	Minimize	linear	41.8	
Constraint	ring2cm-external	Minimize	linear	20	
Constraint	Shell3mm	Minimize	linear	38	
Constraint	Shell3cm	Minimize	linear	20	
Constraint	Smoothing 1st	Minimize	linear	10*A	
Constraint	Smoothing 1st	Minimize	linear	-10*A	
Constraint	Smoothing 2nd	Maximize	quadratic	0.6*0.6*10*A*A	
Constraint	Rectum	Minimize	EUD	28	20
Constraint	Bladder	Minimize	EUD	30.7	20
1	PTV	Minimize	LTCP	0.2	37, 0.9
2	PTV	Minimize	LTCP	2.2	57, 0.07
3	Rectum	Minimize	EUD	0	20
4	Bladder	Minimize	EUD	0	20
5	Rectum	Minimize	mean	0	
6	Bladder	Minimize	mean	0	
7	Shell 2 cm	Minimize	linear	30	

Table 4.1: Wish-list to optimize SBRT dose plans of a prostate patient. This wish-list is the starting point for the generation of new treatment plans steering MDE coverage. A is equal to the prescribed tumor dose dose, 38 Gy.

By treatment plan optimization based on this wish-list, the optimizer first minimizes the underdosed volume in the PTV and ensures PTV coverage (priorities 1 and 2). Next, it reduces the high doses in the rectum and bladder as much as possible (priorities 3 and 4). After, it minimizes the mean dose in both OARs (priorities 5 and 6). At last, it tries to reduce the dose and improve the conformality of the dose distribution with the shell 2 cm objective (priority 7). While optimizing these aspects, constraints are always active to fulfill the clinical requirements (table 2.1).

Most constraints used in the wish-list directly reflect the clinical protocol. Some additional structures were automatically created to help the optimizer to control different aspects of the dose distribution better, i.e., the rectum dummy structure improves control of the high doses to the rectum. Three extra constraints, called smoothing, are used to control the complexity of the delivery of the dose distribution (smoothing 1st limits the variation that a beamlet can have compared to the adjacent ones while smoothing 2nd controls the overall homogeneity of the fluence map).

Below, various wish-lists are discussed with changes in objective functions to promote dose delivery to MDEs. Mostly, the constraints were not changed. For two wish-lists, two constraints were converted into objectives. For all alternative wish-lists, only the part with the objective functions was reported.

4.1.2. Plan generation for MDE coverage improvement

With the developed plan generation for steering MDE coverage, we investigated different trade-offs between OAR and MDE doses. For all studies, objective functions for enhancing MDE coverage were added to the wish-list. For delivery of doses to the MDE volume, we investigated two scenarios:

1. **MDE coverage with 25 Gy up to 12 mm**
   For the first scenario, we aimed to maximize voxel doses in the region up to 12 mm from the PTV to receive preferentially an EQD_2 of 55 Gy. We assumed an EQD_2 of 55 Gy as a sufficient dose level for MDEs [26] [29] [30]. To translate the EQD_2 of 55 Gy into a fraction dose, d, in our specific fractionation scheme, we used the following formula:

   $$EQD_2 = N_f \cdot d \cdot \left(\frac{d + (\alpha/\beta)}{2 + (\alpha/\beta)}\right) \tag{4.2}$$

   With $N_f = 4$ and α/β=1.5, as commonly used for prostate tumor cells [39]. An EQD_2 of 55Gy, results in a total dose of 25 Gy in our treatment plans.

   Three expansion structures, of 5, 5-8 and 8-12 mm, were created surrounding the PTV. This was based on findings by Davis et al. [4], Sohayda et al [20], Teh et al. [12] [21] and Schwartz et al. [22] (see section 3.1.1). Instead of taking a single expansion of 12 mm, creating 3 separate structures allowed for more refined steering of MDE coverage at different distances from the PTV. The volume subdivisions into 5, 5-8 and 8-12 mm are referred to as the expansion 5, expansion 5-8 and expansion 8-12, respectively.

2. **MDE coverage with 38 Gy up to 5 mm**
   For the second scenario, only the expansion of 5 mm (expansion 5) was used for enhancing dose outside the PTV. Instead of maximizing the dose up to 25 Gy, the dose was optimized to the prescribed dose of 38 Gy (same as used for PTV). Here the MDE volume should receive the prescribed dose, based on the suggestion from the article of Chao et al. [23], where they conclude that for patients with a high risk of MDEs the CTV margin should be expanded.

Depending on the priorities allocated to the MDE objective functions, different compromises between MDE coverage and dose delivery to OARs can be made during plan optimization. Several wish-lists were generated to explore a range in trade-offs. Because the treatment plans should be clinically acceptable, PTV objectives always kept the highest priority. Below descriptions of plans generated with various wish-lists are given. Most of them are used for both MDE coverage up to 12 mm with 25 Gy and MDE coverage up to 5 mm with 38 Gy, unless commented.

- **Orig (Original)**
  This was the plan without any modification made to the wish-list as presented in table 4.1.

- **MDEvsNothing (MDE versus Nothing)**
  The intention was to enhance MDE coverage without sacrificing other objectives. To do so, the MDE objective was added at the lowest priority to the wish-list (see table 4.2). Contrary to Orig, goal values for the bladder and rectum EUD and mean were set per patient (Set PP); parameter values obtained in Orig plans were used as goal values. By replacing the original goal values of 0 (table 4.1) by these new goals, we made sure that if there was any space created, the optimizer would use it for improving MDE coverage and not for further improvement of rectum and bladder doses.

- **MDEvsLHD (MDE versus Low and High (OAR) Doses)**
  These plans investigate the MDE trade-off with OAR Low and High Doses (LHD). The OAR EUD and mean objectives (high and low dose minimization) were moved to a lower priority, after MDE coverage objectives (table 4.2).

- **MDEvsHD (MDE versus High (OAR) Doses)**
  The plan investigates MDE trade-off with OAR High Doses (HD). The OAR EUD objectives (i.e. high doses optimization) are moved to a lower priority, after OAR mean dose and MDE coverage objectives (table 4.2).

- **MDEvsLD (MDE versus Low (OAR) Doses)**
  The plans investigate MDE trade-off with OAR Low Doses (LD). The OAR mean objectives were moved to a lower priority, after OAR high dose and MDE coverage objectives (table 4.2).

- **MDEvsLHDpartially (MDE versus Low and High (OAR) Doses partially)**
  The plans investigate a partial trade-off between MDE coverage and both OAR Low and High doses (LHDpartially). With the previous wish-lists, the OAR doses were either optimized towards their goal values, when having higher priorities than the MDE objective or worsened as much as necessary to maximize MDE coverage, when having lower priorities. With this wish-list, intermediate plans were generated, where OAR doses was worsened to improve MDE coverage, but in a controlled way. To this purpose, OAR objectives were kept at high priorities, but their goal values were relaxed. This was done to leave space for MDE coverage optimization that had a lower priority. EUD values were multiplied by a factor x = 1.05, while x = 2 was used for mean values for MDE coverage up to 12 mm (see table 4.2).

- **MDEvsDD (MDE vs Dose Distribution)**
  The plans investigate MDE trade-off with the Dose Distribution (DD). The dose distributions generated with the wish-lists as introduced above are conformal, enforced mainly by the shell constraints. By switching them off as constraints and including them as objectives with the lowest priority, space was created for improving on other objectives (see table 4.2).

- **MDEvsLHD+DD (MDE vs Low and High (OAR) Doses and Dose Distribution)**
  The plans investigate MDE trade-off with the OAR Low and High (OAR) Doses and the Dose Distribution (DD). The plan was evaluated for MDE coverage up to 5 mm with 38 Gy only, due to limitations of the other plans for coverage with 38 Gy (further discussed in the results section).

MDEvsNothing

Priority	Structure	Min/Max	Type	Goal value
3	*Rectum*	Min	EUD	Set PP
4	*Bladder*	Min	EUD	Set PP
5	*Rectum*	Min	Mean	Set PP
6	*Bladder*	Min	Mean	Set PP
7	*Expansion5*	Max	Linear	25
8	*Expansion5-8*	Max	Linear	25
9	*Expansion8-12*	Max	Linear	25

MDEvsLHD

Priority	Structure	Min/Max	Type	Goal value
3	*Expansion5*	Max	Linear	25
4	*Expansion5-8*	Max	Linear	25
5	*Expansion8-12*	Max	Linear	25
6	*Rectum*	Min	EUD	Set PP
7	*Bladder*	Min	EUD	Set PP
8	*Rectum*	Min	Mean	Set PP
9	*Bladder*	Min	Mean	Set PP

MDEvsHD

Priority	Structure	Min/Max	Type	Goal value
3	*Rectum*	Min	Mean	Set PP
4	*Bladder*	Min	Mean	Set PP
5	*Expansion5*	Max	Linear	25
6	*Expansion5-8*	Max	Linear	25
7	*Expansion8-12*	Max	Linear	25
8	*Rectum*	Min	EUD	Set PP
9	*Bladder*	Min	EUD	Set PP

MDEvsLD

Priority	Structure	Min/Max	Type	Goal value
3	*Rectum*	Min	EUD	Set PP
4	*Bladder*	Min	EUD	Set PP
5	*Expansion5*	Max	Linear	25
6	*Expansion5-8*	Max	Linear	25
7	*Expansion8-12*	Max	Linear	25
8	*Rectum*	Min	Mean	Set PP
9	*Bladder*	Min	Mean	Set PP

MDEvsLHDpartially

Priority	Structure	Min/Max	Type	Goal value
3	*Rectum*	Min	EUD	Set PP*1.05
4	*Bladder*	Min	EUD	Set PP*1.05
5	*Rectum*	Min	Mean	Set PP*2.0
6	*Bladder*	Min	Mean	Set PP*2.0
7	*Expansion5*	Max	Linear	25
8	*Expansion5-8*	Max	Linear	25
9	*Expansion8-12*	Max	Linear	25

MDEvsDD

Priority	Structure	Min/Max	Type	Goal value
3	*Rectum*	Min	EUD	Set PP
4	*Bladder*	Min	EUD	Set PP
5	*Rectum*	Min	Mean	Set PP
6	*Bladder*	Min	Mean	Set PP
7	*Expansion5*	Max	Linear	25
8	*Expansion5-8*	Max	Linear	25
9	*Expansion8-12*	Max	Linear	25
10	*Shells*	Min	Linear	0

Table 4.2: Objective functions of the prostate wish-lists for MDEvsNothing, MDEvsLHD, MDEvsHD, MDEvsLD, MDEvsLHDpartially and MDEvsLHD. Set PP refers to Set Per Patient. The goal values were predefined from the outcome of corresponding Orig plans. In orange are changes relative to the wish-list in table 4.1. As mentioned above, constraints were the same as used for the Orig plans (table 4.1).

4.1.3. Treatment plan evaluation

Several methods were used for the evaluation of the generated plans.

Dosimetric parameters

The dosimetric parameters that were evaluated in this study are listed in table 4.3. These parameters included the clinical requirements, other commonly reported values to evaluate the dose distribution and some new parameters relevant for this study.

Underdosed volume graphs

A second method used to compare dose delivered to the MDE volume is by the “underdosed MDE volume” graph. For these graphs, the volume around the PTV was sampled in expansion volumes with 1 mm thickness. The expansion at 1 mm contained all voxels between 0 and 1 mm from the PTV, etc. The underdosed MDE volume was plotted for all the expansion structures created, ranging from 1 to 12 mm distance from the PTV.

Dose Volume Histograms

The third method of treatment plan evaluation and comparison was by inspection of DVHs. These histograms can be used to structure-wise compare the dose delivered with different dose plans (see section 2.4.2 for more background information).

Dose distributions

As last evaluation tool, the (relevant) dose distributions are provided. The dose distributions show important OARs and target structures and provide the isodose areas for 10, 25 and 38 Gy (volumes receiving a dose starting at 10, 25, or 38 Gy, respectively).

Structure	Parameter
Expansion	*expansion 5 V<25Gy*
	expansion 5 V<38Gy
	expansion 5-8 V<25Gy
	expansion 8-12 V<25Gy
	expansion 5 D98%
	expansion 5-8 D98%
	expansion 8-12 D98%
	PTV expansion (ring) fully covered by 25 Gy
Patient	*V10Gy*
	V20Gy
	V30Gy
PTV	*V38Gy*
	Dmean
Prostate	*Dmin*
Rectum	*D0.03cc*
	D1cc
	V27Gy
	V18.2Gy
	Dmean
Bladder	*D0.03cc*
	D1cc
	Dmean
Urethra	*D50%*
	D10%
	D5%

Table 4.3: Overview of the parameters used for plan evaluations. The expansion parameters are for either for both 12mm/25 Gy and 5mm/38 Gy approach (black), for the 12mm/25 Gy approach (blue) or for the 5mm/38 Gy approach (orange). V<25Gy and V<38Gy represent the expansion volumes receiving a dose <25 and <38 Gy, respectively and D98% are near-minimum doses: 98% of the structure gets a higher dose. PTV expansion (rings) fully covered by 25 Gy represents the distance up to where the full volume is covered by a dose of 25 Gy. The patient parameters V10Gy, V20Gy, V30Gy represent the patient volumes receiving dose of >10, >20 and >30 Gy, respectively. V18.2Gy and V27Gy for the rectum correspond to EQD2's of 40 and 60 Gy.

4.2. Results

In this section, the results of the prioritized optimization approach will be discussed. The first section starts with the results of using prioritized optimization for MDE coverage up to 12 mm. Followed by the results for MDE coverage up to 5 mm. Graphical representations provide information of one example patient out of the five evaluated patients (similar for all figures). This patient was randomly selected. Unless commented, the results of other patients showed similar behaviour as the example patient.

4.2.1. MDE coverage up to 12 mm with 25 Gy

Orig

For the plans made with the Orig wish-list, part of the MDE volume was already covered by 25 Gy (figures 4.1 , 4.2, and 4.3). This was due to the unavoidable finite dose fall-off resulting from delivery of 38 Gy at the PTV border. However, this was only a significant for expansion 5; V<25Gy of expansions 5, 5-8, and 8-12 were 14.4% (9.8 cc), 42.9% (25.1 cc) and 64.4% (58.0 cc), respectively (figure 4.2). In figure 4.1 it can clearly be seen that V<25Gy gets worse for distances further from the PTV. The PTV expansion (ring) fully covered with 25 Gy was on average at 1.0 mm (table 4.4).

MDEvsNothing

When adding the MDE objectives behind all OAR objectives to cover more MDE (MDEvsNothing), the plans showed only minor increases in MDE coverage compared to the original plan Orig (figure 4.1 and table 4.4). As intended, this happened without deteriorating the rest of the plan. On average over all patients, the PTV expansion fully covered with 25 Gy increased from 1.0 mm to 1.6 mm. The MDEvs-Nothing plans will be used as reference for the other plan evaluations, discussed below.

	Parameter	Unit	Clinical constraint	Orig	MDEvs Nothing	MDEvs LHD	MDEvs HD
Expansion	*expansion 5 V<25Gy*	%		14.4	14.4	0	14.1
	expansion 5-8 V<25Gy	%		44.6	44.5	0	44.5
	expansion 8-12 V<25Gy	%		64.4	64.2	0.7	63.5
	expansion 5 D98%	Gy		16.5	17.2	26.8	16.5
	expansion 5-8 D98%	Gy		8.2	9	26.3	8.2
	expansion 8-12 D98%	Gy		3.3	3.6	25.5	3.3
	PTV expansion (ring) fully covered by 25 Gy	mm		1	1.6	11.2	1.8
Patient	*V10Gy*	%		5.9	6.1	8.5	6.2
	V20Gy	%		1.2	1.3	1.9	1.3
	V30Gy	%		0.6	0.6	0.6	0.6
PTV	*V38Gy*	%	95.0	95.3	95	94.5	94.8
	Dmean	Gy		46.7	46.7	46.8	46.8
Prostate	*Dmin*	Gy	34.0	36.4	36.3	36.3	35.9
Rectum	*D0.03cc*	Gy	38	33.8	34	34.2	34.9
	D1cc	Gy	32.3	26.7	27.3	30.2	28
	V27Gy	%		1.4	1.6	7.5	1.9
	V18.2Gy	%		5.1	5.5	30.6	5.9
	Dmean	Gy		3.1	3.2	10.1	3.2
Bladder	*D0.03cc*	Gy	41.8	38.8	38.9	38.3	40.7
	D1cc	Gy	38.0	34.6	34.6	34.9	35.9
	Dmean	Gy		5.9	5.8	11.7	5.8
Urethra	*D50%*	Gy	40.0	38.5	38.5	38.5	38.4
	D10%	Gy	42.5	40.5	40.5	40.6	40.7
	D5%	Gy	45.0	41.3	41.1	41.4	41.3

Table 4.4: Population-mean dosimetric parameters for Orig, MDEvsNothing, MDEvsLHD and MDEvsHD plans.

MDEvsLHD

The plans prioritizing MDE coverage above OAR high and low dose objectives (MDEvsLHD) showed significant increases in MDE coverage compared to MDEvsNothing. Up to 12 mm, almost the entire MDE volume was irradiated with at least 25 Gy dose (figures 4.1, 4.2 and table 4.4). The price paid was mainly in the OAR low and medium-high doses as seen in the DVHs in figure 4.2, i.e. the solid/dashed vs the dotted line. On average, the rectum Dmean increased by 6.9 Gy (217%) and the bladder Dmean by 5.9 Gy (100%). The rectum D1cc increased by 2.9 Gy (11%), and the bladder D1cc by 0.3 Gy (0.9%). Large increases were also observed for rectum V18.2Gy and V27 Gy; 25.1% (456%) and 5.9% (369%), respectively.

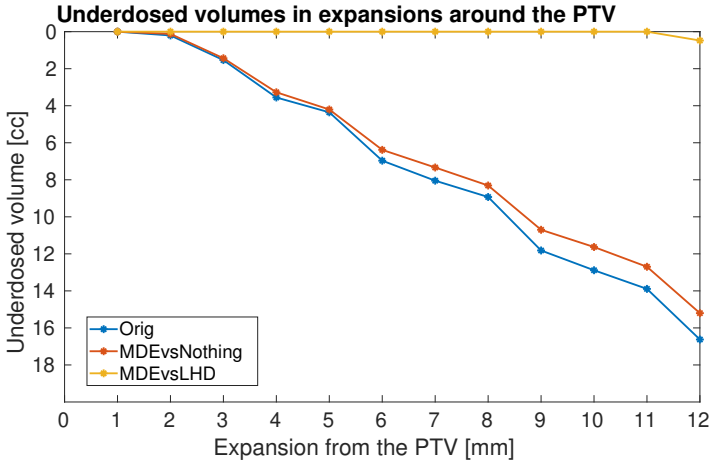

Figure 4.1: Volumes in an example patients, receiving doses <25 Gy in rings around the PTV for Orig, MDEvsNothing and MDEvsLHD plans. The expansion at 1 mm, ring 1, contains voxels at distances for 0-1 mm from the PTV, etc.

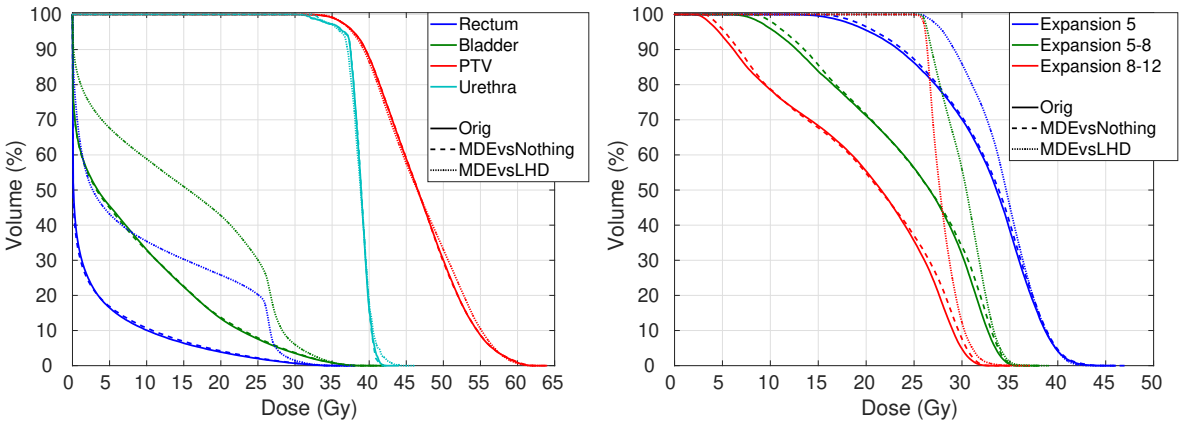

Figure 4.2: DVHs for an example patient for Orig, MDEvsNothing and MDEvsLHD plans.

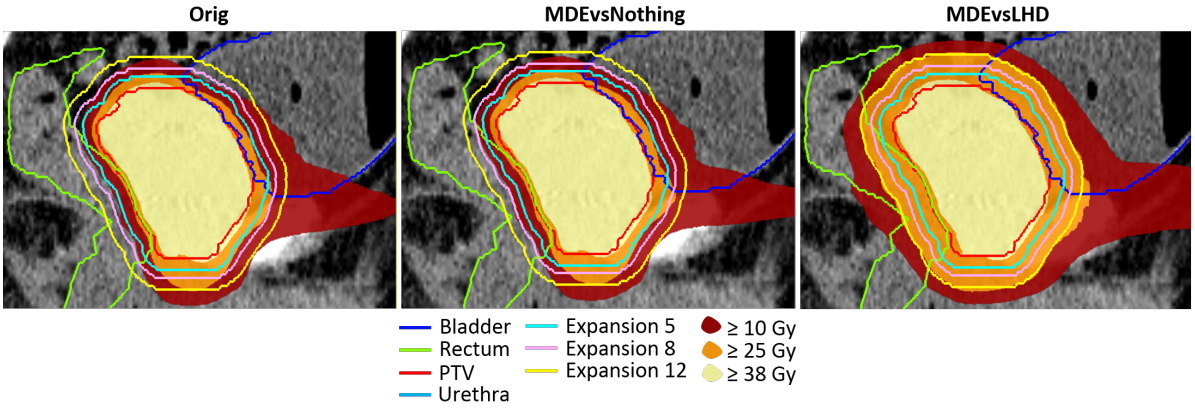

Figure 4.3: Sagittal dose distributions for Orig, MDEvsNothing and MDEvsLHD of an example patient.

MDEvsHD

Lowering the priority of the OAR high doses (MDEvsHD) did only marginally enhance MDE coverage compared to MDEvsNothing. On average, V<25Gy in expansions 5, 5-8 and 8-12 only improved by 0.26% (0.3 cc), 0.01% (0.1 cc) and 0.69% (0.5 cc), see figure 4.4, table 4.4 . Also the PTV and OAR doses remained basically the same (figure 4.5).

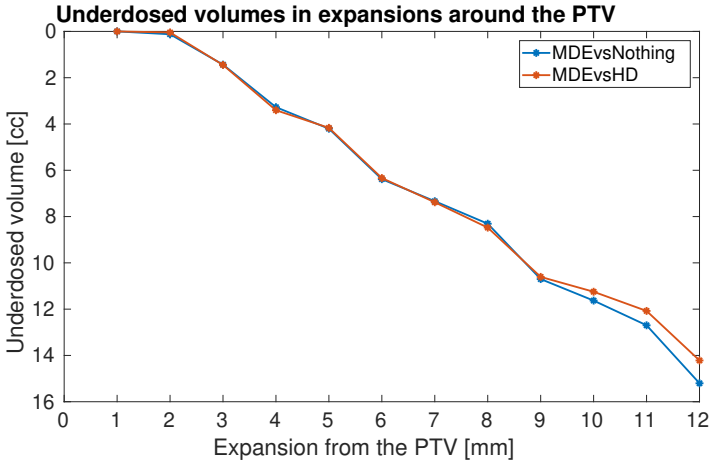

Figure 4.4: Volumes in an example patients, receiving doses <25 Gy in expansions (rings) around the PTV for MDEvsNothing and MDEvsHD plans.

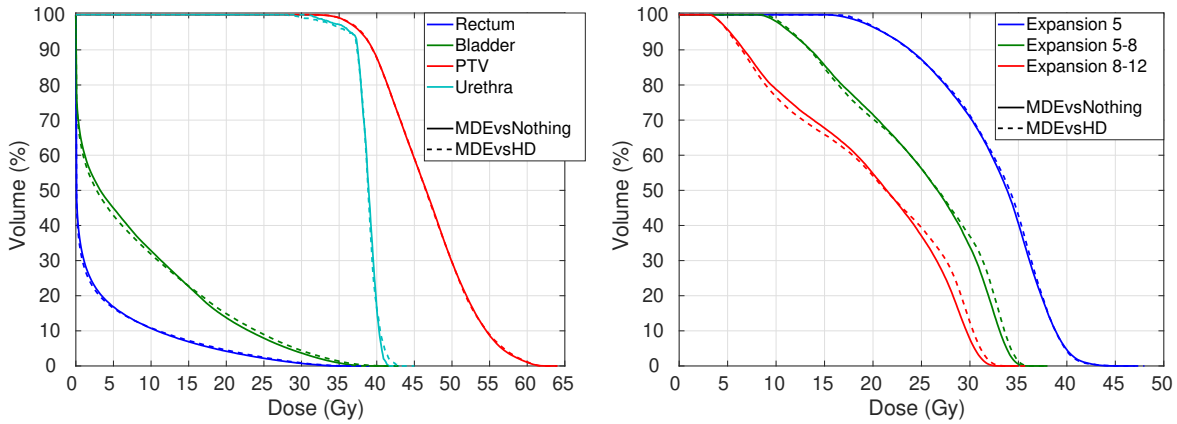

Figure 4.5: DVHs for an example patient for MDEvsNothing and MDEvsHD plans.

MDEvsLD

Giving lower priority to low OAR doses (MDEvsLD), clearly increased MDE coverage compared to MDEvsNothing. The improvement in the underdosed volume is visualized in figure 4.6 and figure 4.7. For expansions 5, 5-8 and 8-12, V<25Gy improved by 84% (8.1 cc), 68% (15.9 cc) and 46% (24.2 cc), respectively (table 4.5). The PTV expansion fully covered with 25 Gy was 3.2 mm, a 200% increase compared to MDEvsNothing. Unfortunately, lowering the priorities for the OAR low dose objectives also led to a clear rise in the rectum and bladder Dmean (figure 4.7). The rectum Dmean increased by 7.1 Gy (224%) and the bladder Dmean by 5.6 Gy (95%). The rectum V18.2Gy increased by 24.6% (427%) and the rectum V27Gy by 1.5% (94%). The increase in the OAR lower doses was also clearly visible in the dose distributions (figure 4.8).

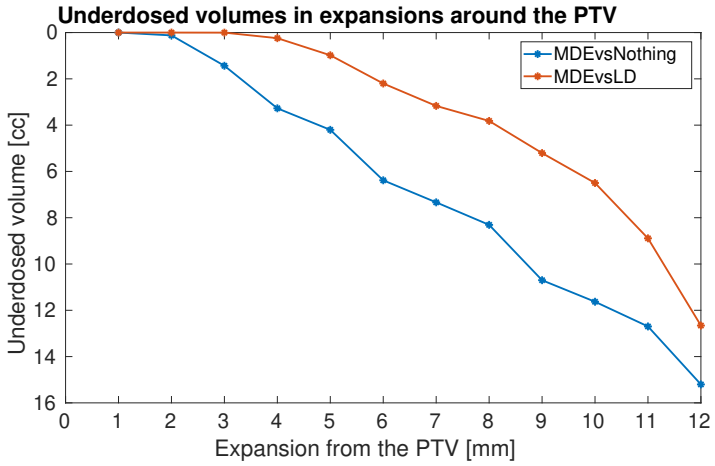

Figure 4.6: Volumes in an example patients, receiving doses <25 Gy in expanions (rings) around the PTV for MDEvsNothing and MDEvsLD plans.

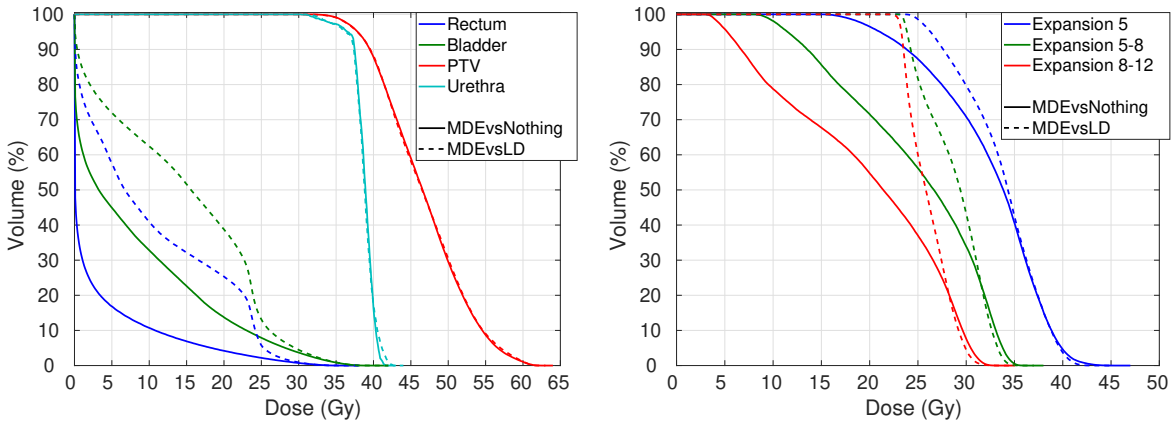

Figure 4.7: DVHs for an example patient for MDEvsNothing and MDEvsLD plans.

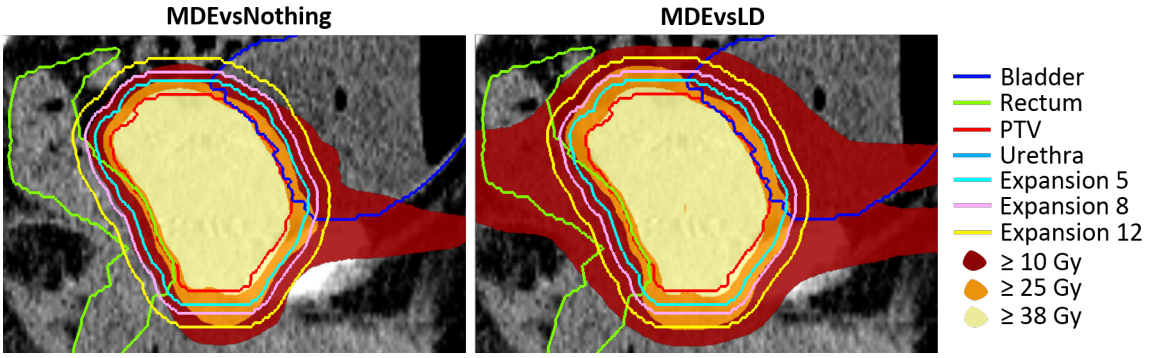

Figure 4.8: Sagittal dose distributions for Orig, MDEvsNothing and MDEvsLHD of an example patient.

MDEvsLHDpartially

For MDEvsLHDpartially, the treatment plans gave up a bit on the high and low doses. The V<25 Gy in expansion 5, 5-8 and 8-12 improved by 99% (9.7 cc), 65% (15.2 cc) and 17% (9.3 cc), compared to MDEvsNothing. Additionally, the PTV expansion fully covered with 25 Gy increased from 1.6 mm to 4.8 mm (table 4.5). Rectum and bladder D1cc were increased by 2.8 Gy (10%), and 1.5 Gy (4.3%), while Dmean values were increased by 3.4 Gy (106%), and 5.1 (89%), respectively. Rectum V18.2Gy and V27Gy increased by 12.2% (222%) and 3.3% (206%).

Compared to MDEvsLD, the V<25Gy of expansion 5 improved by 96% (1.6 cc), but the V<25Gy of expansion 8 and 12 mm worsened by 12% (0.7 cc) and 53% (14.9 cc), respectively, with MDEvsLHDpartially. The improvement in the coverage of expansion 5 V<25 Gy comes at the cost of a higher OAR high doses (table 4.5). On the other hand, the increased underdosage in expansion 8 and 12, V<25Gy, with MDEvsLHDpartially, corresponds to lower OAR Dmean, compared to MDEvsLD (table 4.5 and figure 4.10 and 4.11).

Comparing MDEvsLHDpartially to MDEvsLHD, the V<25Gy for expansion 5,8 and 12 worsened (table 4.5). On the other hand, MDEvsLHDpartially reduced the rectum and bladder Dmean compared to MDEvsLHD, while the high dose (D1cc) was comparable.

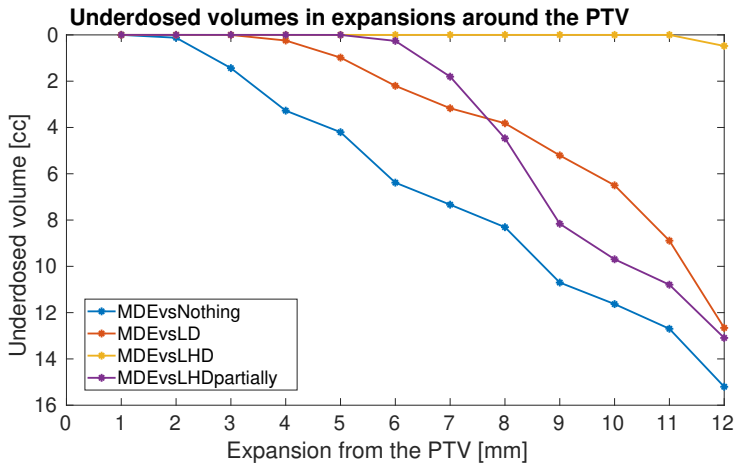

Figure 4.9: Volumes in an example patients, receiving doses <25 Gy in expansions (rings) around the PTV for MDEvsNothing, MDEvsLD, MDEvsLHD and MDEvsLHDpartially.

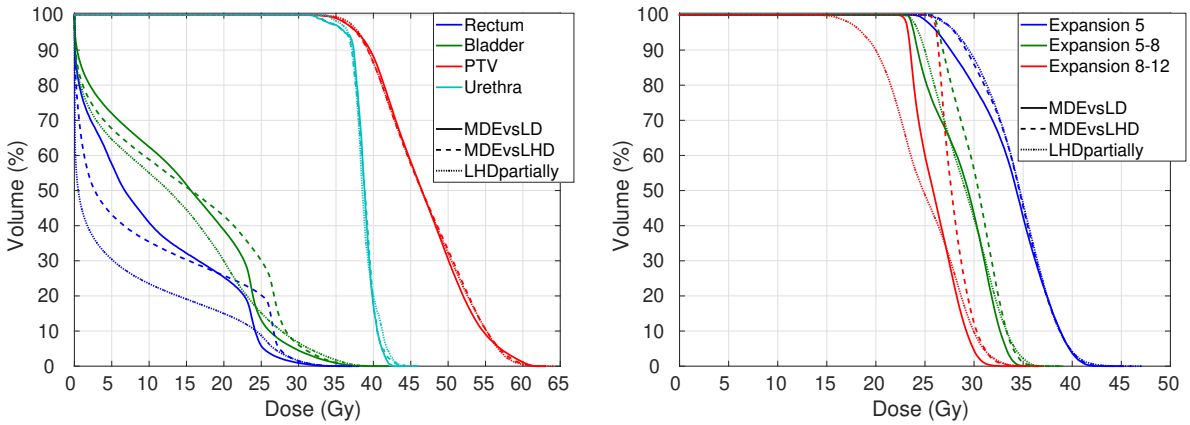

Figure 4.10: DVHs for an example patient for MDEvsLD, MDEvsLHD and MDEvsLHDpartially.

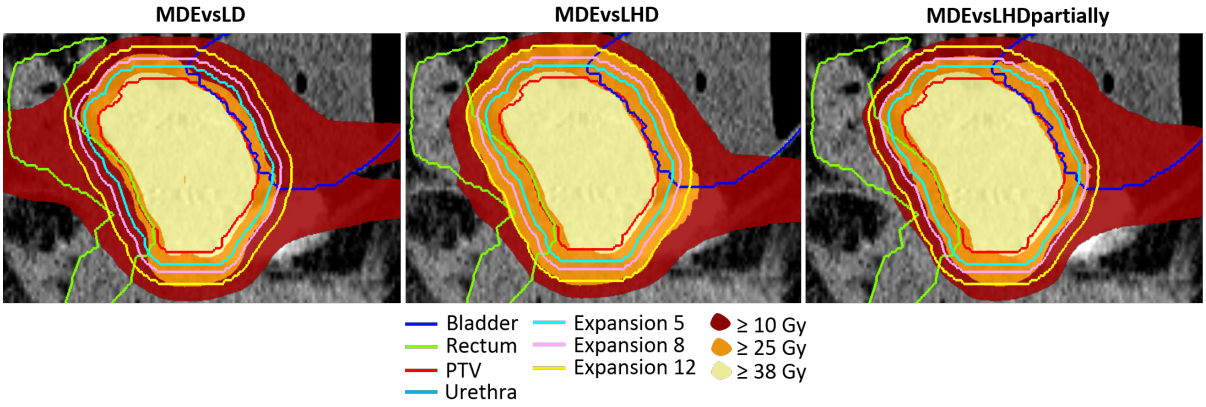

Figure 4.11: Sagittal dose distributions of MDEvsLD, MDEvsLHD, and MDEvsLHDpartially of an example patient.

MDEvsDD

Converting dose distribution constraints into lowest priority objectives, with the MDE objectives just above them, slightly improved the MDE covered at higher distances from the PTV, when compared to MDEvsNothing. However, this did not hold for volumes closer to the PTV boundary. V<25Gy in expansion 5 deteriorated by 2.6% (0.2 cc), and for expansions 5-8 and 8-12 mm V<25Gy improved by 0.4% (2.1 cc) and 21% (11 cc), respectively. The PTV expansion fully covered with 25 Gy remained similar, i.e. 1.6 mm. A higher dose was delivered to the expansion 5, 5-8 and 8-12 with MDEvsDD compared to MDEvsNothing, as visualized in figure 4.14, even if not desired or intended. As expected, no significant changes were observed for OAR doses (figure 4.13 and table 4.5). Giving up on conformality, there is a limited enhancement in the MDE coverage. However, as could be seen in figure 4.14, a huge price is paid regarding dose conformality.

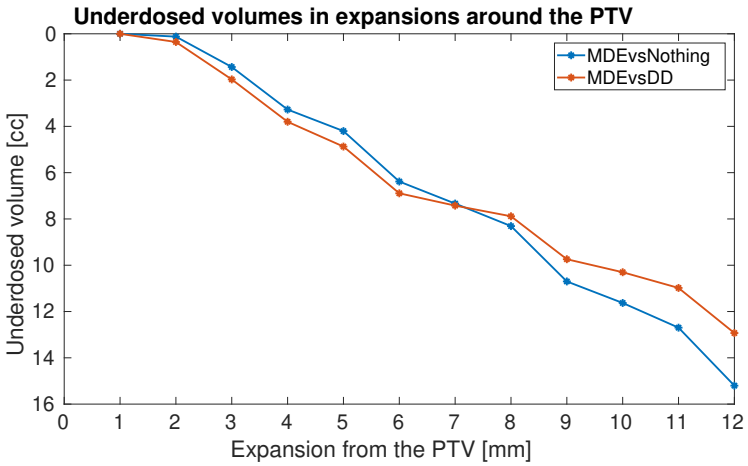

Figure 4.12: Volumes in an example patients, receiving doses <25 Gy in expansions (rings) around the PTV for MDEvsNothing and MDEvsDD.

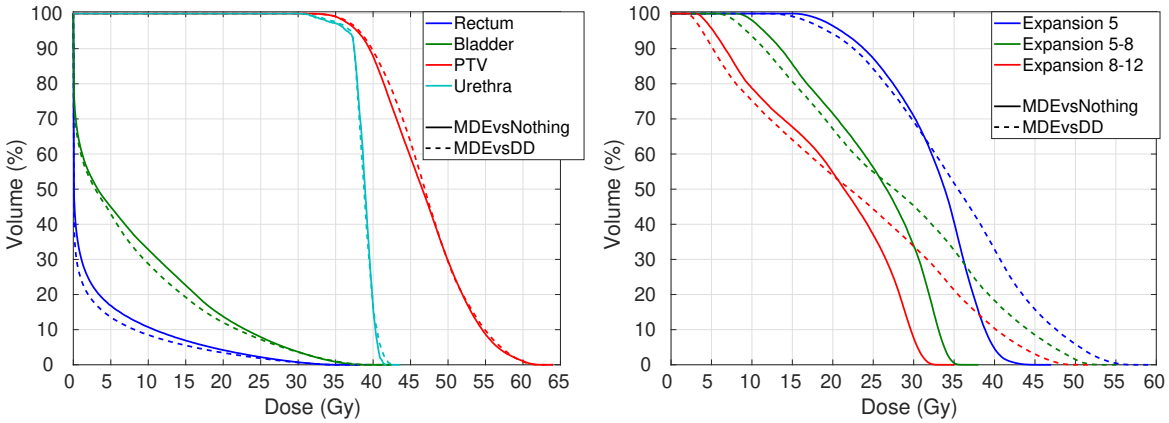

Figure 4.13: DVHs for an example patient for MDEvsNothing and MDEvsDD.

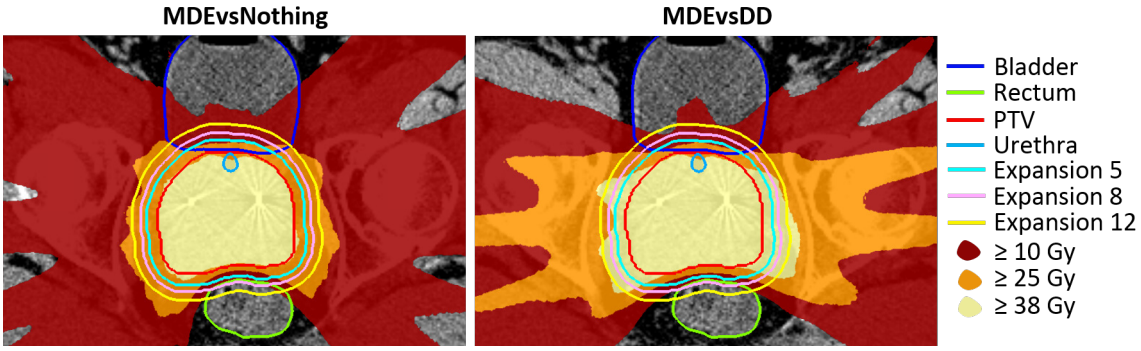

Figure 4.14: Axial dose distributions of MDEvsNothing and MDEvsDD of an example patient.

	Parameter	Unit	Clinical constraint	MDEvs Nothing	MDEvs LD	MDEvs LHDpartially	MDEvs DD
Expansion	*expansion 5 V<25Gy*	%		14.4	2.3	0.1	14.8
	expansion 5-8 V<25Gy	%		44.5	14	15.7	40.7
	expansion 8-12 V<25Gy	%		64.2	34.9	53.4	50.8
	expansion 5 D98%	Gy		17.2	17.2	26.8	17.7
	expansion 5-8 D98%	Gy		9	9	26.3	9.2
	expansion 8-12 D98%	Gy		3.6	3.6	25.5	3.6
	PTV expansion (ring) fully covered by 25 Gy	mm		1.6	3.2	4.8	1.6
Patient	*V10Gy*	%		6.1	7.5	7.2	7
	V20Gy	%		1.3	1.7	1.5	2.1
	V30Gy	%		0.6	0.6	0.6	0.8
PTV	*V38Gy*	%	95.0	95	95.1	95.3	95.4
	Dmean	Gy		46.7	46.7	46.7	47.2
Prostate	*Dmin*	Gy	34.0	36.3	36.4	36.1	36.5
Rectum	*D0.03cc*	Gy	38	34	33.6	34.2	33.9
	D1cc	Gy	32.3	27.3	28.9	30.1	27.5
	V27Gy	%		1.6	3.1	4.9	1.7
	V18.2Gy	%		5.5	30.1	17.7	5.8
	Dmean	Gy		3.2	10.3	6.6	3.1
Bladder	*D0.03cc*	Gy	41.8	38.9	38.6	39.4	38.8
	D1cc	Gy	38.0	34.6	34.8	36.1	34.8
	Dmean	Gy		5.8	11.4	10.9	5.6
Urethra	*D50%*	Gy	40.0	38.5	38.5	38.3	38.5
	D10%	Gy	42.5	40.5	40.6	40.8	40.5
	D5%	Gy	45.0	41.1	41.5	41.6	41.2

Table 4.5: Population-mean dosimetric parameters for MDEvsNothing, MDEvsLD, MDEvsLHDpartially and MDEvsDD plans.

Overview of all dose plans

Figure 4.15 provides an overview of underdosed MDE volumes (V<25Gy) of the seven different treatment plans and of the PTV expansions fully covered with 25 Gy. Figure 4.16 shows corresponding OAR D1cc and Dmean values. Clearly, MDE dose delivery is only substantially enhanced with MDEvsLD, MDEvsLDHpartially and MDEvsLHD, always at the cost of some increases in OAR doses. For MDEvsLD, the rectum and bladder D1cc are hardly enhanced, while for MDEvsLDHpartially, the mean doses are less enhanced than for MDEvsLD and MDEvsLHD.

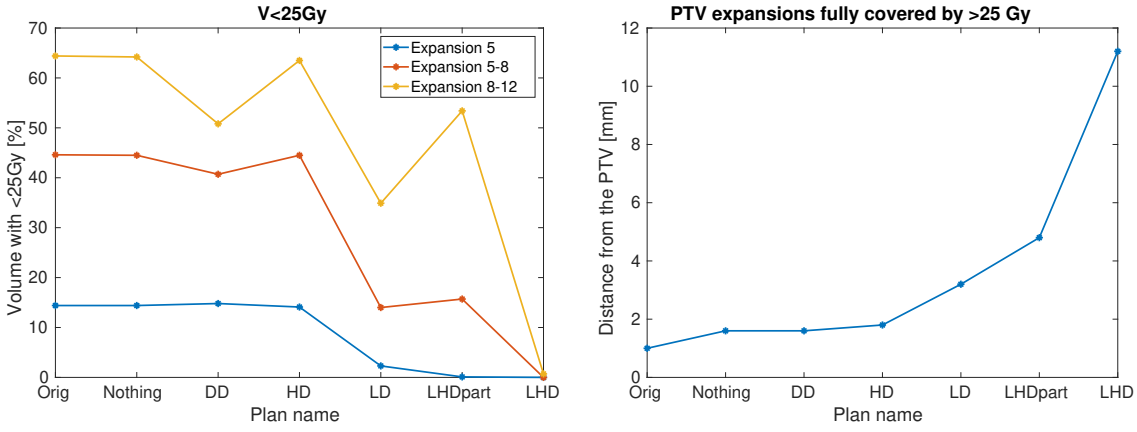

Figure 4.15: Population-mean underdosed MDE volumes (V<25Gy) of the seven different treatment plans on the left and on the right the population-mean of the PTV expansions fully covered with 25 Gy. Names are abbreviated, from left to right: Orig, MDEvsNothing, MDEvsDD, MDEvsHD, MDEvsLD, MDEvsLHDpartially and MDEvsLHD.

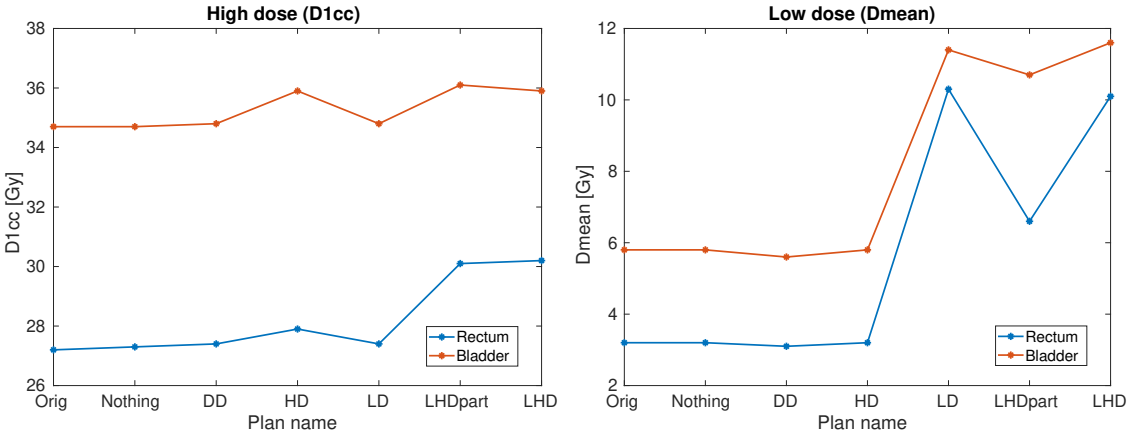

Figure 4.16: Population-mean values of the rectum and bladder D1cc on the left and Dmean on the right in the seven different treatment plans. Names are abbreviated, from left to right: Orig, MDEvsNothing, MDEvsDD, MDEvsHD, MDEvsLD, MDEvsLHDpartially and MDEvsLHD.

4.2.2. MDE coverage up to 5 mm with 38 Gy

The results for MDE coverage up to 12 mm showed that only the MDEvsLHD, MDEvsLD and MDEvsLHDpartially plans (almost) covered the volume up to 5 mm from the PTV edge with a dose of 25 Gy. Therefore, those were the only ones promising for being able to deliver dose up to 38 Gy. Apart from these plans, Orig, MDEvsNothing, and MDEvsLHD+DD plans were generated. For all plans except for Orig and MDEvsNothing, the constraint value of the Shell 3 mm was increased from 38 Gy to 42 Gy, to not upfront restrict delivery of 38 Gy in expansion 5. This is denoted by a '+' behind the plan names. (Orig+ is the original plan, but with the constraint of the shell 3 mm set to 42 Gy, etc.). PTV expansions every 1 mm from the PTV were found to be less informative for MDE coverage up to 5 mm. The near-minimum dose, $D_{98\%}$ in expansion 5 is reported instead of the PTV expansion with full coverage with 38 Gy. Doses in expansions 5-8 and 8-12 are not reported here.

Orig

In the original plans, a significant part of expansion 5 was already covered with 25 Gy as previously seen, but a negligible part is covered by 38 Gy, as visible in figures 4.17 and 4.18. V<25Gy in expansion 5 was on average 13.4%, but V<38Gy was 85.5% (table 4.6). The $D_{98\%}$ was 16.9 Gy, so rather far from the aimed 38 Gy.

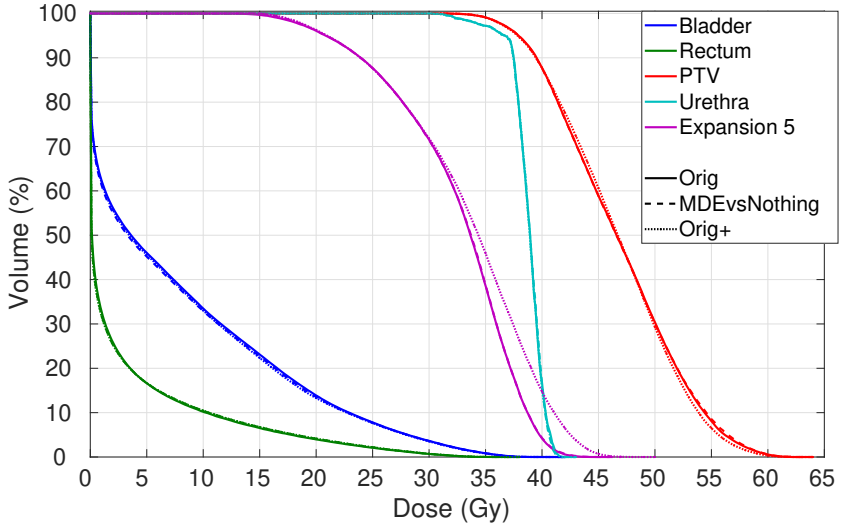

Figure 4.17: DVHs for an example patient for Orig, MDEvsNothing.

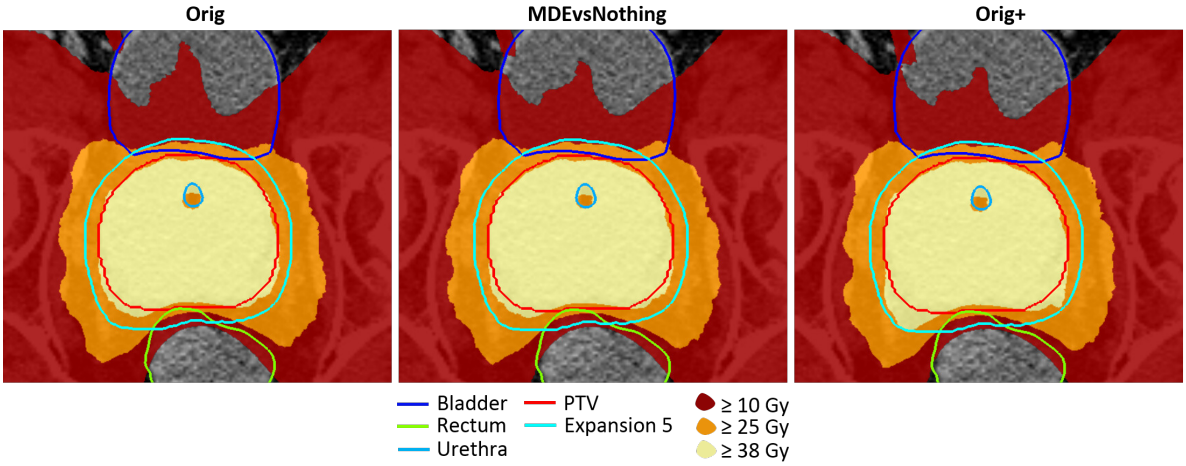

Figure 4.18: Axial dose distributions of Orig, MDEvsNothing and Orig+ of an example patient.

MDEvsNothing

By only adding an MDE objective at the lowest priority, no significant differences were visible compared to Orig (see figures 4.17 and 4.18).

Orig+

Increasing the constraint value of the shell 3 mm from 38 Gy to 42 Gy in Orig, resulting in the Orig+ wish-list, allowed to reduce V<38Gy of expansion 5 from 85.5% to 75.4% (see table 4.6). V<25Gy remained basically the same, as visible in figure 4.17. The effect of increasing the constraint value from 38 to 42 is also well visualized in the dose distributions in figure 4.18; PTV dose conformality closely around the 3 mm shell decreased. The impact is most evident in the volume close to the rectum.

	Parameter	Unit	Clinical constraint	Orig	MDEvs Nothing	Orig+	MDEvs LHD+
	expansion 5 V<25Gy	%		13.4	13.7	13.7	0.9
Expansion	*expansion 5 V<38Gy*	%		85.5	86.2	75.4	71.6
	expansion 5 D98%	Gy		16.9	17.1	17.3	25.6
Patient	*V10Gy*	%		5.8	5.8	5.9	6.5
	V20Gy	%		1.2	1.2	1.2	1.4
	V30Gy	%		0.6	0.5	0.6	0.6
PTV	*V38Gy*	%	95.0	95.2	94.9	94.9	94.7
	Dmean	Gy		46.7	46.7	46.6	46.6
Prostate	*Dmin*	Gy	34.0	36.5	36.3	36.4	36.1
Rectum	*D0.03cc*	Gy	38.0	33.9	34.1	34.1	34.1
	D1cc	Gy	32.3	26.9	27.3	27.4	30.2
	V27Gy	%		1.5	1.6	1.7	4.5
	V18.2Gy	%		5.2	5.5	5.6	15.9
	Dmean	Gy		3.2	3.2	3.2	6.1
Bladder	*D0.03cc*	Gy	41.8	38.8	38.9	38.7	37.9
	D1cc	Gy	38.0	34.6	34.6	34.6	34.9
	Dmean	Gy		6	5.9	5.8	7.3
Urethra	*D50%*	Gy	40.0	38.5	38.5	38.5	38.4
	D10%	Gy	42.5	40.5	40.5	40.5	40.7
	D5%	Gy	45.0	41.2	41.1	41.1	41.6

Table 4.6: Population-mean dosimetric parameters for Orig, MDEvsNothing, Orig+ and P-MDEvsLHD+ plans.

MDEvsLHD+

Adding the MDE objective at the highest priority, V<25Gy and V<38Gy clearly improved relative to orig (figure 4.19). The $D_{98\%}$ in expansion 5 increased by 8.7 Gy (51%), to a value of 25.6 Gy (table 4.6). The improved MDE coverage was mainly at the cost of OAR Dmean values(figure 4.19). The rectum and bladder Dmean increased by 2.9 Gy (89%) and 1.3 Gy (22%), respectively, compared to Orig. Figure 4.20 clearly shows the increases in both the volume coverage and Dmean values in the OARs.

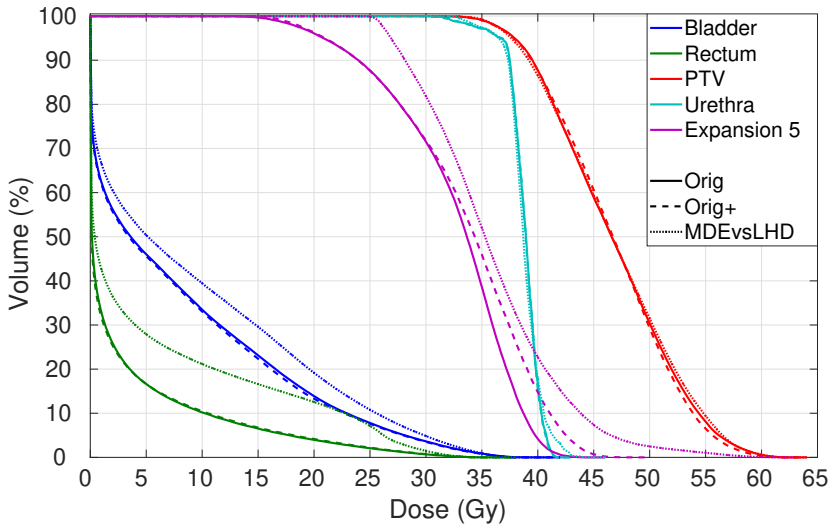

Figure 4.19: DVHs for an example patient for Orig, Orig+ and MDEvsLHD+ plans.

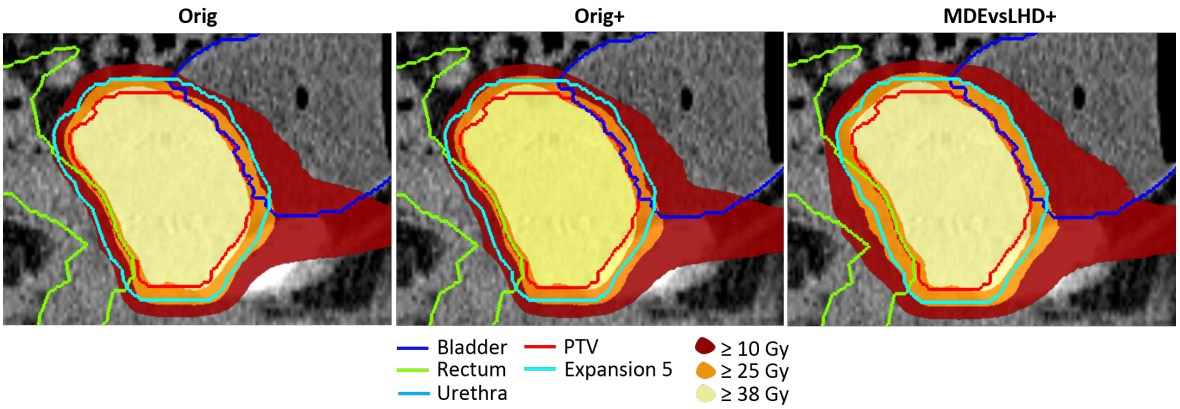

Figure 4.20: Sagittal dose distributions of Orig, Orig+ and MDEvsLHD+ of an example patient.

MDEvsLD+

Giving up on the low doses only in MDEvsLD+, V<25Gy reduced on average from 13.4% to 5.2% and V<38Gy from 85.5 to 70.2% compared to Orig. There also was a 6.8 Gy (40%) increase in the $D_{98\%}$ to a value of 23.7 Gy (table 4.7). Lowering the OAR mean dose objective priorities did not only lead to improved MDE coverage, but also to notable increases in the bladder and rectum Dmean, of 3.1 Gy (94%) and 1.1 Gy (19%), respectively (see also figure 4.21).

Compared to MDEvsLD+, MDEvsLHD+ improved the V<25Gy (477%), the D98% (1.9 Gy), with comparable V<38Gy (see figure 4.21, table 4.7). This came at the cost of enhanced OAR high doses and slightly lower OAR Dmean values as also visible in figure 4.21 and in the dose distribution in figure 4.22.

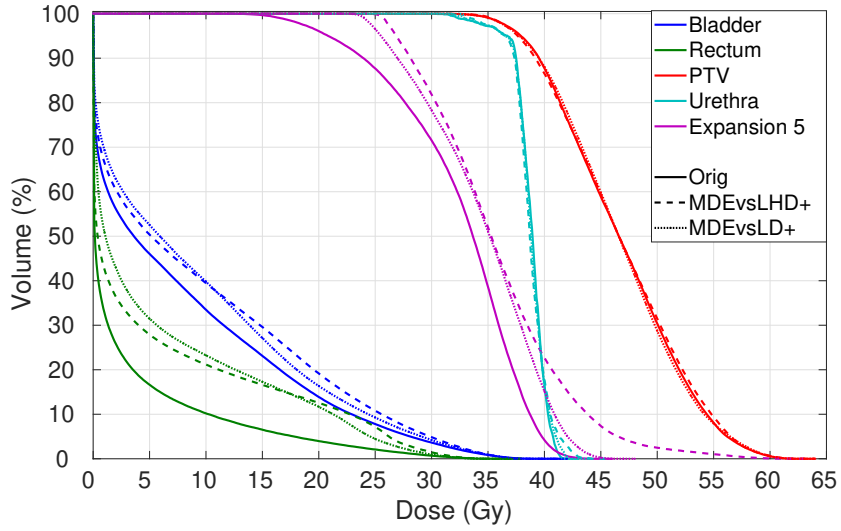

35

Figure 4.21: DVHs for an example patient for Orig, MDEvsLHD+ and MDEvsLD+ plans.

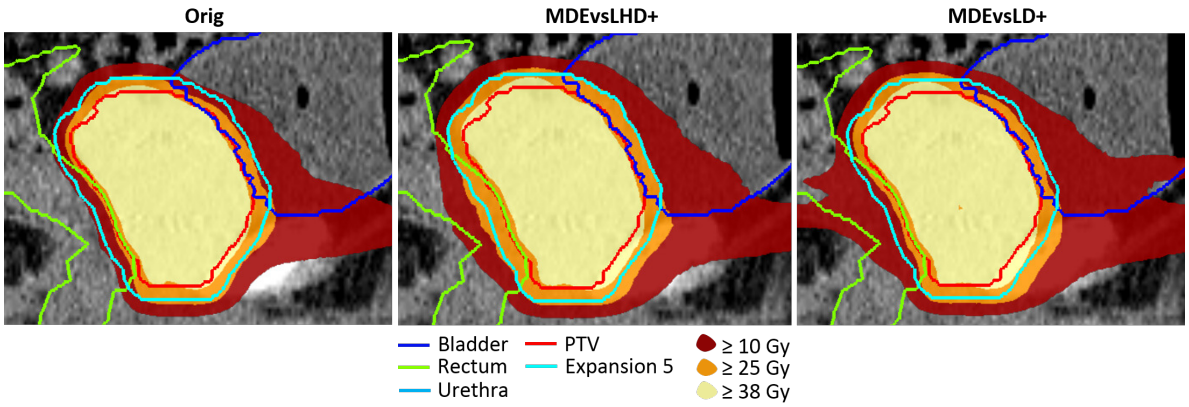

Figure 4.22: Sagittal dose distributions for Orig, MDEvsLHD+ and MDEvsLD+ plans of an example patient.

MDEvsLHDpartially+
MDEvsLHDpartially+ improved the V<25Gy and V<38Gy by 46% and 8.1%, respectively, compared to Orig. $D_{98\%}$ increased with 5.4 Gy (32%) to a value of 22.5 Gy. Both D1cc and Dmean values in rectum and bladder deteriorated. D1cc in the rectum and bladder increased with 2.3 Gy (8.4%) and 0.6 Gy (1.7%), respectively. The rectum Dmean increased by 1.6 Gy (50%), the bladder Dmean by 0.4 Gy (6.8%) (table 4.7).

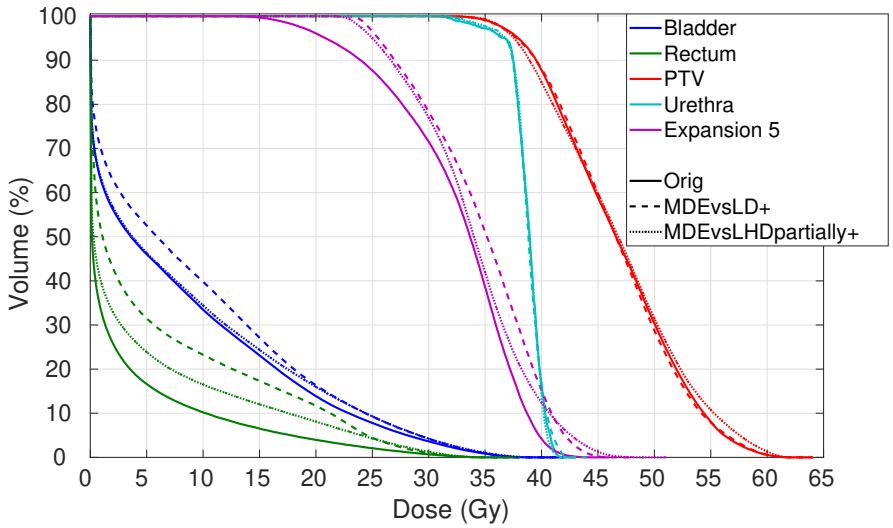

Figure 4.23: DVHs for an example patient for Orig, MDEvsLD+ and MDEvsLHDpartially+.

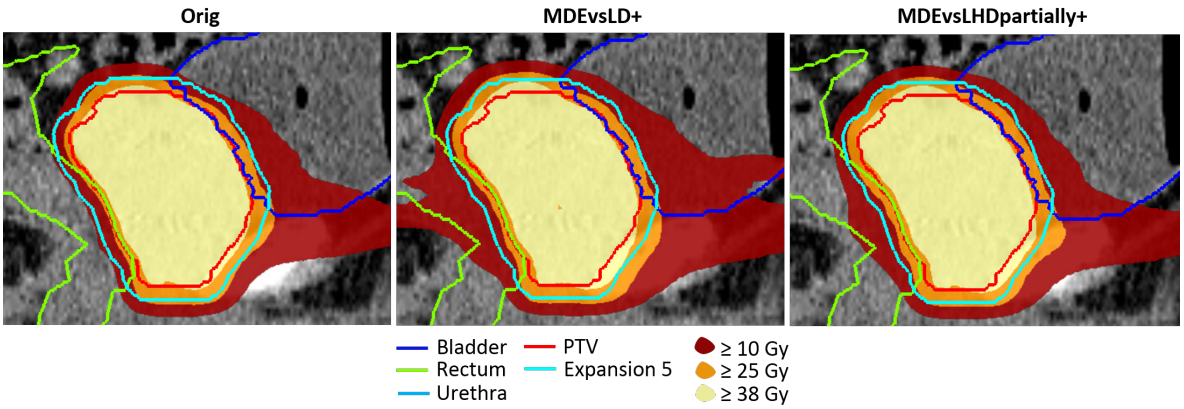

Figure 4.24: Sagittal dose distributions for Orig, MDEvsLD+ and MDEvsLHDpartially+ of an example patient.

MDEvsLHD+DD

By abandoning both low and high OAR doses as well as the dose distribution with MDEvsLHD+DD, the V<38Gy improved by 37% and 24% compared to Orig and MDEvsLHD, respectively. This improvement can also be seen in the DVH in figure 4.25 and the dose distribution in figure 4.26, especially in the areas where the OARs are not physically present.

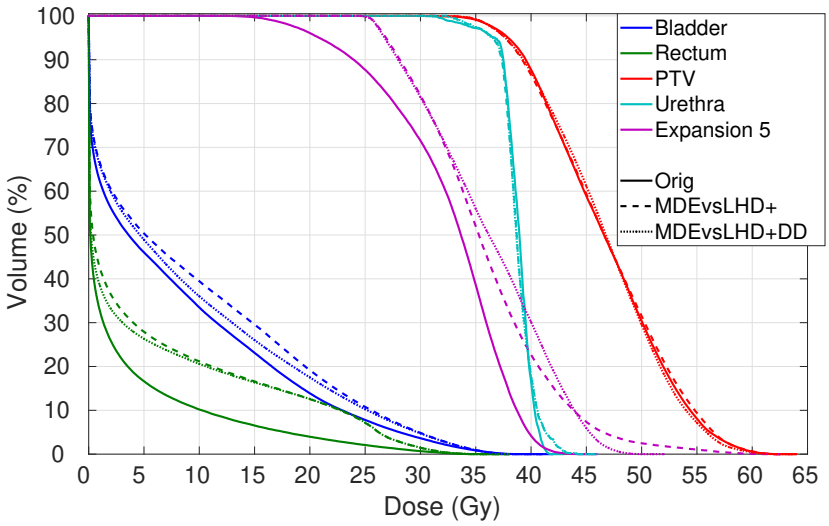

Figure 4.25: DVHs for an example patient for Orig, MDEvsLHD+ and MDEvsLHD+DD.

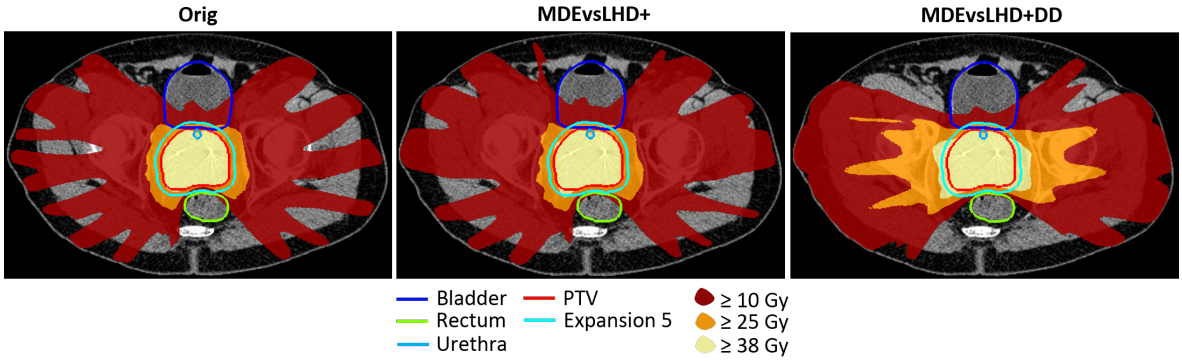

Figure 4.26: Axial dose distributions of Orig, MDEvsLHD+ and MDEvsLHD+DD of an example patient.

	Parameter	Unit	Clinical constraint	Orig	MDEvs LD+	MDEvs LHDpartially+	MDEvs LHD+DD
	expansion 5 V<25Gy	%		13.4	5.2	7.4	0.9
Expansion	*expansion 5 V<38Gy*	%		85.5	70.2	79.2	54.5
	expansion 5 D98%	Gy		16.9	23.7	22.5	25.6
Patient	*V10Gy*	%		5.8	6.1	5.9	6.8
	V20Gy	%		1.2	1.3	1.2	2
	V30Gy	%		0.6	0.6	0.6	0.8
PTV	*V38Gy*	%	95.0	95.2	95	93.9	94.7
	Dmean	Gy		46.7	46.6	46.8	46.9
Prostate	*Dmin*	Gy	34.0	36.5	36.4	36.3	36.1
Rectum	*D0.03cc*	Gy	38.0	33.9	33.7	34	34.1
	D1cc	Gy	32.3	26.9	29.1	29.6	30.1
	V27Gy	%		1.5	3	3.1	4.5
	V18.2Gy	%		5.2	14.6	10.5	15.8
	Dmean	Gy		3.2	6.2	4.8	5.8
Bladder	*D0.03cc*	Gy	41.8	38.8	38.3	38.7	37.8
	D1cc	Gy	38.0	34.6	34.8	35.2	34.8
	Dmean	Gy		6	7.1	6.3	6.7
Urethra	*D50%*	Gy	40.0	38.5	38.5	38.6	38.4
	D10%	Gy	42.5	40.5	40.6	40.4	40.8
	D5%	Gy	45.0	41.2	41.4	40.9	41.8

Table 4.7: Population-mean parameters of Orig, MDEvsLHD+, MDEvsLD+, MDEvsLHDpartially+ and MDEvsLHD+DD plans.

Overview of all plans

Figure 4.27 shows V<25Gy, V<38Gy and $D_{98\%}$ in expansion 5 of all plans. Figure 4.28 shows corresponding OAR D1cc and Dmean values. MDE dose delivery is only substantially enhanced with MDEvsLHDpartially+, MDEvsLD+, MDEvsLHD+ and LHD+DD+. For V<38Gy, we clearly see the effect of shells, there is a considerably improved V<38Gy for both Orig+ compared to Orig and for MDEvsLHD+DD compared to MDEvsLHD. This suggests that MDE dose delivery up to 38 Gy is limited by the shell constraints in the other plans. Improved MDE doses is always at the cost of some increase in OAR doses. The bladder D1cc is hardly increased, but for MDEvsLHDpartially+, MDEvsLD+, MDEvsLHD+ and MDEvsLHD+DD an increase is visible in the rectum D1cc. Also mean doses are enhanced, whereby the effect is largest for the rectum Dmean doses. Plan MDEvsLD+ and MDEvsLHD+ show the biggest enhancements in low doses.

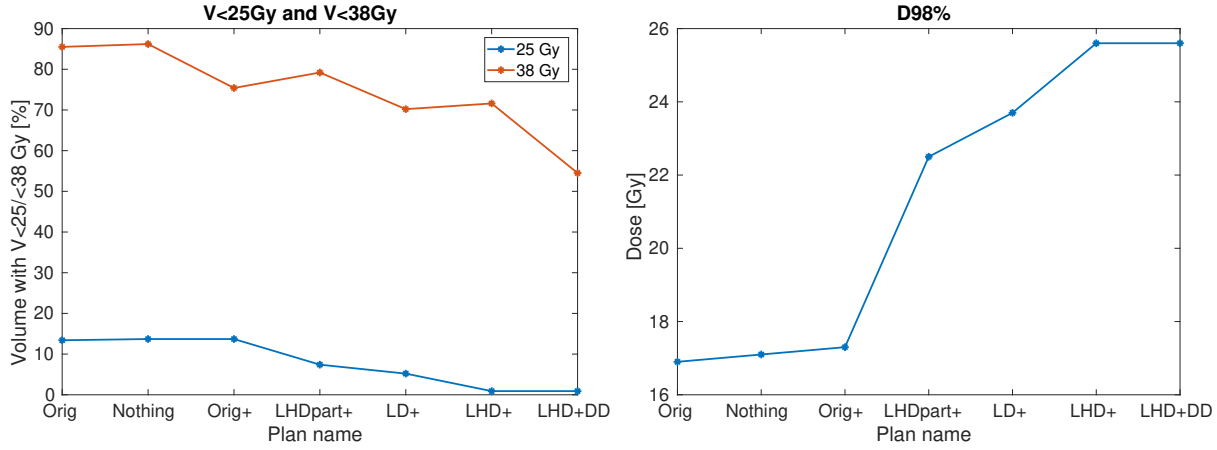

Figure 4.27: Population-mean underdosed MDE volumes (V<25Gy or V<38 Gy) of the seven different treatment plans on the left and on the right the $D_98\%$ population-mean. Names are abbreviated, from left to right: Orig, MDEvsNothing, Orig+, MDEvsLHDpartially+, MDEvsLD+, MDEvsLHD+, MDEvsLHD+DD

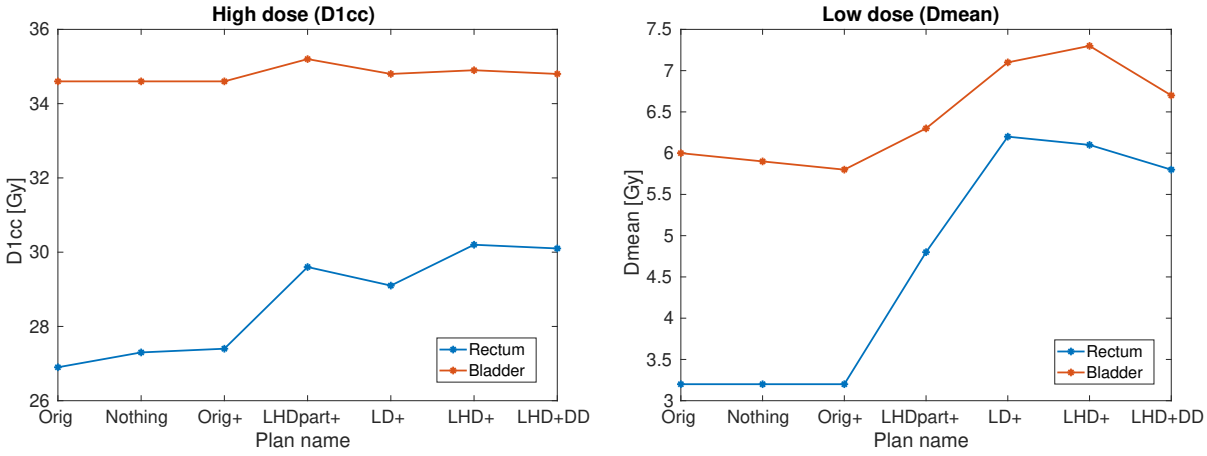

Figure 4.28: Population-mean values for the rectum and bladder D1cc on the left and Dmean on the right in the seven different treatment plans. Names are abbreviated, from left to right: Orig, MDEvsNothing, Orig+, MDEvsLHDpartially+, MDEvsLD+, MDEvsLHD+, MDEvsLHD+DD

4.3. Conclusions

4.3.1. MDE coverage up to 12 mm with 25 Gy

- **Orig**
  The original dose plans, generated without addition of cost functions for enhancement of MDE dose, already cover a big part of expansion 5 with 25Gy, but not of expansions 5-8 and 8-12 .

- **MDEvsNothing**
  MDEvsNothing plans aimed at 'free' improvements in MDE dose coverage. However, only negligible improvements could be obtained for free, i.e. without allowing enhanced doses in the OARs.

- **MDEvsLHD**
  MDEvsLHD resulted in the most extreme plans regarding opportunities to enhance MDE coverage. Almost >99% of the expansion 5, 5-8, and 8-12 mm were covered with 25 Gy. However, big prices were paid in OAR high and (especially) low doses, even if always within clinical constraints for the OARs.

- **MDEvsHD**
  MDEvsHD plans showed that giving up on only the high OAR doses did not result in meaningful increases in MDE coverage.

- **MDEvsLD**
  Giving up on low OAR doses alone with MDEvsLD resulted in significant improvements in MDE coverage. This approach might be interesting for further exploration for introduction in the clinic, because currently there are no clinical constraints for the low OAR doses. Focus is on limiting the high doses mainly.

- **MDEvsLHDpartially**
  Relaxing both the goal of the OAR high and low dose values with MDEvsLHDpartially provided some important insights. First, it showed that giving up on the high doses created space for MDE dose improvement. However, in order for the high doses to provide this space, both the high and low doses needed to be relaxed. Relaxing both high and low doses provided a bit more improvement in the areas close to the PTV compared full relaxation of only the low doses in MDEvsLD. At larger distances, MDEvsLD resulted in higher MDE volume coverage.

- **MDEvsDD**
  By setting the shell constraints as objectives with the lowest priority in MDEvsDD, the dose distributions lost a lot of conformality, as expected, but with a negligible gain in MDE coverage, compared to MDEvsNothing.

- **Overall conclusion**
  The three approaches that were most promising for improving MDE coverage were MDEvsLD, MDEvsLHDpartially and MDEvsLHD. Depending on the situation and preferred requirements, an optimal trade-off plan can be selected. If the focus is on covering most volume up to 12 mm only, MDEvsLHD gives the best result. However, if MDE coverage at larger distances is nonessential, MDEvsLHDpartially provides the most optimal outcome, because the sacrifice in OAR low doses is smaller. If limiting high rectum and bladder doses is crucial (like in current clinical practice), MDEvsLD is an appropriate choice.

4.3.2. MDE coverage up to 5 mm with 38 Gy

- **Orig**
  With the original wish-list, Orig, not having a cost function for dose enhancement in volumes with MDE, 14.5% of expansion 5 was covered with doses >38 Gy.

- **MDEvsNothing**
  Compared to Orig, plans generated with MDEvsNothing did not show increased coverage of expansion 5 with 38 Gy, showing that there was no ‘free’ improvement in coverage possible.

- **Orig+**
  With enhancement of the constraint dose of the Shell 3 mm, there was a higher coverage of expansion 5 possible at the 38 Gy level. For all OAR doses, it showed similar results to Orig.

- **MDEvsLHD+**
  MDEvsLHD+ offered the best coverage of expansion 5, both at 25 and 38 Gy level. However, both OAR high and low doses deteriorated. The deterioration was more moderate than for MDE coverage up to 12 mm.

- **MDEvsLD+**
  Lowering only the priorities of the cost functions for reductions in low OAR doses with MDEvsLD+, showed similar coverage effects as obtained with MDEvsLHD+. This suggests that the effect of lowering the priorities for the high doses is smaller than that of lowering the priorities of the mean doses. Since the clinical impact of higher doses in the OARs is larger than of the lower doses, MDEvsLD+ provides an interesting trade-off.

- **MDEvsLHDpartially+**
  MDEvsLHDpartially+ still increased both low and high OAR doses, but less than MDEvsLHD+ and MDEvsLD+. Similar MDE coverage at 25 Gy was obtained as with MDEvsLD, but the coverage was lower at the 38 Gy level. Compared to MDEvsLHD+, coverage for 25 Gy and 38 Gy decreased, but OAR doses improved.

- **MDEvsLHD+DD**
  Plans generated with MDEvsLHD+DD showed that shell constraints that control the conformality of the dose distribution can be a big limitation for obtaining MDE coverage at the 38 Gy level. By removing these constraints, significant improvements could be obtained, reaching a population mean coverage at the 38 Gy level of 45.5%, compared to 14.5% with Orig. This improvement was at the cost of a big loss in conformality of the dose distribution.

- **Overall conclusion**
  Fully covering the MDE volume up to 5 mm from the PTV with doses above 38 Gy was not possible, due to existing rectum, rectum mucosa and bladder constraints. However, by introducing dedicated OAR dose trade-off against dose coverage in expansion 5, it was possible to enhance MDE irradiation. MDEvsLHD offered largest improvements in MDE coverage with OAR parameters that were still within clinical constraints. However, the gain from allowing an increase in high doses in the rectum and bladder was relatively small compared to allowing an increase in the low doses only with MDEvsLD. Therefore, MDEvsLD offered the clinically most interesting plans for improving MDE coverage up to 5 mm.

4.3.3. Conclusion prioritized optimization

In general, we can conclude that with the current approach for multi-criteria optimization, we can steer MDE coverage. Covering more MDE volume outside of the PTV is possible when making trade-offs with the OAR doses. The effect of accepting slightly higher OAR low doses is larger than for the high doses. The is an exciting outcome, as this is less impacting for the OARs than elevated high doses. Changing wish-list priorities is a straightforward way to better account for MDEs, making this approach relevant for introduction in the clinic.

4.4. Future research

Improvement of treatment outcomes

For each patient, we always needed to run Orig, before creating the other plans. This makes treatment planning more time-consuming. On the other hand, if by enhancing MDE coverage, treatment outcomes advance, this extra step might be worth it. Future research should investigate if treatment outcomes can indeed be improved. Prior to this investigation, more patients need to be included in studies on the most promising approaches, in order to draw more definitive conclusions.

The effect of shell constraints

It might be worth taking a more in-depth look at the effect of shell constraints in the wish-lists. Currently, the shells are limiting increased doses to MDE volume. Finding out more about the exact effects of increasing their doses, might offer potential for improved MDE coverage/OAR dose trade-offs.

Anisotropic PTV expansions

In the investigations in this study, PTV expansions were always isotropic. It could be interesting to perform additional analyses with expansions that exclude overlaps with rectum and bladder, especially if the MDE cost functions have high priority.

Replacing the CTV margin

Another point that needs more investigation is whether this method can really replace the current CTV margin. The idea behind prioritized optimization as a method to improve MDE coverage is that the CTV margin is neglected, and planning is performed on the GTV directly.

Preferences in the clinic

As last, it would be interesting to include physicians in the project. By letting them evaluate the dose distributions, information could be gathered about which trade-offs they would prefer to use in the clinic.

5

Probabilistic planning

This chapter focuses on treatment planning to improve dose control to the MDE volume, steered by the probability that MDEs are located at a specific distance from the macroscopic tumor. This will be achieved by constructing and implementing a probabilistic cost function, instead of changing objective priorities in the wish-list and assuming that the volume up to 5, or 12 mm should be covered, as performed in the previous chapter. The first section explains the methods used. Secondly, the results are presented and discussed, and the final part addresses the conclusions.

5.1. Methods

The goal of the probabilistic planning approach is to deduce a probabilistic cost function and incorporate it into Erasmus-iCycle. This way, the function can be used in plan optimization. Instead of using the linear, LTCP, EUD or mean functions (section 4.1.2), an expected Tumor Control Probability (TCP) function is derived for this purpose in the next sections.

5.1.1. Deriving the probabilistic cost function

The TCP model

As explained in section 2.1.1, the TCP describes the probability of local tumor control. Since the aim of the cost function is to improve dose control in the MDE volume, which can be seen as possible tumor volume, the use of the TCP model can be justified.

We start from the most general TCP model, which follows from the dependence on the Poisson distribution for cell kill

$$TCP = e^{-N_0 e^{-(\alpha D + \beta D^2/N_f)}} \tag{5.1}$$

with N_0 the initial number of tumor cells, α, β, the radiosensitivity parameters of the tumor tissue and N_f the number of fractions. N_0 can be written as $N_0 = \rho * Volume$, where ρ is the tumor cell density and $Volume$ the tumor volume. Instead of taking N_0, a volume integral can be included in the TCP model, integrating from 0 to r_{max}, the maximum radius of the tumor volume.

It is known that in general there is a high probability of finding MDEs close to the tumor boundary and that this value decreases for distances further away. We want Erasmus-iCycle to increase dose in volumes where there is a high probability of finding MDEs. This means that the TCP should include a spatially dependent dose factor. Instead of taking one value for the dose, D, the model is adapted to accommodate the parameter $D(\vec{r})$. $D(\vec{r})$ is the spatially dependent dose distribution. The TCP in equation 5.1 can be written as

$$TCP = e^{-\int_0^{rmax} \rho e^{-(\alpha D(\vec{r}) + \beta D(\vec{r}^2)/N_f)} d\vec{r}} \tag{5.2}$$

For a spherically symmetric problem, D($\vec{r}$) = D(r) and the volume of a sphere equals: $V(r) = \frac{4}{3}\pi r^3$, where r is the radius of the sphere. The TCP can be written as

$$TCP = e^{-\int_0^{rmax} \rho e^{-(\alpha D+\beta D^2/N_f)} 4\pi r^2 dr} \tag{5.3}$$

This section continues with a simple concept patient model, where both the PTV and MDE volumes are considered to be symmetrical spheres. The PTV refers to the tumor target volume. In principle the approach could also start from the GTV. However, we use the PTV to be consistent with the prioritized optimization approach (Chapter 4). Assuming that the TCP of the tumor should ideally be one, the TCP for the MDE volume starts at the PTV boundary and goes up to the maximum MDE distance, Δ. Figure 5.1 shows a phantom example of the assumed model.

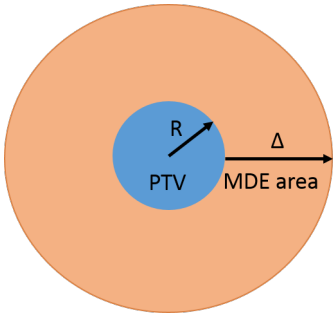

Figure 5.1: Geometry for the concept model. R is the radius of the PTV and Δ the maximum distance from the PTV boundary up to where there is a possibility of finding MDEs.

Volume integration starts at the PTV boundary (radius R), and goes up to the MDE border (R + Δ). The volume integral over r now goes from R to $R + \Delta$, resulting in

$$TCP(\Delta) = e^{-\int_R^{R+\Delta} \rho e^{-(\alpha D(r)+\beta D(r)^2/N_f)} 4\pi r^2 dr} \tag{5.4}$$

It is assumed that ρ is also spatially dependent, just like the dose distribution, resulting in

$$TCP(\rho,\Delta) = e^{-\int_R^{R+\Delta} \rho(r) e^{-(\alpha D(r)+\beta D(r)^2/N_f)} 4\pi r^2 dr} \tag{5.5}$$

The expected TCP

Both the parameters ρ and Δ are uncertain for individual patients. These uncertainties should be taken into account when calculating the TCP. The expected TCP allows to handle these parameter uncertainties. The expected TCP includes the distribution of the possible parameter values, described by a probability function. We assumed that the values for ρ and Δ are described by their respective probability density functions; $P(\rho)$ and $P(\Delta)$. The expected TCP, E(TCP), can then be written as

$$E(TCP) = \int_\rho \int_\Delta TCP(\rho,\Delta) P(\Delta) P(\rho) d\Delta d\rho \tag{5.6}$$

The tumor density probability is considered to be uniformly distributed in a pre-defined range and is considered to be independent of space, with

$$P(\rho) = U(\rho_0, \rho_1) \tag{5.7}$$

U denotes the uniform distribution of ρ, between ρ_0 and ρ_1. With ρ_0 and ρ_1 possible tumor cell densities for the MDE area. Section 5.1.2 elaborates on the exact values used for this approach.

The probability of finding an MDE between Δ and $d\Delta$ is given by $P(\Delta)d\Delta$. We assume that the probability density, $P(\Delta)$, is described by an exponential

$$P(\Delta) = \frac{1}{L} e^{-\frac{\Delta}{L}} \tag{5.8}$$

Here L is a normalization constant. The function is based on literature findings [24] (see section 3.1.2 on probability density functions). Integrating the density function from 0 to infinity results in a probability of 1

$$\int_0^\infty P(\Delta)d\Delta = 1 \tag{5.9}$$

Clinically it is not possible to irradiate the total patient volume, therefore, equation(5.9) is replaced by

$$\int_0^{R_{max}} P(\Delta)d\Delta = 0.99 \tag{5.10}$$

So the assumption is that 99% of the MDE is within Rmax from the tumor border. To obtain values for L, and describe the distal spread of MDEs, three different models were investigated. These models were, similarly to the previous chapter, based on MDE literature findings.

1. For the first model, we set the maximum distance to 5 mm. This results in:

$$\int_0^5 \frac{1}{L} e^{-\frac{\Delta}{L}} = 0.99 \tag{5.11}$$

$$L \approx 1.1 \text{ mm} \tag{5.12}$$

   So L equals 1.1 mm (rounded off to one decimal); using a normalization constant of 1.1, there is a 99% chance of finding MDEs up to 5 mm.

2. For the second model, the maximum distance was set to 8 mm. This results in an L of 1.7 mm (rounded off to one decimal).

3. For the third approach, we assumed the maximum distance to be 12 mm. The corresponding normalization constant L is 2.6 mm (rounded off to one decimal).

Calculating the expected TCP
Since we cannot implement the expected TCP as a continuous distribution function (as it is in equation 5.6, due to the uncertainties), we need to discretize it. This cannot be done analytically, therefore, the quadrature rule is used for the numerical integration [40] (see section 5.1.5 for the technical background).
Using the quadrature rule, the expected TCP can be calculated by two summations, instead of integrals; one summation for replacing the integral over ρ and one for the integral over Δ.

Combining both summations for values over Δ and ρ results in an expected TCP of

$$E(TCP) \approx \sum_{i=1}^{n_\Delta} \sum_{j=1}^{n_\rho} w_i^\Delta w_j^\rho TCP(\Delta_i, \rho_j) \tag{5.13}$$

1. First there is a summation over ρ, from j=1 up to j=n_ρ (the quadrature level). For each level, there is a weight w_j^ρ and function value ρ_j, specified by the quadrature. i.e, if we take n_p=30, for one Δ value, the expected TCP will be a summation of the TCP's for all 30 different values of ρ multiplied with their according weights.

2. A similar summation happens for the Δ values, the parameters belonging to this summation are; the quadrature level for Δ, n_Δ, and the weights and function values for each level, w_i^Δ and Δ_i, respectively.

Using the expected TCP
To study optimization based on the expected TCP, two experiments were performed. In the first experiment, the effect is shown for a simple model, this is mainly a proof-of concept model (section 5.1.3). For the second experiment, the cost function was implemented in Erasmus-iCycle (section 5.1.4). This way it could be used for the dose optimization in real patient plans.

5.1.2. Parameter selection

To use the expected TCP as a cost function, the parameters α, β and ρ need to be provided. The parameters used for this project are based on an article by Pedicini et al.[41]. Their estimate for the α, β parameters provides values compatible with a realistic tumor cell density ρ, of approximately 10^5cm^{-3}, for the prostate tumor cells [41]. Values for α, β and ρ are 0.15 Gy^{-1}, 0.058 Gy^{-2} and 10^5cm^{-3}, respectively. These α, β values have an α/β ratio of 2.6 Gy. In this project, results, unless commented, were investigated for a α/β ratio of 1.5 (see section 4.1.2), as commonly used for prostate tumor cells [39] and because of better optimizer performance (appendix A). The α and β provided by Pedicini et al. were adapted to a ratio of 1.5 Gy by plotting and evaluating several combinations of α and β. Parameters were selected that resulted in significantly improved dose coverage of the MDE volume in the Erasmus-iCycle approach (section 5.1.4). However, they also resulted in very high expected TCP values. The proposed α and β values are 0.15 Gy^{-1} and 0.103 Gy^{-2}, respectively.

The assumption is made is that the tumor cell density in the MDE area is lower compared to the PTV as tumor volume [42]. In the expected TCP, the value for ρ is uniformly distributed between ρ_0 and ρ_1. ρ_0 and ρ_1 were set to 10^2 and 10^5cm^{-3}, respectively.

5.1.3. Concept model

The goal of the concept model is to show that with proper constraining of the total delivered energy to the MDE area, maximizing the expected TCP will indeed result in highest doses close to the PTV edge. This is to be expected because of the exponential shape of the probability density function of the MDEs (equation 5.8). Furthermore, sensitivity to parameters α, β and ρ will be shown.

The starting point is the formula for the expected TCP from equation 5.13. We assume that both the PTV, as target volume, and the MDE volume surrounding the PTV can be described by spheres. Instead of using the volume distribution over r, the volume ranging from the PTV to the maximum value of delta was subdivided into spherically shaped subdomains with volumes V_k. These subdomains are represented by equally spaced rings around the PTV. Figure 5.2 shows a graphical representation of the model.

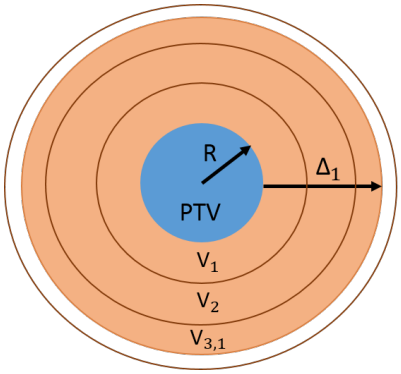

Figure 5.2: An example of the simple TCP model, for which the PTV is a circle with radius R. Rings with radius r around the PTV are plotted as circles with respective volumes V_k and represent the subdomains. With maximum MDE distance Δ_1, the volumes of ring 1 and 2, V_1 and V_2, respectively, completely fall within distance Δ_1, and ring volume 3 partly (denoted by $V_{3,1}$ partial ring volume 3 for Δ_1)

The total TCP is a multiplication of the TCP values for the separate ring volumes within Δ_i. If part of the ring volume falls within distance Δ_i, the calculation will only include the TCP for this partial volume. The volumes included are denoted with subscripts; $V_{k,i}$, here k represents the ring number and i is used when a partial ring volume should be included (i becomes the specific Δ for which the partial volume should be included). Taking a look at figure 5.2, the ring volume of the third ring k=3 is only partially located within the first delta, Δ_1, therefore we denote the volume of the third ring to be included in the calculation as $V_{3,1}$. The volume equals zero for all (partial) rings outside of Δ_i.

$$E(TCP) = \sum_{i=1}^{n_\Delta} \sum_{j=1}^{n_\rho} w_i^\Delta w_j^\rho e^{-\sum_{k \in \Delta_i} \rho_j e^{-(\alpha D_k + \beta D_k^2 / N_f)} V_{k,i}} \tag{5.14}$$

The Matlab function fmincon, maximizes the expected TCP. Fmincon is a nonlinear programming solver that finds the minimum/maximum of a problem [43]. Several rules can be used to constrain the problem. The constraints used for this approach were:

1. $0 \leq D_k \leq D_{max}$
   This constraint makes sure that the dose in each ring is larger or equal to zero and smaller than the maximum dose to be specified.

2. $\sum_k V_k D_k = E_{max}$
   If only the first constraint would be used, the function would administer maximum doses to the entire MDE volume. The second rule constrains the integral dose in the volume; there is a maximum energy to be distributed throughout the volume and the expected TCP determines in which way the doses should be distributed to have an optimal outcome. The total of all ring volumes (V_k) times the dose per ring (D_k) is equal to this maximum energy value. We assumed that $E_{max} = V_{MDE} C D_{max}$; the MDE volume, V_{MDE} times the maximum dose D_{max} multiplied by a constant C. The MDE volume is the possible volume up to where MDEs are located according to literature, i.e. the resulting volume of a sphere with a radius of 5, 8 or 12 mm, starting at the tumor border. C was varied to investigate the effect of having different maximum energy values.

For our optimization of E(TCP), we also specified the gradient, the first derivative of the E(TCP) with respect to dose

$$\frac{\partial E(TCP)}{\partial D_l} = -\sum_{i=1}^{m}\sum_{j=1}^{n} w_i w_j e^{-\sum_{k\in\Delta_i}\rho_j e^{-(\alpha D_k+\beta D_k^2/N_f)V_{k,i}}} \times \rho_j e^{-(\alpha D_l+\beta D_l^2/N_f)} V_{l,i}\left(-\alpha - \frac{2\beta D_l}{N_f}\right) \tag{5.15}$$

For all rings with volumes $V_{l,i}$ within Δ. Otherwise, $V_{l,i}$ and therefore the derivative equals zero. This can be simplified to

$$\frac{\partial E(TCP)}{\partial D_l} = -E(TCP) \times \rho_j e^{-(\alpha D_l+\beta D_l^2/N_f)} V_{l,i}\left(-\alpha - \frac{2\beta D_l}{N_f}\right) \tag{5.16}$$

The objective of using fmincon is to maximize the value of the expected TCP, taking into account the function, the first derivative, and the constraints in order to find the optimal dose values in the rings, D_k.

This was calculated for all 3 models; L=1.1, L=1.7, and L=2.6 mm. For each approach the maximum ring distance to the PTV was 10*L and the ring thickness was set to 0.25 mm (resulting in 44, 68 and 104 rings for L=1.1, L=1.7 and L=2.6 mm, respectively). For all models, the α, β and ρ from section 5.1.2 were used (0.15 Gy^{-1}, 0.103 Gy^{-2} and uniformly distributed between 10^2 to $10^5 cm^{-3}$, respectively), unless commented. The maximum dose was set to 38 Gy and the maximum energy constraint was varied by using different values for the constant C. The values used were C=0.5, C=1, C=2, and no constraint in total energy.

Evaluation

The results were evaluated by calculating the expected TCP values for the three models and for the different energy constraints. Also plots were created showing the optimal dose value for each distance from the PTV. The latter was done by optimizing the dose values per ring and plotting the optimal dose values against the distance from the PTV, i.e. ring 1 has a 0.25 mm distance from the PTV, so the first point in the graph will be at 0.25 mm.

Next to dependence of the model on the maximum energy constraint, the dependence on parameter ρ was tested. In the expected TCP model as in equation 5.12, ρ is uniformly distributed between 10^2 to $10^5 cm^{-3}$. Next to taking a distribution over ρ, three constant values were tested; ρ_0=$10^2 cm^{-3}$, the lower limit of the uniform distribution, $\rho_1 = 10^5 cm^{-3}$, the upper limit and ρ_M which represents the median value between ρ_0 and ρ_1 (10^2 and $10^5 cm^{-3}$) and is equal to $5.005 \cdot 10^5 cm^{-3}$.

As last, the sensitivity of the expected TCP to the α/β ratio was evaluated. The proposed values for α and β are 0.15 Gy^{-1} and 0.103 Gy^{-2}, respectively, resulting in an α/β ratio of 1.5 Gy. To evaluate the effect of a higher α/β ratio on the expected TCP, also the values suggested by Pedicini et al. [41], $\alpha = 0.15 Gy^{-1}$, $\beta = 0.058 Gy^{-2}$ and $\alpha/\beta = 2.6$ Gy, were tested.

5.1.4. Expected TCP in Erasmus-iCycle

For the second model, the expected TCP was implemented as a cost function in Erasmus-iCycle. This way it can be used in treatment plan optimization.

By evaluating the resulting dose distributions, the effect of using the new cost function on real patient plans could be investigated.

Maximizing the expected TCP in Erasmus-iCycle was done by optimization of the beamlet weights, i.e. the weights of narrow pencil beams entering the patient. Contrary to the simple model, the volume domain is divided into voxels instead of rings. The volume is described by PTV expansions (further explanation below). In the expansion structure the voxel distances to the PTV boundary are calculated. This is done by finding the nearest point of each voxel to the PTV. All voxels with distances located within a specific Δ_i are included in the expected TCP calculation. Also in this approach the values of Δ_i are determined by the quadrature rule. Instead of taking the total volume of all rings falling within Δ_i, the volume of all voxels inside the integration bound is taken. To account for the fact that the integration bound Δ_i partially includes a subvolume or voxel, we denote the relevant volumes as $V_{v,i}$ (subscript v for voxel, instead of k). However, for simplicity, we assumed that the voxels either entirely fall in- or outside of Δ_i. As volumes are given per voxel, also the resulting spatial dose distribution will be provided per voxel.

For implementing the expected TCP as a cost function in Erasmus-iCycle, both the gradient and the hessian function are ideally used. The gradient is similar to the one in equation 5.25. The doses are calculated per voxel instead of per subregion (D_k becomes D_v). Because Erasmus-iCycle optimizes pencil beam weights, x_i (unit fluence), also the gradient with respect to the beam weights should be obtained. This can be done by:

$$\frac{\partial E(TCP)}{\partial x_j} = \sum_v \frac{\partial D_v}{\partial x_j} \frac{\partial E(TCP)}{\partial D_l} \tag{5.17}$$

The dose of a voxel is given by: $D_v = d_v^T x$. Here d_v gives the dose per beam weight and vector x contains all beam weights. The derivative of the dose matrix D to the beam weights would simply be:

$$\frac{\partial D_v}{\partial x_j} = d_v^j \tag{5.18}$$

d_v^j is the j-th entry of d_v^T. The derivative is simply an entry of the dose matrix, hence the gradient is a vector multiplication of the first derivative with the transpose of the dose matrix.

In this project, we have not used the Hessian in the Erasmus-iCycle implementation. The Hessian is a difficult format to be written in an efficient canonical form, the format needed for implementation, and it will increase computation times. The Hessian is not needed to measure convergence, as this is measured with the first derivative only. As long as the first derivative is defined correctly, a (local) optimal solution is found. The impact of ignoring the Hessian is slower convergence.

To use the cost function, treatment plans were created using the expected TCP cost function to increase coverage in the MDE volume. This was done for the 5 SBRT patients. Before the cost function could be used, original plans had to be created, called *Orig* plans. These plans were created with the prostate wish-list that reflects the clinical protocol previously developed at the Erasmus MC [38] and that has been introduced in section 4.1.1 (also see table 4.1).

For the treatment plans with expected TCP optimization, specified as the *ETCP* plans, an objective for MDE coverage was added to the wish-list. The MDE objective is an expansion structure of either 5, 8, or 12 mm surrounding the PTV, referred to as expansion 5, 8, or 12, respectively. The objective was added with the highest priority, above rectum and bladder EUD and mean objectives (see table 5.1). This way the optimizer first optimizes the expected TCP of the MDE volume, towards a value of 1, and then reduces rectum and bladder high and low doses. For expected TCP optimization in expansion 5, 8 and 12, the three different models as introduced in section 5.1.1 were used (i.e., for expansion 5, L=1.1 mm, for expansion 8, L=1.7 mm, and for expansion 12, L=2.6 mm).

Another change to the initial wish-list (table 4.1) is that the shell 3 mm constraint was ignored. This allows an increase in the dose values above 38 Gy, without being limited by the shell constraint.

		ETCP		
Priority	**Structure**	**Min/Max**	**Type**	**Goal value**
3	*Expansion 5/8/12*	Max	E(TCP)	1
4	*Rectum*	Min	EUD	0
5	*Bladder*	Min	EUD	0
6	*Rectum*	Min	Mean	0
7	*Bladder*	Min	Mean	0

Table 5.1: Objective functions of the prostate wish-lists for ETCP. In orange are changes relative to the wish-list in table 4.1. As mentioned above, constraints were the same as used for the Orig plans, apart from ignoring the shell 3 mm constraint (table 4.1).

Since the focus was on increased MDE coverage in expansion 5, 8, or 12, the corresponding ETCP plan names are: ETCP5, ETCP8, and ETCP12, respectively. By creating these expansions, the probabilistic planning approach becomes comparable to the prioritized optimization approach (chapter 4, section 4.1.2 and evaluation section below). Because voxel distances are only calculated up to 5, 8, or 12 mm, respectively, instead of up to the maximum Δ_i (see equation 5.13), not all quadrature points are included in the numerical integration anymore. However, the weights belonging to the omitted points only make up 1.3% of the total summation. Therefore, the summation is still a reasonable approximation of the integral.

Evaluation

To investigate the effect of using the new expected TCP cost function on real patient plans, several evaluation methods were used. Evaluation is performed separately for the three different plans, ETCP5, ETCP8 and ETCP12. Results from ETCP plans will be compared to the original plans without the expected TCP optimization, Orig plans, and to the MDEvsLHD plans, having MDE trade-off with Low and High OAR Doses. These are the treatment plans of the prioritized optimization approach (see chapter 4, section 4.1.3) being most similar to the ETCP plans regarding their objective order (see table 5.2). Similar as for the ETCP plans, MDEvsLHD plans were created for maximizing MDE coverage up to 5, 8, or 12 mm from the PTV to a dose of 38 Gy, referred to as MDEvsLHD5, MDEvsLHD8, and MDEvsLHD12, respectively. The plans were generated by creating expansions of 5, 8, or 12 mm around the PTV and maximizing the dose in this expansion volume to 38 Gy. Also for these plans the shell 3 mm constraint was ignored. The results of ETCP5, ETCP8, and ETCP12, were compared to MDEvsLHD5, MDEvsLHD8 and MDEvsLHD12, respectively. i.e., ETCP5, aiming for an optimal dose distribution depending on the MDE probability function (99% probability of findings MDEs up to 5 mm, L=1.1 mm), is compared to MDEvsLHD5, aiming for dose maximization to 38 Gy in the entire region up to 5 mm from the PTV. Even though only small deviations are expected, also the Orig plans are created for all three plans separately to include the right expansion structure.

		ETCP		
Priority	**Structure**	**Min/Max**	**Type**	**Goal value**
3	*Expansion 5/8/12*	Max	E(TCP)	1
4	*Rectum*	Min	EUD	0
5	*Bladder*	Min	EUD	0
6	*Rectum*	Min	Mean	0
7	*Bladder*	Min	Mean	0

		MDEvsLHD		
Priority	**Structure**	**Min/Max**	**Type**	**Goal value**
3	*Expansion 5/8/12*	Max	Linear	38
4	*Rectum*	Min	EUD	0
5	*Bladder*	Min	EUD	0
6	*Rectum*	Min	Mean	0
7	*Bladder*	Min	Mean	0

Table 5.2: Objective functions of the prostate wish-lists for ETCP and MDEvsLHD. In orange are changes relative to the wish-list in table 4.1. As mentioned above, constraints were the same as used for the Orig plans (table 4.1), apart from ignoring the shell 3 mm constraint.

The first and foremost way to evaluate and compare the plans is by the obtained expected TCP value, where a value of 1 is the best obtainable result.

The second way of comparison is by relevant dosimetric parameters, which include clinical requirements and other commonly reported values to evaluate the whole dose distribution. Additional parameters for the expansion volume of either 5, 8, or 12 mm, referred to as expansion 5, 8 or 12, include the expected TCP, reported as E(TCP), V38Gy, the expansion volume receiving a dose of 38 Gy, and $D_{98\%}$, the near minimum dose to the expansion volume. Contrary to all other dosimetric parameters, the E(TCP) is reported in three decimals.

The third method of treatment plan evaluation and comparison is by DVHs. Trade-offs between MDE coverage and OAR doses should be well visible in these graphs.

Similar to Chapter 4, all plans were performed for 5 SBRT patients. Even if the patient number is low for a statistically robust analysis, the goal of the project was to propose, build and investigate the feasibility of a clinically usable approach

5.1.5. Technical background of the quadrature rule

As pointed out above, the quadrature rule was used to approximate the E(TCP) expressed in equation (5.6) by equation (5.13). Here the use of the quadrature rule is explained in more detail.

Use of quadrature is possible for any function to be integrated, as long as it resembles a polynomial. For this study, we assumed the TCP to be a polynomial function. The quadrature rule gives an approximation of the definite integral, calculated by a weighted sum of function values, whereby the function values, abscissas, are at specific points in the domain of the integral and the weights belong to these individual points [44] [40]. The weights (w) and quadrature points in the summation depend on the quadrature rule used and on the probability function P. The number of terms included in the summation goes up to a specified quadrature level (n). Increasing this level increases the number of weights and quadrature points that are taken into consideration in the integral approximation. A higher level will result in a more accurate approximation, but also in increased computation times.

There are several different kinds of quadrature rules. For our research we used both the Gauss-Legendre quadrature and the Gauss-Laguerre quadrature.

Gauss-Legendre quadrature

The Gauss-Legendre quadrature is the simplest quadrature format, where f(x) can be approximated by polynomials on [-1, 1].

$$\int_{-1}^{1} f(x)dx \approx \sum_{j=1}^{n} w_j f(x_j) \tag{5.19}$$

The subscript *j* denotes the *j*th quadrature point with its belonging weight. For the integral over ρ we can use the Gauss-Legendre quadrature, as in fact it is the TCP function on the interval $[\rho_0, \rho_1]$

$$E(TCP) = \int_{\rho} TCP(\rho)P(\rho)d\rho = \int_{\rho_0}^{\rho_1} TCP(\rho)d\rho \tag{5.20}$$

$$\int_{\rho_0}^{\rho_1} TCP(\rho)d\rho \approx \sum_{j=1}^{n_\rho} w_j^\rho TCP(\rho_j) \tag{5.21}$$

Because the general weights for the Gauss-Legendre quadrature are for the [-1,1] range, the weights need to be rescaled for the correct range of the uniform distribution. This means that ρ_j depends on x_j through transformations.

Gauss-Laguerre quadrature
The Gauss-Laguerre quadrature can be used for more advanced integrals, including an exponential. In order to use this type of quadrature, integrals should resemble the following format:

$$\int_0^\infty e^{-x} f(x) dx \tag{5.22}$$

For this case, it holds that

$$\int_0^\infty e^{-x} f(x) dx \approx \sum_{i=1}^{n} w_i f(x_i) \tag{5.23}$$

The integral over Δ, can be written as:

$$E(TCP) = \int_\Delta TCP(\Delta) P(\Delta) d\Delta = \int_0^\infty TCP(\Delta) \frac{1}{L} e^{-\frac{\Delta}{L}} d\Delta \tag{5.24}$$

The quadrature rule can only be used for simple exponents. To rewrite the exponent, $-\Delta/L$ is replaced by Δ' with $\Delta' = \frac{\Delta}{L}$

$$E(TCP) = \int_0^\infty TCP(\Delta' L) \frac{1}{L} e^{-\Delta'} d\Delta' L = \int_0^{\Delta' L} TCP(\Delta' L) e^{-\Delta'} d\Delta' \tag{5.25}$$

Now the Gauss-Laguerre can be used for approximating the values of the integral

$$\int_0^\infty TCP(\Delta' L) e^{-\Delta'} d\Delta' \approx \sum_{i=1}^{\infty} w_i TCP(\Delta_i) \tag{5.26}$$

5.2. Results

In this section the results of dose optimization using the expected TCP will be discussed. The first section shows the results of the proof of concept model, followed by the results obtained with the Erasmus-iCycle implementation.

5.2.1. Proof of concept model

Dependence of resulting dose and expected TCP on the total energy constraint

Figure 5.3 shows optimal dose values as a function of distance from the PTV for the three different L constants (section 5.1.1) used and for four maximum energy constraints, represented by C-values (section 5.1.3) and table 5.3 corresponding expected TCP values. As expected, by increasing the total delivered energy, dose is distributed over a larger volume. For instance, for L=1.1 mm and C=0.5, dose is delivered up to 5.5 mm from the PTV and this increases to 8.8 mm for C=2 and a similar L value. In line with the observations for dose, for a higher maximum energy value, also the expected TCP increases, as can be seen in table 5.3. Without any constraint being present (bottom right in figure 5.3), the expected TCP reaches one and the maximum dose, 38 Gy, is deposited in the entire volume. The expected TCP values are similar for all 3 models, as expected.

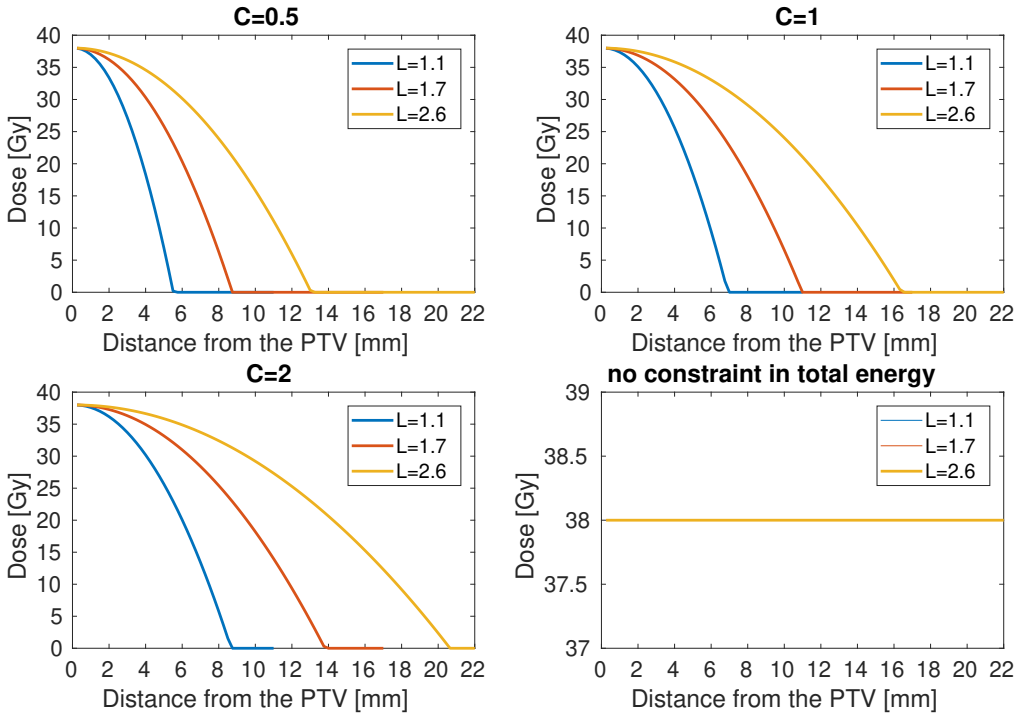

Figure 5.3: Optimal dose values for three different expected TCP models with L=1.1, L=1.7 and L=2.6 mm as a function of the constraint in total delivered dose, represented by C. For the panel without energy constraint, the curves for L=1.1 and L=1.7 mm are superimposed by the curve for L=2.6 mm .

Energy constraint	L=1.1	L=1.7	L=2.6
C = 0.5	0.960	0.960	0.960
C = 1	0.984	0.985	0.976
C = 2	0.990	0.990	0.988
no constraint	1.000	1.000	1.000

Table 5.3: Optimized expected TCP values for models with L=1.1, L=1.7 and L=2.6 mm and for four constraints in total delivered energy.

Dependence of expected TCP on the tumor cell density
To test the sensitivity of the expected TCP on the tumor cell density, expected TCPs were calculated for different values of ρ (section 5.1.3). Table 5.4 shows that when ρ takes values from a uniform distribution between ρ_0 and ρ_1, U(ρ_0, ρ_1) (determined by the quadrature rule), the expected TCP is in between of what it would be for either ρ_0 or ρ_1. The expected TCP for U(ρ_0, ρ_1) is not exactly similar to the expected TCP for the median value of ρ, ρ_M, as expected. The values provided are for L=1.1 mm, but results were similar for L=1.7 and 2.6 mm.

Energy constraint	U(ρ_0, ρ_1)	$\rho_0=10^2$	$\rho_1=10^5$	ρ_M
C = 0.5	0.960	0.961	0.960	0.960
C = 1	0.984	0.987	0.981	0.984
C = 2	0.990	0.997	0.988	0.989
no constraint	1.000	1.000	1.000	1.000

Table 5.4: Optimized expected TCP values for the model with L=1.1 mm, as a function of tumor cell density in the area with microscopic disease.

Dependence of the expected TCP on the α/β ratio
Table 5.5 shows the expected TCP values depending on the α/β ratio used. As can be seen a higher α/β ratio results in a lower expected TCP for all three models. This is as expected, since a higher α/β ratio contributes to a higher surviving fraction and so a higher TCP (section 2.1.1).

	L=1.1		L=1.7		L=2.6	
Energy constraint	α/β=1.5	α/β=2.6	α/β=1.5	α/β=2.6	α/β=1.5	α/β=2.6
C = 0.5	0.960	0.902	0.960	0.898	0.960	0.889
C = 1	0.984	0.954	0.985	0.946	0.976	0.919
C = 2	0.990	0.970	0.990	0.964	0.988	0.955
no constraint	1.000	0.998	1.000	0.982	1.000	0.989

Table 5.5: Dependence of optimized Expected TCPs for various models (L) and total energy constraints (C) on α/β ratio of 1.5 and 2.6 Gy (see section 5.1.2 parameter selection and section 5.1.3 evaluation)

5.2.2. Expected TCP in Erasmus-iCycle

Graphical representations, presented for easier interpretation of the data, provide information of one example patient out of the five evaluated patients. Unless commented, the results of the other patients showed similar behaviour.

MDE coverage up to 5 mm
Maximizing the expected TCP in Erasmus-iCycle, in ETCP5, the expected TCP value, referred to as E(TCP) value, was 0.931 (table 5.6). This is an increase of 0.344 (59%) compared to the E(TCP) of Orig (section 5.1.4 for the evaluation methods). The high E(TCP) value is a result of the parameter selection (section 5.1.2).

Dose values increased considerably in expansion 5, V38Gy increased by 21.4% (147%), while the $D_{98\%}$ increased by 4.6 Gy (27%). The enhanced dose in expansion 5 is also visible in the DVH in figure 5.4 (solid vs dashed line) and in the dose distribution in figure 5.5.

To obtain the higher E(TCP) and expansion dose, a price is paid in the OAR doses. For the rectum; D1cc increased by 1.7 Gy (6.3%), V27Gy by 0.9% (60%), V18.2Gy by 3.3% (63%) and Dmean by 1.0 Gy (31%), compared to Orig. For the bladder Dmean increased slightly by 0.4 Gy (6.7%) (table 5.6).

Compared to MDEvsLHD5 (section 5.1.4), the E(TCP) worsened from 1.000 to 0.931 (table 5.6). The reduced E(TCP) of ETCP5 is an effect of the lower dose in expansion 5 compared to MDEvsLHD5, $D_{98\%}$ decreased from 25.6 to 21.5 Gy. The lower expansion dose in ETCP5 can also be seen in the DVH in figure 5.4 (solid vs dotted line) and in the dose distribution in figure 5.5. The results suggest that the E(TCP) reaches a value of 1 for MDE volume coverage with 25 Gy.

The decreased E(TCP) and expansion coverage correspond to improved OAR doses; for the rectum D1cc decreased by 1.5 Gy (5.0%), V27Gy by 2.1% (47%), V18.2Gy by 7.4% (47%) and the rectum Dmean by 1.8 Gy (24.6%). For the bladder D1cc decreased by 0.2 Gy (0.57%) and Dmean by 0.9 Gy (12.3%).

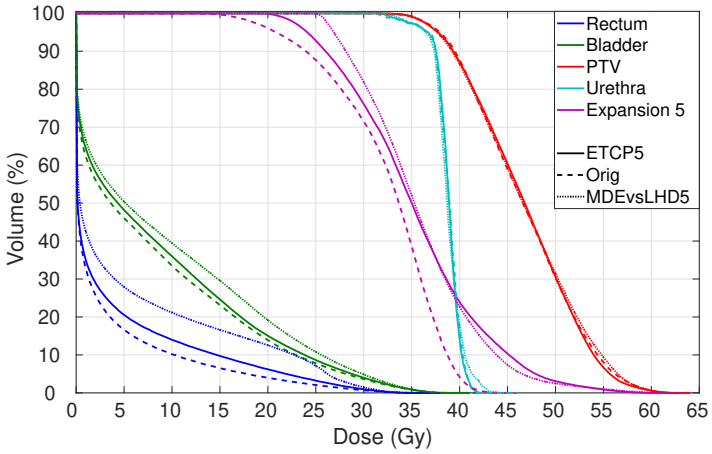

Figure 5.4: DVHs for an example patient for ETCP5, Orig, and MDEvsLHD5 plans.

Structure	Parameter	Unit	ETCP5	Orig	MDEvsLHD5
Expansion 5	*E(TCP)*	-	0.931	0.587	1.000
	V38Gy	%	36.0	14.6	34.8
	D98%	Gy	21.5	16.9	25.6
Patient	*V10Gy*	%	6.4	5.8	6.8
	V20Gy	%	1.4	1.2	1.4
	V30Gy	%	0.6	0.6	0.7
PTV	*V38Gy*	%	95	95.3	94.6
	Dmean	Gy	46.7	46.7	46.7
Prostate	*Dmin*	Gy	36.4	36.4	36.1
Rectum	*D0.03cc*	Gy	33.8	33.9	34.1
	D1cc	Gy	28.7	27	30.2
	V27Gy	%	2.4	1.5	4.5
	V18.2Gy	%	8.5	5.2	15.9
	Dmean	Gy	4.2	3.2	6
Bladder	*D0.03cc*	Gy	38	38.7	37.7
	D1cc	Gy	34.6	34.6	34.8
	Dmean	Gy	6.4	6	7.3
Urethra	*D50%*	Gy	38.6	38.5	38.4
	D10%	Gy	40.4	40.5	40.7
	D5%	Gy	41.1	41.2	41.7

Table 5.6: Population-mean dosimetric parameters for ETCP5, Orig and MDEvsLHD5 plans.

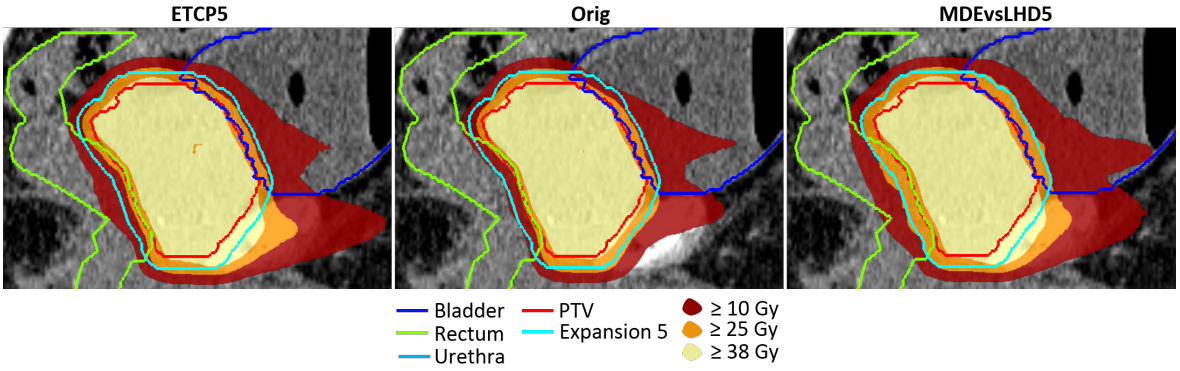

Figure 5.5: Sagittal dose distributions of ETCP5, Orig and MDEvsLHD5 of an example patient

MDE coverage up to 8 mm

Maximizing the expected TCP in Erasmus-iCycle to increase MDE coverage up to 8 mm, the E(TCP) of ETCP8 becomes 0.966. This is an improvement of 0.626 (184%), compared to Orig (table 5.7). The enhanced dose in both expansion 8 and OARs is well visualized in the DVH in figure 5.6 and the dose distribution in figure 5.7. In expansion 8, V38Gy and $D_{98\%}$ increased by 16.2% (195%) and 12.9 Gy (130%), respectively.

Compared to Orig, for the rectum, D1cc increased by 2.6 Gy (9.7%), V27Gy by 2.2 Gy (147%), V18.2Gy by 11.7 Gy (225%) and Dmean by 3.1 Gy (97%). For the bladder, the biggest change was observed in the bladder Dmean; an increase of 2.5 Gy (42%).

Compared to MDEvsLHD8 (section 5.1.4), the E(TCP) marginally worsened in ETCP8, from 1.000 to 0.966. This could be explained by the reduced dose in the expansion 8, $D_{98\%}$ decreased from 25.6 to 22.8 Gy (table 5.7). The reduced expansion dose is also visible in figure 5.6 and figure 5.7.

In a relative sense, the decreased expansion dose is negligible compared to the improved OAR doses. Especially the OAR low and medium-high doses improved (figure 5.6 and table 5.7). On average, the rectum V27Gy decreased by 2.1% (36%), V18.2Gy by 4.6% (21%) and Dmean by 1.3 Gy (17%).

For ETCP5, the E(TCP) of the corresponding Orig plan had an E(TCP) value lower than that of the Orig plan of ETCP8. However, the E(TCP) value of ETCP8 was 0.035 (3.8%) higher compared to the value of ETCP5. This suggests that the optimizer better succeeds in increasing the E(TCP) values when the values of the plan to be optimized, Orig plan, are lower. This behaviour could also be seen in figure 5.6 and 5.4, i.e, a larger increase in doses in both the expansion volume and OARs can be seen for ETCP8 compared to Orig (figure 5.6) than for ETCP5 with its corresponding Orig plan (figure 5.4).

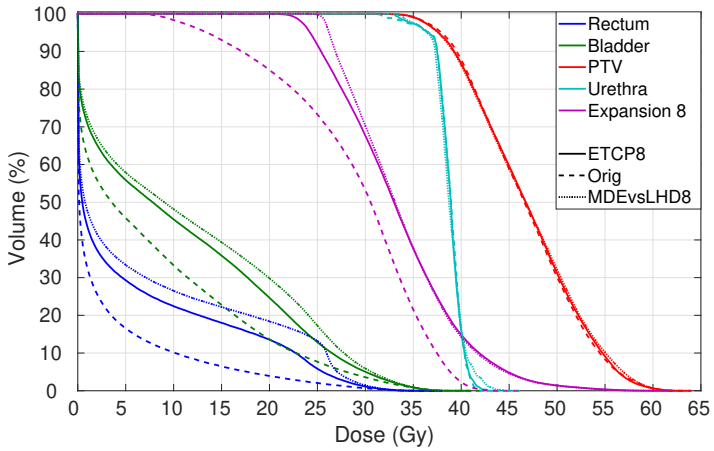

Figure 5.6: DVHs for an example patient for ETCP8, Orig, and MDEvsLHD8 plans.

Structure	Parameter	Unit	ETCP8	Orig	MDEvsLHD8
Expansion 8	*E(TCP)*	-	0.966	0.340	1.000
	V38Gy	%	24.5	8.3	24.0
	D98%	Gy	22.8	9.9	25.6
Patient	*V10Gy*	%	7.1	5.9	7.5
	V20Gy	%	1.5	1.2	1.6
	V30Gy	%	0.7	0.6	0.7
PTV	*V38Gy*	%	94.7	95.2	94.5
	Dmean	Gy	46.7	46.7	46.7
Prostate	*Dmin*	Gy	36.4	36.5	36.3
Rectum	*D0.03cc*	Gy	33.9	33.9	34.1
	D1cc	Gy	29.5	26.9	30.2
	V27Gy	%	3.7	1.5	5.8
	V18.2Gy	%	16.9	5.2	21.5
	Dmean	Gy	6.3	3.2	7.6
Bladder	*D0.03cc*	Gy	37.9	38.7	37.8
	D1cc	Gy	34.8	34.6	34.8
	Dmean	Gy	8.5	6.0	9.3
Urethra	*D50%*	Gy	38.5	38.5	38.4
	D10%	Gy	40.6	40.6	40.7
	D5%	Gy	41.4	41.3	41.7

Table 5.7: Population-mean dosimetric parameters for ETCP8, Orig and MDEvsLHD8 plans.

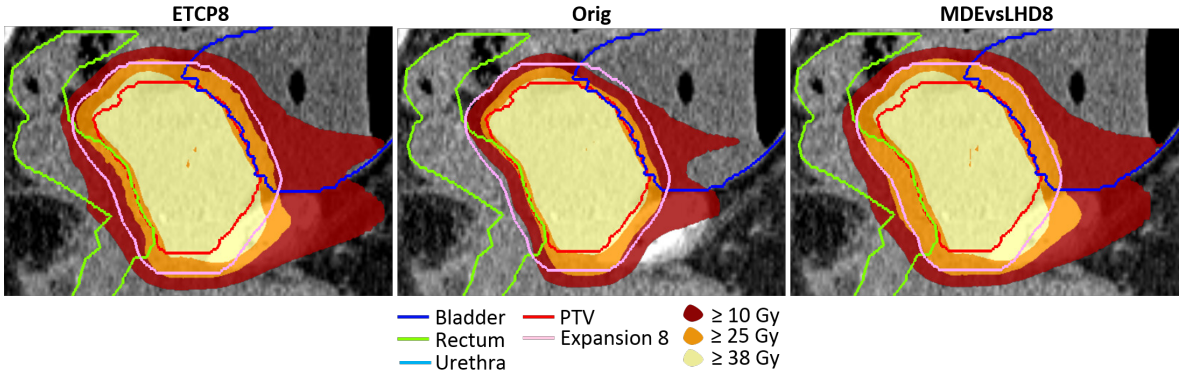

Figure 5.7: Sagittal dose distributions of ETCP8, Orig and MDEvsLHD8 of an example patient

MDE coverage up to 12 mm

Maximizing the expected TCP in ETCP12, the average E(TCP) was 0.970. This is an improvement of 0.630 (185%), compared to Orig.

The DVH in figure 5.8 and dose distribution in figure 5.9 show a remarkable enhancement in coverage of expansion 12 in ETCP12 compared to Orig. The V38Gy increased by 10.8% (216%) and the $D_{98\%}$ by 19.7 Gy (469%).

Unfortunately, OAR doses deteriorated a result of the increased MDE coverage. For the rectum; D1cc increased by 3.2 Gy (12%), V27Gy by 3.4% (243%), V18.2Gy by 20% (417%) and Dmean by 5.4 Gy (180%). For the bladder D1cc increased by 0.2 Gy (0.58%) and Dmean by 4.9 Gy (90.7%). Even though there are no dosimetric parameters to evaluate the volume receiving the medium-high doses (around V18.2Gy), the DVH shows a clear increase in volume coverage with these doses (see figure 5.8).

Compared to MDEvsLHD12, expansion 12 received a slightly lower dose (see figure 5.8 purple solid vs dotted line) in ETCP12. The lower dose is especially visible close to the edges of the expansion border in figure 5.9. This explains the reduced E(TCP) value of ETCP12; a decrease of 0.029 (2.9%) compared to MDEvsLHD12 (table 5.8).

As expected this is only a small decrease, since MDE coverage closer to the PTV is of higher importance due to the MDE probability function in the expected TCP model (section 5.1.1).

As expected, the decrease in E(TCP) and MDE coverage complements improved OAR doses in ETCP12 compared to MDEvsLHD12. The impact is most evident in the low and medium-high doses, the rectum V27Gy, V18.2Gy and Dmean decreased by 1.5% (23.8%), 3.7% (13.0%), and 1 Gy (10.6%), respectively. The bladder Dmean decreased by 0.5 Gy (4.6%).

Comparison between ETCP12 and ETCP8, showed a minor increase in E(TCP) of 0.032 (0.33%) for ETCP12. At the same time, the E(TCP) of MDEvsLHD12 is 0.001 (0.11%) lower compared to the E(TCP) of MDEvsLHD8. This implies that the difference between the E(TCP) of ETCP and MDEvsLHD plans decreases for larger MDE distances from the PTV. This is in line with the comparison between ETCP5 and ETCP8; using the expected TCP cost function, Erasmus-iCycle applies more pressure to increase the E(TCP) when initial values (of the plans to be optimized, Orig plans) are lower.

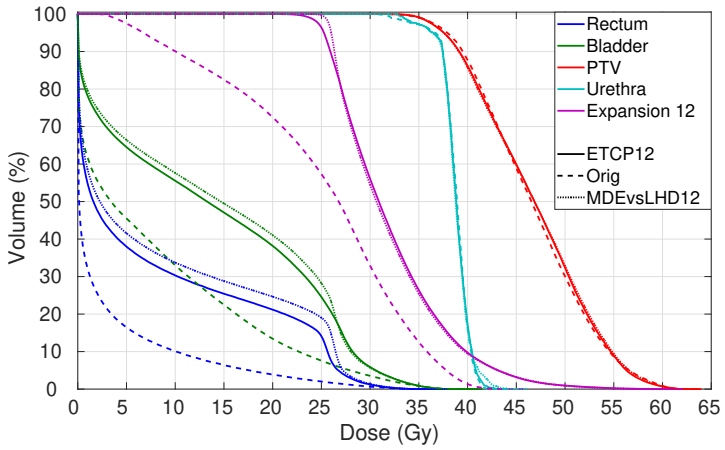

Figure 5.8: DVHs for an example patient for ETCP12, Orig, and MDEvsLHD12 plans.

Structure	Parameter	Unit	ETCP12	Orig	MDEvsLHD12
Expansion 12	*E(TCP)*	-	0.969	0.340	1.000
	V38Gy	%	15.8	5.0	14.3
	D98%	Gy	23.9	4.2	25.4
Patient	*V10Gy*	%	7.3	5.2	7.4
	V20Gy	%	1.6	1.1	1.6
	V30Gy	%	0.6	0.5	0.6
PTV	*V38Gy*	%	94.5	95.3	94.3
	Dmean	Gy	46.7	46.7	46.8
Prostate	*Dmin*	Gy	36.2	36.3	36.1
Rectum	*D0.03cc*	Gy	34.0	33.9	34.3
	D1cc	Gy	29.7	26.5	30.1
	V27Gy	%	4.8	1.4	6.3
	V18.2Gy	%	24.8	4.8	28.5
	Dmean	Gy	8.4	3.0	9.4
Bladder	*D0.03cc*	Gy	37.8	38.7	37.8
	D1cc	Gy	34.7	34.5	34.7
	Dmean	Gy	10.3	5.4	10.8
Urethra	*D50%*	Gy	38.5	38.4	38.4
	D10%	Gy	40.8	40.7	40.9
	D5%	Gy	41.8	41.5	41.8

Table 5.8: Population-mean dosimetric parameters for ETCP12, Orig and MDEvsLHD12 plans.

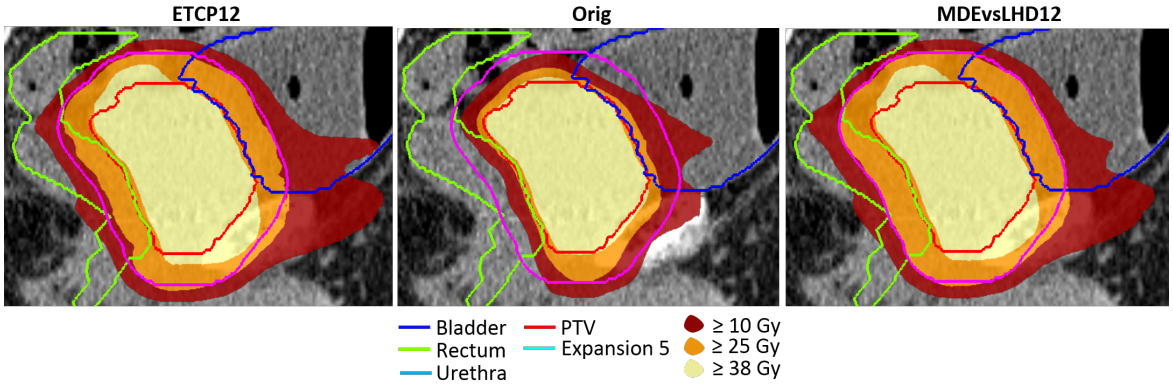

Figure 5.9: Sagittal dose distributions of ETCP12, Orig and MDEvsLHD12 of an example patient

Overview of all dose plans

Figure 5.10 shows E(TCP) and $D_{98\%}$ values in expansion 5, 8 and 12 for Orig, ETCP and MDEvsLHD plans. Figure 5.11 and 5.12 show corresponding OAR D1cc and Dmean values. Increased E(TCP) values go together with an increased $D_{98\%}$, as expected. E(TCP) values are enhanced for ETCP5, ETCP8 and ETCP12, with most enhancement for ETCP8 and ETCP12 compared to Orig. MDEvsLHD results in higher E(TCP) values for all plans (MDEvsLHD5, MDEvsLHD8 and MDEvsLHD12), however the improved E(TCP) is at the cost of increased OAR doses (figure 5.11 and 5.12). D1cc and Dmean in the rectum and Dmean in the bladder are always higher for MDEvsLHD than for ETCP plans. Only D1cc does not deteriorate in MDEvsLHD8 and MDEvsLHD12 compared to ETCP8 and ETCP12.

Table 5.9 gives an overview of the numbers of iterations needed for treatment plan optimization and table 5.10 the corresponding optimization times. The number of iterations and optimization times for the Orig plans deviate slightly for the different expansion volumes, as expected. The number of iterations and optimization times do not scale linearly. However, both the number of iterations and optimization times needed for the optimization of the ETCP plans are considerably higher than for the MDEvsLHD plans, especially for larger expansion structures. i.e. the number of iterations and the optimization time of ETCP12, are 7.9 and 4.7 times the values of MDEvsLHD12, respectively.

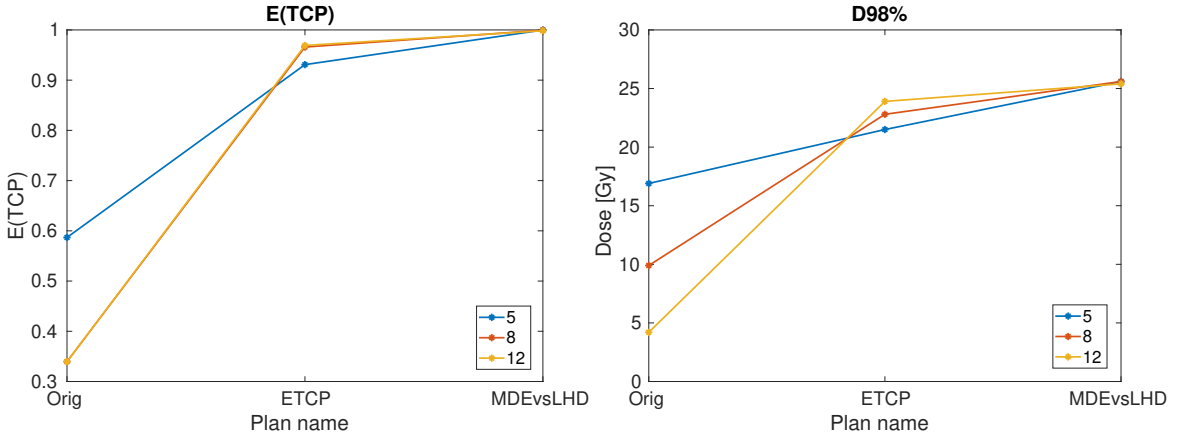

Figure 5.10: Population-mean values of the E(TCP) on the left and $D_{98\%}$ on the right in expansion 5, 8, or 12 mm of Orig, ETCP(5/8/12) and MDEvsLHD(5/8/12).

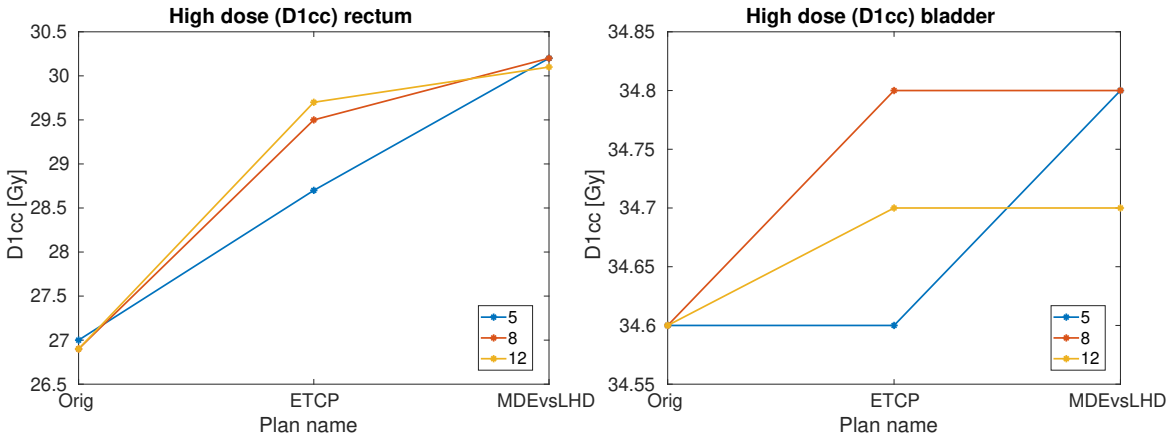

Figure 5.11: Population-mean values of the rectum D1cc on the left and the bladder D1cc on the right of Orig, ETCP(5/8/12) and MDEvsLHD(5/8/12).

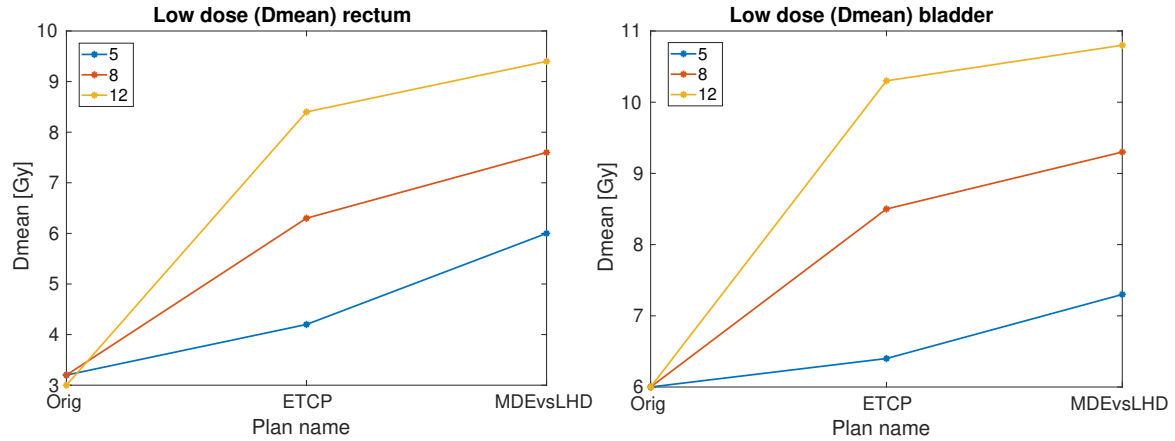

Figure 5.12: Population-mean values the rectum Dmean on the left and the bladder Dmean on the right of Orig, ETCP(5/8/12) and MDEvsLHD(5/8/12).

	ETCP	Orig	MDEvsLHD
5	684	259	337
8	1236	267	362
12	2187	277	374

Table 5.9: Population-mean values of the number of iterations needed for plan optimization of ETCP(5/8/12), Orig and MDEvsLHD(5/8/12).

	ETCP	Orig	MDEvsLHD
5	2326	652	1261
8	9242	765	1671
12	10236	819	2161

Table 5.10: Population-mean values of the optimization times in seconds needed for plan optimization of ETCP(5/8/12), Orig and MDEvsLHD(5/8/12).

5.3. Conclusions

5.3.1. Proof of concept model

The concept model shows that with proper constraining of the total dose delivered to the MDE volume, the expected TCP results in highest doses close to the PTV edge. When there is no constraint in the doses to be delivered, the entire volume will receive the maximum dose. Furthermore, the expected TCP model is sensitive to the biological parameters used. For tumor cell density, ρ, using a uniform distribution between ρ_0 and ρ_1 provides an improved expected TCP compared to when using the median value between ρ_0 and ρ_1 as single input. An increased α/β ratio reduced the expected TCP, with the largest effect for MDE probabilities up to high distances from the PTV.

5.3.2. Expected TCP in Erasmus-iCycle

Using the expected TCP as a cost function in Erasmus-iCycle, the E(TCP) values of real patient plans can be increased compared to the plans without expected TCP optimization. Especially for low E(TCP) values in the plan to be optimized, the cost function pushes to increase doses in the specified MDE volume. This implies that the expected TCP succeeds in optimizing the tumor control probability and is able to improve MDE coverage depending on the MDE distance to the PTV. The effect of the expected TCP optimization is milder than that of MDEvsLHD from the multi-citeria optimization approach. Even though the E(TCP) values are slightly lower, the doses to the OARs are improved. This is a promising outcome, as we want to improve on the E(TCP) as much as possible - accounting for more MDEs, and at the same time spare the OARs. However, the number of iterations and optimization time increased considerably compared to the original plans without use of the novel cost function.

5.4. Future research

Parameter selection

By definition, the expected TCP is sensitive to parameter choices. Because the optimization results were better for a lower α/β ratio (see appendix A), these values were used for the expected TCP in Erasmus-iCycle. Future research should take a deeper look into the effect of using different values for α and β. A possible approach would be to include the uncertainties in α and β values in a similar way as currently done for the values of Δ and ρ. It would also be interesting to test for extreme values, not only for α and β, but also for the tumor cell density, ρ.

Trade-off with OARs

The expected TCP was implemented with a priority higher than the OAR objectives; rectum and bladder EUD and Dmean values. It is worth investigating different trade-offs with OARs and the impact that these modifications have on E(TCP) values. A similar approach could be used as for prioritized optimization (chapter 4), where different compromises in the dose distribution are made; MDE coverage with expected TCP vs OAR doses.

Erasmus-iCycle optimization

In this project, we have decided not to use the Hessian in Erasmus-iCycle implementation (as explained in section 5.1.4). However, the number of iterations and optimization time when using the cost function increased considerably compared to without use of the expected TCP cost function and to the MDEvsLHD plans. Future research should conclude whether there will be a faster convergence of the function when implementing the Hessian next to the original and gradient function.

MDE probability function

The distribution of the probability of finding an MDE at a certain location from the tumor edge, describes an exponential. However, it is not a given fact that the MDE function is an exponential, since there are still many uncertainties in the MDE distribution. Therefore, the use of different probability functions might provide insights into the optimal dose distribution for various situations.

Furthermore, the currently used MDE probability function, only depends on probabilities of finding MDEs at a certain distance and therefore suggests that all patients have MDEs. However, histopathological studies have shown that there are patients that have no microscopic extensions while for others microscopic disease can be found up to 12 mm from the tumor edge.

To improve accuracy of the function, also the probability that a patient has MDEs should be included.

Implementation of the expected TCP
For the use of the expected TCP in Erasmus-iCycle, the MDE volume domain in the current approach is described by PTV expansions of either 5, 8 or 12 mm around the PTV. Only the voxels within the expansion volume are considered in the expected TCP calculation. This way, not all quadrature points are included in the numerical integration, as the voxel distances do not go up to the maximum value for Δ_i. The correct way of calculating the expected TCP is by including all voxels outside of the PTV and not only the ones in the expansion volumes. Future research should investigate the effect on E(TCP) values when including all voxels in the expected TCP calculation.

6

Conclusions

In this work, two novel approaches have been introduced to account for MDE uncertainties in treatment planning; multi-criteria prioritized optimization and probabilistic planning. Feasibility studies have been performed for each approach. An overall conclusion and directions for future research are provided below.

By using multi-criteria prioritized optimization, it was possible to steer the dose distribution towards improved MDE coverage. Irradiating a larger volume outside of the PTV, where MDEs can be present, was feasible, but always in exchange for enhanced OAR doses. By accepting higher low OAR doses and only moderately deteriorated high OAR doses, the MDE coverage increased significantly.

The probabilistic planning approach showed that with optimization of the expected TCP (tumor control probability) as a cost function in Erasmus-iCycle, the volume close to the PTV would receive the highest dose. This means that dose coverage is enhanced for volumes with a high probability of holding MDEs. Implementation of the new cost function resulted in treatment plans with an increased expected TCP, as wanted.

The most significant improvement of the new automated treatment planning approaches is that instead of using a fixed applied margin for all prostate patients, more patient-specific dose distributions could be obtained compared to the current CTV margin.

Both prioritized optimization and probabilistic planning have shown to be capable of enhancing dose to the area with likely MDE presence, in a trade-off with OAR doses. Although OAR doses increased, treatment planning did not violate the clinical constraints for any of the proposed plans. Therefore it implies that prioritized optimization and probabilistic planning can improve optimal tumor control, and thereby radiotherapy outcomes, while at the same time avoiding severe radiotherapy-induced toxicity. In this way, it is possible to patient-specifically decide on the balance between improved MDE irradiation and reduced OAR sparing.

Future research
This work focused on accounting for uncertainties in microscopic disease extensions only. However, the investigated approaches could, in principle, also be applied for the macroscopic tumor delineation uncertainties. Future research can evaluate how prioritized optimization and probabilistic planning could also be used to define the GTV margin in a novel way.

For both approaches, feasibility studies have been performed, based on five patient plans. The inclusion of a higher number of patients as well as the involvement of treating clinicians will be the next steps to investigate whether the approaches could lead to changes in clinical practice.

Both prioritized optimization and probabilistic planning could be used for other tumor sites than the prostate. This way, the performance of both promising approaches can be evaluated for different anatomies, including other OARs, and with the use of different protocols and CTV margins.

7

Appendix

A.

The α and β parameters that were first used for the expected TCP optimization were $\alpha = 0.15$ Gy^{-1} and $\beta = 0.058$ Gy^{-2}, having an α/β ratio of 2.6 Gy. However, in Chapter 4, we assumed the α/β ratio to be 1.5 Gy (section 4.1.2). To be consistent, the α/β ratio was adapted to 1.5 Gy and the outcomes for the Erasmus-iCycle approach (section 5.1.4) of ETCP5 and ETCP8 were evaluated. DVHs of an example patient can be seen in figure 7.1 and corresponding optimized expected TCP values in table 7.1. Especially for ETCP8 (right plot in figure 7.1) it is clearly visible that for an α/β ratio of 1.5 Gy, the optimizer focuses more on increasing dose received by the full expansion volume compared to when using an α/β ratio of 2.6 Gy. The α/β ratio of 1.5 Gy also corresponds to higher expected TCP values (table 7.1). Because better optimizer performance was obtained using the α/β ratio of 1.5 Gy, this ratio was used for the project (here better performance was defined by the largest dose increase to the full expansion volume). Future research is needed for more definitive conclusions regarding the optimal expected TCP parameters (also see section 5.4).

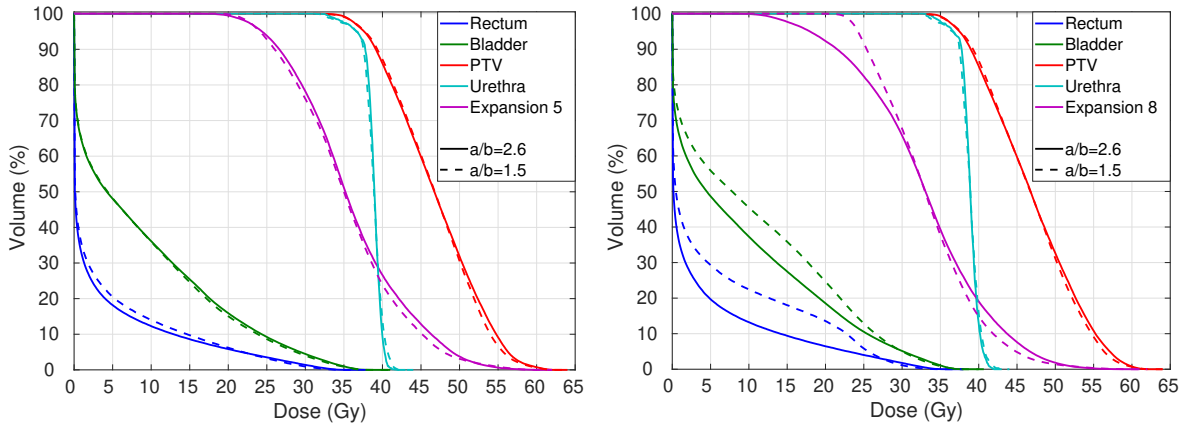

Figure 7.1: DVHs for an example patient for expected TCP optimization with Erasmus-iCycle of plan ETCP5 on the left and ETCP8 on the right (as introduced in section 5.1.4) using an α/β ratio of 2.6 or 1.5 Gy.

Plan name	α/β=2.6	α/β=1.5
ETCP5	0.92	0.99
ETCP8	0.84	0.99

Table 7.1: Expected TCP values of an example patient for expected TCP optimization with Erasmus-iCycle of plan ETCP5 on the left and ETCP8 on the right (as introduced in section 5.1.4) using an α/β ratio of 2.6 or 1.5 Gy.

Bibliography

[1] World Health Organization. Key facts cancer. https://www.who.int/news-room/fact-sheets/detail/cancer.

[2] Nigel P. Murray. Minimal residual disease in prostate cancer patients after primary treatment: Theoretical considerations, evidence and possible use in clinical management. *Biological Research*, 51(1):1–14, 2018.

[3] F. Menegoz, J. M. Lutz, M. Mousseau, H. Orfeuvre, and R. Schaerer. Descriptive Epidemiology of Prostate Cancer. 10(2):1–6, 2019.

[4] B J Davis, T M Pisansky, R P Myers, H J Rothenberg, A Pacelli, D W Hillmun, D J Sargent, and D G Bostwick. The radial distance of extraprostatic extension of prostatic adenocarcinoma: implications for prostate brachytherapy. *I. J. Radiation Oncology*, 42(1):1998, 1998.

[5] Murat Beyzadeoglu, Gokhan Ozyigit, and Cuneyt Ebruli. *Radiobiology*. Springer Berlin Heidelberg, 2010.

[6] NIH National Cancer Institute. Nci dictionary of cancer terms. https://www.cancer.gov/publications/dictionaries/cancer-terms/def/hypofractionated-radiation-therapy.

[7] C.K. Chris Wang. The progress of radiobiological models in modern radiotherapy with emphasis on the uncertainty issue. *Mutation Research/Reviews in Mutation Research*, 704(1):175 – 181, 2010.

[8] S Webb and A E Nahum. A model for calculating tumour control probability in radiotherapy including the effects of inhomogeneous distributions of dose and clonogenic cell density. 38(6):653–666, jun 1993.

[9] Darek Michalski, M. Huq Saiful, and Brian F. Hasson. *Normal Tissue Complication Probability (NTCP)*, pages 560–560. Springer Berlin Heidelberg, Berlin, Heidelberg, 2013.

[10] John T Lyman. Complication probability as assessed from dose-volume histograms. *Radiation Research*, 104(2s):S13–S19, 1985.

[11] T. Landberg, J. Chavaudra, J. Dobss, G.Hanks, K.A. Johannson, T. Moller, and J. Purdy. *Prescribing, Recording and Reporting Photon Beam Radiotherapy*. 1993.

[12] B.S. Teh, M.D. Bastasch, W.Y. May, and T.M. Wheeler E.B. Butler. Predictors of extracapsular extension and its radial distance in prostate cancer: implications for prostate imrt, brachytherapy, and surgery. *Cancer J*, 9:454–60, 2003.

[13] Marcel van Herk. Errors and margins in radiotherapy. *Seminars in Radiation Oncology*, 14(1):52 – 64, 2004. High-Precision Radiation Therapy of Moving Targets.

[14] Paul M. DeLuca and Stephen M. Seltzer. *Journal of the ICRU: Preface*, volume 8. 2008.

[15] H. Rodney Withers, Jeremy M.G. Taylor, and Boguslaw Maciejewski. Treatment volume and tissue tolerance. *International Journal of Radiation Oncology*Biology*Physics*, 14(4):751 – 759, 1988.

[16] Sebastiaan Breedveld, Pascal R.M. Storchi, Peter W.J. Voet, and Ben J.M. Heijmen. ICycle: Integrated, multicriterial beam angle, and profile optimization for generation of coplanar and noncoplanar IMRT plans. *Medical Physics*, 39(2):951–963, 2012.

[17] Brian F. Hasson. *Dose Volume Histogram (DVH)*, pages 166–166. Springer Berlin Heidelberg, Berlin, Heidelberg, 2013.

[18] Rudi Apolle, Maximilian Rehm, Thomas Bortfeld, Michael Baumann, and Esther G.C. Troost. The clinical target volume in lung, head-and-neck, and esophageal cancer: Lessons from pathological measurement and recurrence analysis. *Clinical and Translational Radiation Oncology*, 3:1 – 8, 2017.

[19] Hanan Goldberg, Abu-Hijlih Ramiz, Rachel Glicksman, Noelia S. Salgado, Thenappan Chandrasekar, Zachary Klaassen, Christopher J.D. Wallis, Ali Hosni, Fabio Ynoe Moraes, Sangeet Ghai, Girish S. Kulkarni, Robert J. Hamilton, Nathan Perlis, Ants Toi, Peter Chung, Andrew Evans, Theo van der Kwast, Antonio Finelli, Neil Fleshner, and Alejandro Berlin. Extraprostatic extension in core biopsies epitomizes high-risk but locally treatable prostate cancer. *European Urology Oncology*, 2(1):88 – 96, 2019.

[20] Chris Sohayda, Patrick A Kupelian, Howard S Levin, and Eric A Klein. Extent of extracapsular extension in localized prostate cancer. *Urology*, 55:382–6, 04 2000.

[21] Bin S Teh, Michael D Bastasch, Thomas M Wheeler, Wei-Yuan Mai, Anna Frolov, Barry M Uhl, Hsin H Lu, L.Steven Carpenter, J.Kam Chiu, John McGary, Shiao Y Woo, Walter H Grant, and E.Brian Butler. Imrt for prostate cancer: Defining target volume based on correlated pathologic volume of disease. *International Journal of Radiation Oncology*Biology*Physics*, 56(1):184 – 191, 2003.

[22] David J. Schwartz, Shomik Sengupta, David W. Hillman, Daniel J. Sargent, John C. Cheville, Torrence M. Wilson, Lance A. Mynderse, Richard Choo, and Brian J. Davis. Prediction of radial distance of extraprostatic extension from pretherapy factors. *International Journal of Radiation Oncology*Biology*Physics*, 69(2):411 – 418, 2007.

[23] K. Kenneth Chao, Neal S. Goldstein, Di Yan, Carlos E. Vargas, Michel I. Ghilezan, Howard J. Korman, Kenneth M. Kernen, Jay B. Hollander, Jose A. Gonzalez, Alvaro A. Martinez, Frank A. Vicini, and Larry L. Kestin. Clinicopathologic analysis of extracapsular extension in prostate cancer: Should the clinical target volume be expanded posterolaterally to account for microscopic extension? *International Journal of Radiation Oncology*Biology*Physics*, 65(4):999 – 1007, 2006.

[24] Christian Siedschlag, Liesbeth Boersma, Judith van Loon, Maddalena Rossi, Angela van Baardwijk, Kenneth Gilhuijs, and Joep Stroom. The impact of microscopic disease on the tumor control probability in non-small-cell lung cancer. *Radiotherapy and Oncology*, 100(3):344–350, 2011.

[25] Judith van Loon, Christian Siedschlag, Joep Stroom, Hans Blauwgeers, Robert-Jan van Suylen, Joost Knegjens, Maddalena Rossi, Angela van Baardwijk, Liesbeth Boersma, Houke Klomp, Wouter Vogel, Sjaak Burgers, and Kenneth Gilhuijs. Microscopic disease extension in three dimensions for non–small-cell lung cancer: Development of a prediction model using pathology-validated positron emission tomography and computed tomography features. *International Journal of Radiation Oncology*Biology*Physics*, 82(1):448 – 456, 2012.

[26] Inga S. Grills, Dwight L. Fitch, Neal S. Goldstein, Di Yan, Gary W. Chmielewski, Robert J. Welsh, and Larry L. Kestin. Clinicopathologic Analysis of Microscopic Extension in Lung Adenocarcinoma: Defining Clinical Target Volume for Radiotherapy. *International Journal of Radiation Oncology Biology Physics*, 69(2):334–341, 2007.

[27] Thu Tran, Chandru P. Sundaram, Clinton D. Bahler, John N. Eble, David J. Grignon, M. Francesca Monn, Novae B. Simper, and Liang Cheng. Correcting the shrinkage effects of formalin fixation and tissue processing for renal tumors: toward standardization of pathological reporting of tumor size. *J Cancer*, 6:759–766, 2015.

[28] Tao Zhang Jing Jin Shulian Wang Yueping Liu Yongwen Song Xinfan Liu Zihao Yu Weihu Wang, Xiaoli Feng and Yexiong Li. Prospective evaluation of microscopic extension using whole-mount preparation in patients with hepatocellular carcinoma: Definition of clinical target volume for radiotherapy. *Radiation Oncology*, 5(1):1–7, 2010.

[29] Michael C. Roach, Jeffrey D. Bradley, and Cliff G. Robinson. Optimizing radiation dose and fractionation for the definitive treatment of locally advanced non-small cell lung cancer. *Journal of Thoracic Disease*, 10(21), 2018.

[30] A. J. Mundt and J.C. Roeske. *Intensity Modulated Radiation Therapy: A Clinical Perspective*. Pmph-USA, Ltd., 2005.

[31] Román Bohoslavsky, Marnix G Witte, Tomas M. Tomas M. Janssen, and Marcel van Herk. Probabilistic objective functions for margin-less IMRT planning. *Physics in Medicine and Biology*, 58(11):3563–3580, 2013.

[32] Jan Unkelbach, Markus Alber, Mark Bangert, Rasmus Bokrantz, Timothy C.Y. Chan, Joseph O. Deasy, Albin Fredriksson, Bram L. Gorissen, Marcel Van Herk, Wei Liu, Houra Mahmoudzadeh, Omid Nohadani, Jeffrey V. Siebers, Marnix Witte, and Huijun Xu. Robust radiotherapy planning. *Physics in Medicine and Biology*, 63(22), 2018.

[33] J. J. Gordon, N. Sayah, E. Weiss, and J. V. Siebers. Coverage optimized planning: Probabilistic treatment planning based on dose coverage histogram criteria. *Medical Physics*, 37(2):550–563, 2010.

[34] Christoph Baum, Markus Alber, Mattias Birkner, and Fridtjof Nüsslin. Robust treatment planning for intensity modulated radiotherapy of prostate cancer based on coverage probabilities. *Radiotherapy and Oncology*, 78(1):27 – 35, 2006.

[35] Marnix G. Witte, Joris van der Geer, Christoph Schneider, Joos V. Lebesque, Markus Alber, and Marcel van Herk. IMRT optimization including random and systematic geometric errors based on the expectation of TCP and NTCP. *Medical Physics*, 34(9):3544–3555, 2007.

[36] Davide Fontanarosa, Hans Paul van der Laan, Marnix Witte, Georgy Shakirin, Erik Roelofs, Johannes Langendijk, Philippe Larnbin, and Marcel van Herk. An in silico comparison between margin-based and probabilistic target-planning approaches in head and neck cancer patients. *Radiotherapy and Oncology*, 109(3):430–436, 2013.

[37] Nadya Shusharina, David Craft, Yen Lin Chen, Helen Shih, and Thomas Bortfeld. The clinical target distribution: A probabilistic alternative to the clinical target volume. *Physics in Medicine and Biology*, 63(15):aacfb4, 2018.

[38] Linda Rossi, Abdul Wahab Sharfo, Shafak Aluwini, Maarten Dirkx, Sebastiaan Breedveld, and B. Heijmen. First fully automated planning solution for robotic radiosurgery – comparison with automatically planned volumetric arc therapy for prostate cancer. *Acta Oncologica*, 57:1–9, 07 2018.

[39] J. Crezee A. Bel N. A. P. Franken L. J. A. Stalpers H. P. Kok C. M. van Leeuwen, A. L. Oei. The alfa and beta of tumours: a review of parameters of the linear-quadratic model, derived from clinical radiotherapy studies. *Radiation Oncology*, 13(96), 2018.

[40] S.P. Venkateshan and Prasanna Swaminathan. Chapter 9 - numerical integration. In S.P. Venkateshan and Prasanna Swaminathan, editors, *Computational Methods in Engineering*, pages 317 – 373. Academic Press, Boston, 2014.

[41] Piernicola Pedicini, Lidia Strigari, and Marcello Benassi. Estimation of a self-consistent set of radiobiological parameters from hypofractionated versus standard radiation therapy of prostate cancer. *International Journal of Radiation Oncology*Biology*Physics*, 85(5):e231 – e237, 2013.

[42] jian-yue Jin, feng-ming Kong, Dezhi Liu, Lei Ren, Haisen Li, Hualiang Zhong, Benjamin Movsas, and Indrin Chetty. A tcp model incorporating setup uncertainty and tumor cell density variation in microscopic extension to guide treatment planning. *Medical physics*, 38:439–48, 01 2011.

[43] Mathworks. fmincon. `https://www.mathworks.com/help/optim/ug/fmincon.html`.

[44] F.B. Hildebrand. Introduction to numerical analysis. In *Introduction to numerical analysis*, pages 319–323. McGraw-Hill Book Company, New York, 1956.